Spring 2009

Synthesis of inorganic heptazine-based materials

James Robert Holst
University of Iowa

SYNTHESIS OF INORGANIC HEPTAZINE-BASED MATERIALS

by

James Robert Holst

An Abstract

Of a thesis submitted in partial fulfillment
of the requirements for the Doctor of
Philosophy degree in Chemistry
in the Graduate College of
The University of Iowa

May 2009

Thesis Supervisor: Associate Professor Edward G. Gillan

ABSTRACT

This dissertation describes research on the synthesis and characterization of extended heptazine-based, graphite-like carbon nitride materials (CN_x), as well as molecular heptazine (C_6N_7) derivatives. Spurred on by recent triazine to heptazine conversion studies, a structural examination was performed on an amorphous nitrogen-rich carbon nitride material formed via the rapid and exothermic self-propagating decomposition of a triazine (C_3N_3) precursor, trichloromelamine (TCM). The thermally stable and insoluble CN_xH_y product was determined to be composed of heptazine repeat units. This conclusion was supported by ^{13}C solid state NMR and isolation of molecular heptazine anions after base hydrolysis (structural deconstruction) of the CN_xH_y material.

Modifications to the decomposition of TCM were explored. Introduction of a solid template (NaCl or silica) led to morphological changes in the TCM-CN_x product, observed by scanning electron microscopy. It was found that the sodium salts, NaBr and NaN_3, led to chloride exchange with TCM. The use of mixtures of NH_4Cl and NaN_3 also showed changes in the morphology of the material, while leading to slight changes in the IR spectra. A series of reactions between $NaBH_4$ and TCM yield novel thermally stable boron carbon nitride (BCN) materials. Reactions between TCM and Li_2C_2 or aromatic organic solids led to CN_x materials with increased carbon contents.

Crystalline metal-heptazine precipitates were generated by cation exchange reaction with the base hydrolysis product of TCM-CN_x, potassium cyamelurate. A structure solution was attempted for the crystalline copper cyamelurate salt, $KCu[C_6N_7O_3]\cdot 4H_2O$. Neutral molecular heptazines were also synthesized; these species included 2,5,8-tribromo-s-heptazine (TBH), 2,5,8-triphenyl-s-heptazine (TPH), 2,5,8-

tris(diisopropylamino)-s-heptazine (TAmH), and 2-bis(trimethylsilyl)amido-5,8-dichloroheptazine (DCAH). These materials were sublimable and showed interesting optical absorption and emission properties. A polymeric heptazine material was synthesized by thermal decomposition of DCAH.

Several attempts were made to synthesize polymeric materials from heptazine precursors. Extended solids with C_6N_8 and C_9N_7 stoichiometry were made through solid state metathesis reactions between trichloroheptazine and either lithium nitride or lithium carbide. Powder X-ray diffraction indicated that salt formation was occurring during these reactions and products had the desired stoichiometry by elemental analysis. It was generally observed that CN_x materials containing excess carbon displayed increased thermal stability when compared to pure CN_x.

_____

Thesis Supervisor

_____

Title and Department

_____

Date

SYNTHESIS OF INORGANIC HEPTAZINE-BASED MATERIALS

by

James Robert Holst

A thesis submitted in partial fulfillment
of the requirements for the Doctor of
Philosophy degree in Chemistry
in the Graduate College of
The University of Iowa

May 2009

Thesis Supervisor: Associate Professor Edward G. Gillan

Graduate College
The University of Iowa
Iowa City, Iowa

CERTIFICATE OF APPROVAL

_____

PH.D. THESIS

_____

This is to certify that the Ph.D. thesis of

James Robert Holst

has been approved by the Examining Committee
for the thesis requirement for the Doctor of Philosophy
degree in Chemistry at the May 2009 graduation.

Thesis Committee: _____
Edward Gillan, Thesis Supervisor

_____
Darrell Eyman

_____
Julie Jessop

_____
Sarah Larsen

_____
Johna Leddy

To Mom and Dad

I can't live the button-down life like you. I want it all: the terrifying lows, the dizzying highs, the creamy middles.

-Homer Simpson, *The Simpsons*

ACKNOWLEDGMENTS

I want to begin by thanking my wife, Mary. I hope that now you'll finally be able to get sick of me from being around so much. For all their love and support, I want to thank my family: Mom, Dad, Elizabeth, and Philip. When I started college in 1997, I don't think any of you would have expected to me to still be here 11 years later. But here I am and I couldn't have done it without you. Of course, I will insist that you all call me Doctor from now on (just kidding!). I'd also like to thank all my family for their love and support: Grandma Sacquety, Grandma and Grandpa Holst, Uncle Bob and Aunt Rachel, Auntie Sharon and Bill, Jennifer, David, Lauren, Hadley and Bex. We'll be raising some glasses once this thing is over.

Professionally, I would first like to thank the professor. Ed, I want to thank you for being a great mentor. You were very patient with me early on when I had my doubts about this whole chemistry thing, and I appreciate you for seeing me through it. It's also great to see someone who loves what they do for a living…it's infectious. I also want to thank all the members of the Gillan group, past and present: Dr. Dale Miller, Dr. C.J. Choi, Dr. Sujith Perera, Brian Barry, Andrew Zimmerman, Ashley Nelson, Nadiya Zelenski, and Zack Rhodes. Thank you for all your help. Brian, I especially want to thank you thank you for being a great friend and a setting a great example of work ethic.

I also want to thank all my other roommates for their attempts at turning me to the Dark Side: Luke, Will, Willis, Stewie, Hoff, Deardorff, Mike, Brian, and Jon. Thank you for providing me with an occasional outlet to let loose and have fun. I also want to thank all those fellow grad students whom I had to pleasure of meeting for their friendship and camaraderie: Tony Sokolov, Ivan Georgiev, Tamara Hamilton, Tomislav

Friscic, Qianli Chu, Kreso Bucar, Manza Atkinson, Nick Schoenfeldt, Ari Saha, Jennifer Schuttlefield, Cara Bonnema Welch, Joel Welch, Jose Tormos, Jose Yu, Kelly Boss, Nathan Lien, Suhash Harwani, Dave Rotsch, Travis Owen, Matt Kelley, Ani Jordan, Julie Park, Arun Sen, and James Brown.

Thank you to the following UI Faculty members for their various roles during my graduate career: Drs. Harold Goff, Len MacGillivray, Johna Leddy, Julie Jessop, Norb Pienta, and Darrell Eyman. A big thank you is also necessary for the all the UI chemistry department staff members: Shonda Monette, Sharon Robertson, Janet Kugley, Michele Gerot, Vic Parcell, Peter Hatch, Frank Turner, Tim Koon , Andy Lynch, Robert Brown, Brian Morrison, and Earlene Erbe.

Lastly, I would to acknowledge those individuals for their scientific contributions to the work presented in this dissertation. Special attention is given Dr. Santhana Velupillai, Ram Kanthasamy, and Anton Petushkov for performing solid state NMR experiments; Dr. Dale Swenson who performed the data collection on the single crystals collected from Chapter II; Jonas Baltrusaitis for the X-ray Photoelectron Spectroscopy (XPS) data collection in Chapter IV; Vic Parcell and Lynn Teesch for assistance in collect mass spectrometry data; Dr. Darrell Eyman for the use of the residual gas analysis mass spectrometer (RGA-MS); Dr. Vicki Grassian, Jennifer Schuttlefield and Julie Park for the use and assistance with surface area measurements; Brian Morrison for the use of the spectrofluorometer. Finally, I would like to thank the Department of Education in providing the Graduate Assistance in Areas of National Need (GAANN) Fellowship, which allowed me to focus on research, as well as the purchase of replacement parts for the elemental analyzer.

ABSTRACT

This dissertation describes research on the synthesis and characterization of extended heptazine-based, graphite-like carbon nitride materials (CN_x), as well as molecular heptazine (C_6N_7) derivatives. Spurred on by recent triazine to heptazine conversion studies, a structural examination was performed on an amorphous nitrogen-rich carbon nitride material formed via the rapid and exothermic self-propagating decomposition of a triazine (C_3N_3) precursor, trichloromelamine (TCM). The thermally stable and insoluble CN_xH_y product was determined to be composed of heptazine repeat units. This conclusion was supported by ^{13}C solid state NMR and isolation of molecular heptazine anions after base hydrolysis (structural deconstruction) of the CN_xH_y material.

Modifications to the decomposition of TCM were explored. Introduction of a solid template (NaCl or silica) led to morphological changes in the TCM-CN_x product, observed by scanning electron microscopy. It was found that the sodium salts, NaBr and NaN_3, led to chloride exchange with TCM. The use of mixtures of NH_4Cl and NaN_3 also showed changes in the morphology of the material, while leading to slight changes in the IR spectra. A series of reactions between $NaBH_4$ and TCM yield novel thermally stable boron carbon nitride (BCN) materials. Reactions between TCM and Li_2C_2 or aromatic organic solids led to CN_x materials with increased carbon contents.

Crystalline metal-heptazine precipitates were generated by cation exchange reaction with the base hydrolysis product of TCM-CN_x, potassium cyamelurate. A structure solution was attempted for the crystalline copper cyamelurate salt, $KCu[C_6N_7O_3]\cdot 4H_2O$. Neutral molecular heptazines were also synthesized; these species included 2,5,8-tribromo-s-heptazine (TBH), 2,5,8-triphenyl-s-heptazine (TPH), 2,5,8-

tris(diisopropylamino)-s-heptazine (TAmH), and 2-bis(trimethylsilyl)amido-5,8-dichloroheptazine (DCAH). These materials were sublimable and showed interesting optical absorption and emission properties. A polymeric heptazine material was synthesized by thermal decomposition of DCAH.

Several attempts were made to synthesize polymeric materials from heptazine precursors. Extended solids with C_6N_8 and C_9N_7 stoichiometry were made through solid state metathesis reactions between trichloroheptazine and either lithium nitride or lithium carbide. Powder X-ray diffraction indicated that salt formation was occurring during these reactions and products had the desired stoichiometry by elemental analysis. It was generally observed that CN_x materials containing excess carbon displayed increased thermal stability when compared to pure CN_x.

TABLE OF CONTENTS

LIST OF TABLES

LIST OF FIGURES

CHAPTER I

INTRODUCTION AND BACKGROUND

Introduction

The term, "carbon nitride," is used to describe a diverse class of C-N containing solids with nitrogen contents ranging from a few to over 60 mol%, but it is somewhat of a misnomer. Inorganic metal and non-metal nitrides are comprised of nitrogen species that exhibit a range of bonding modes from ionic to covalent and form crystalline networks with well-defined chemical compositions. In contrast to such nitrides, nitrogen-rich carbon nitrides contain covalently bonded nitrogen in disordered structures with variable compositions and little or no long range crystalline order. Regardless of the lack of details of local structure and composition, carbon nitrides and nitrogen-doped carbons have found use as metal free organocatalysts, as components of fuel cell electrodes, and show utility in light-emitting and chemical sensor applications.[1-10] The origin of carbon nitrides will be discussed in the following section.

sp^3-Carbon Nitride: A Theoretical Superhard Material

Interest in covalently bonded carbon nitride (CN_x) materials was initially spurred by theoretical studies on an sp^3-hybridized carbon analog of silicon nitride, C_3N_4 ($CN_{1.33}$), that could have a hardness comparable to that of diamond. In 1984, Cohen and Sung separately began work on calculating bulk moduli for known diamond-like semiconductors.[11,12] In his work, Cohen reported a simple formula relating the bulk modulus, B, with interatomic distance, d: $B = 1761\ d^{-3.5}$. Later, the formula would be iteratively refined to include average coordination number, N_c and bond polarization, λ: $B = (N_c/4)(1971\text{-}220\lambda)\ d^{-3.5}$.[12-14] Along with showing his calculated values had a good

registry to known zinc blende type materials, Cohen also went on to suggest that a similar type of structure with C and N (Figure 1.1a) would have a bulk modulus of up to 483 GPa, which is significantly larger than diamond (440 GPa). Liu and Cohen further refined their model by ruling out that initial zinc blende structure due to it featuring an occupied antibonding orbital.[14] This was deemed to be too unstable a structure to be viable; instead, a C-N solid isotructural to β-Si_3N_4 was proposed as can be viewed in Figure 1.1b. This new β-C_3N_4 phase was recalculated to have a value of 427 GPa, theoretically making it the second hardest material after diamond and ahead of cubic boron nitride (376 GPa).

Researchers began to explore other types of possible structures for C_3N_4 that would be more energetically favorable than α- and β-C_3N_4.[15] Teter and Hemley proposed cubic and pseudocubic phases of C_3N_4 which are shown in Figure 1.2. In a review of

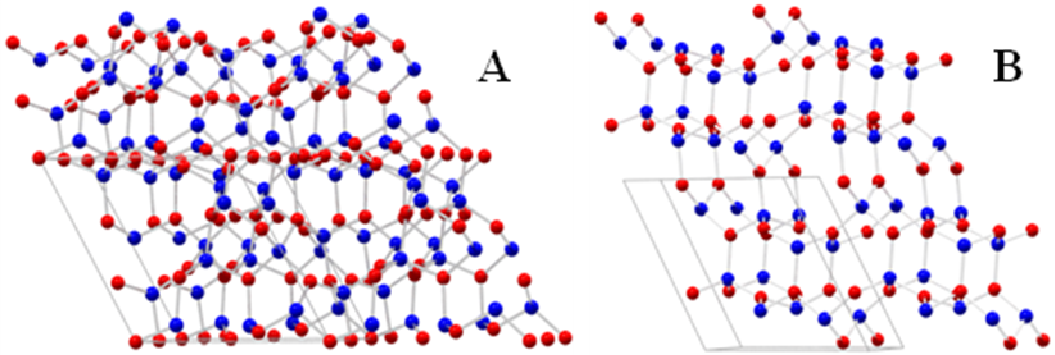

Figure 1.1 - Proposed structure for a) zinc blende or α-C_3N_4 and b) β-C_3N_4. Carbon atoms are in blue and nitrogen atoms are in red. Both structures are shown slightly tilted away from the *c*-axis. Structures were generated in PowderCell 2.4 from data by Teter and Hemley.[15]

superhard materials, Teter also reminded the materials community that the shear modulus of a material is a better predictor of hardness than bulk modulus, i.e. all hard materials have a high bulk modulus, but not all materials with a high bulk modulus are very hard.[16] With that in mind, the calculated shear modulus of the postulated β-C_3N_4 phase, at 320 GPa, pales in comparison to diamond at 535 GPa.

Graphitic-C_3N_4: sp^2 Structures

Teter and Hemley proposed that a layered type of carbon nitride could exist.[15] These planar CN_x materials could be considered to have the same relationship that graphite has to diamond, hence they were referred to as graphitic or g-C_3N_4. Theoretical studies have been able to show that a g-C_3N_4 structure composed of triazine rings (C_3N_3) linked by trigonal planar nitrogen would be slightly more thermodynamically stable than

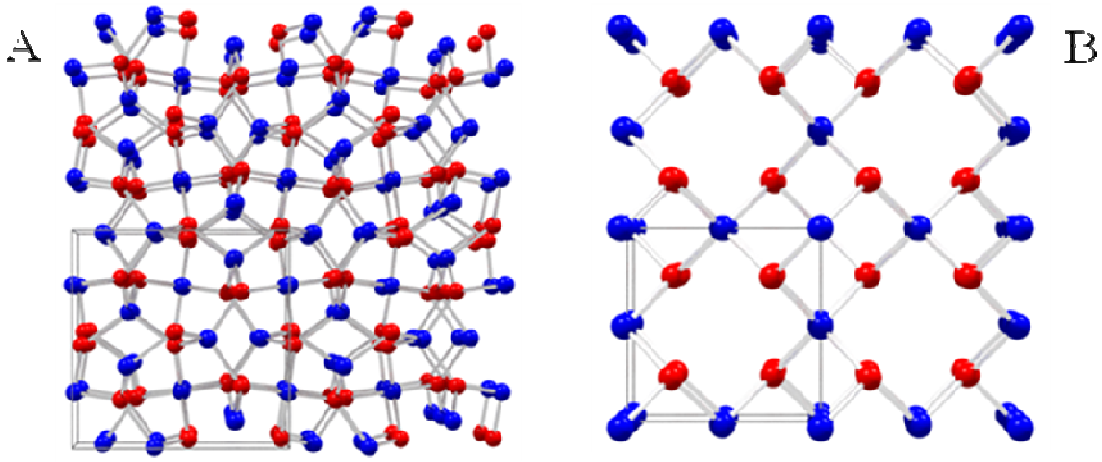

Figure 1.2 - Theoretical structures for: A) cubic C_3N_4 and B) pseudocubic C_3N_4 with carbon atoms shown in blue and nitrogen atoms shown in red. Both structures are shown slightly tilted away from the c-axis. Structures were generated in PowderCell 2.4 from data by Teter and Hemley.[15]

β-C_3N_4.[17] These and other studies postulated structures with different stacking arrangements with interplanar distances of 3.06 to 3.45 Å.[15,18,19] The structure of g-C_3N_4 can be seen in Fig. 1.3. It has been thought that g-C_3N_4 could be used as a precursor to directly convert to dense, hard C_3N_4 materials under pressure, much in the same way that graphite can be converted to diamond under high temperature and pressure.[20]

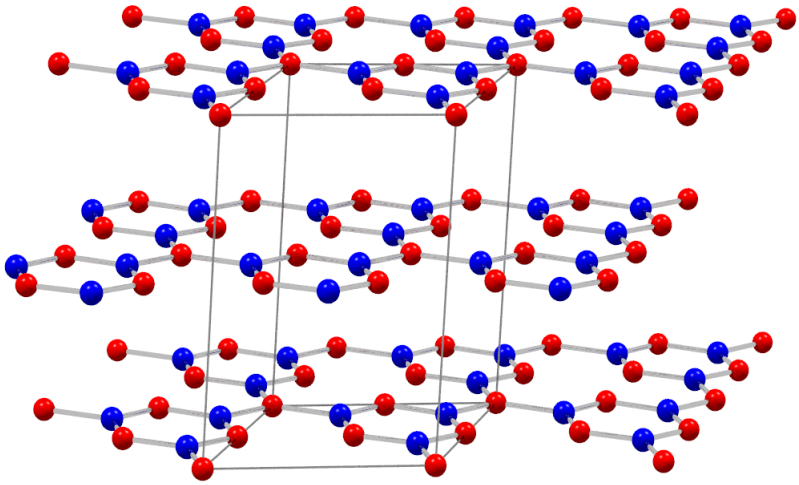

Figure 1.3 - Theoretical structure for the layered g-C_3N_4 with carbon atoms in blue and nitrogen atoms in red. Structures were generated in PowderCell 2.4 from data by Teter and Hemley.[15]

The early work by Cohen and Sung was the spark for the explosion of research into the area of carbon nitride materials that has occurred for nearly 20 years. There have been hundreds of reported attempts to synthesize C_3N_4 and other related carbon nitride (CN_x) materials.[21,22] To date, there have been no reproducible syntheses of the proposed ordered three-dimensional nitrogen-rich carbon nitride structures. Unsatisfactory characterization has cast doubts on the claims of successful syntheses of β-C_3N_4 or α-

C_3N_4.[23] High-energy physical deposition processes (e.g., laser ablation and RF magnetron sputtering) produce nitrogen-poor CN_x materials (where $x << 1$) with nitrogen-doped graphitic sp^2 carbon and amorphous sp^3 carbon regions.[24-28] In carbon nitride syntheses, as the CN_x nitrogen content increases to $x \approx 1$ or greater, the structures transform from disordered (black) graphite analogs to extended cross-linked (tan to brown) polymer-like materials. Despite the lack of success in forming the desired C_3N_4 stoichiometry, many CN_x thin films have shown a wide variety of mechanical, optical, and tribological properties, which are dependent on the composition and structure of the films. Certain nitrogen-rich deposited CN_x films showed thermoluminescent properties,[29,30] solar cell potential,[31] and may be useful as humidity sensors and gas detectors,[32] while others exhibit electrical resistance,[33,34] optical transparency,[35,36] wear resistance,[37,38] and high hardness.[39,40]

A chemical synthetic approach to nitrogen-rich CN_x materials utilized frequently over the past decade involves reactive precursors containing pre-bonded C-N core structures, such as triazine rings (C_3N_3) and related heterocyclic arenes.[22,41-49] Molecular triazines have been widely studied in other areas including pesticide synthesis, molecular organic chemistry, molecular magnetism, and hydrogen bonded crystal formation.[50-54] Concurrent with nitrogen increases in CN_x products, there is very frequently significant hydrogen incorporation in the final product (CN_xH_y), though this is often ignored in many CN_x structural proposals, as was detailed in a review of carbon nitride precursor approaches.[21] Our research focus has been on thermally unstable triazine and heptazine precursors that convert to nitrogen-rich carbon nitride powders and films.[55-61] Chemical

precursors for CN_x synthesis will be further discussed in Chapter II, but an introduction of the aromatic heptazine system will be presented in the following section.

Heptazine: Beyond Triazine-Based C-N Structures

Although the theoretical work previously mentioned instigated much of the modern work in carbon nitrides, the earliest C-N work has its origins in the early 19th century. Jöns Jakob Berzelius, considered a father of modern chemistry and coiner of the word "polymer", synthesized a carbon nitride material during his career through the heating of mercuric thiocyanate, $Hg(SCN)_2$.[62] This product was found to have a formula of $C_6N_9H_3$, which is also the same formula for a material discovered by Justus von Liebig in 1834.[63] His synthesis involved the heating of chlorine with potassium thiocyanate to form the yellow, amorphous, and insoluble product he dubbed melon. Liebig also went on to describe its properties and the related compounds melem ($C_6N_{10}H_6$), melam ($C_6N_{11}H_9$), and hydromelonic acid ($C_9N_{13}H_3$).[64-66] It is interesting to note that there was some discrepancies in the elemental analysis of melon, as Liebig could not generate a clearly reproducible formula.[67] In 1835, Leopold Gmelin, found that when potassium ferricyanide, $KFe(CN)_6$, was heated with sulfur, he could generate a species called potassium hydromelonate, $K_3C_9N_{13}$.[68] When acidified, this material would form the aforementioned hydromelonic acid. In 1855, Hennenberg found that when heated in aqueous alkali, hydromelonate salts would form products with the formula $C_6N_7O_3$. Soon after this report, interest in these lesser known "ammono carbonic acids" faded.

In 1922, Edward C. Franklin published a review of the carbon-nitrogen family of compounds which also included the more well-known guanidine, biguanidine, melamine, cyanamide, and dicyanodiamide.[69] A brief description of a "carbonic nitride" with the

formula $(C_3N_4)_x$ is mentioned as possibly being the final deammonation product from the heating of Liebig's melon, though actual evidence was far from unequivocal. Franklin proposed some possible structures based on linked triazines for these lesser known ammono carbonic acids, but without X-ray analysis, was only able to conjecture. In 1933, Franklin gave some crystals with the formula $Na_3C_6N_9 \cdot 3H_2O$ to Linus Pauling for him to perform an X-ray study. After studying this material, Pauling and Sturdivant reexamined its parent acid tricyanomelamine ($H_3C_6N_9$) and the related material hydromelonic acid. On the merits of resonance stabilization, they asserted that the most likely structure would be a coplanar arrangement of three fused rings. Therefore, Pauling introduced the cyameluric nucleus, C_6N_7, which is shown in Figure 1.4; the same nucleus was predicted to be contained in both hydromelonic acid and cyameluric acid.[70] Redemann and Lucas were able to extend this work a few years later and showed,

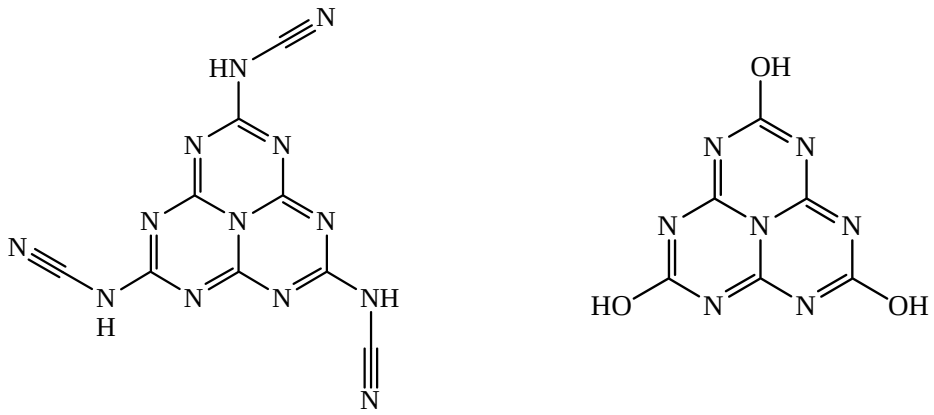

a b

Figure 1.4 - Pauling's proposed structure for a) hydromelonic acid, $H_3C_9N_{13}$ and b) cyameluric acid $C_6N_7O_3H_3$.

through acid-base titrations and hydrolytic degradation, the cyameluric nucleus was the most likely candidate for hydromelonic acid and cyameluric acid.[71] In a subsequent article, they also postulated that Liebig's melon contained the cyameluric nucleus and managed to report the successful synthesis of chlorine cyameluric chloride, $C_6N_7Cl_3$.[72]

After Redemann and Lucas, Finkel'shtein of the Soviet Union explored the spectroscopic and thermal properties of these known cyameluric molecules over the next forty years.[73-85] They did much to advance the understanding of melem, hydromelonic acid and others, although no new derivatives were reported. It was also during this time they began referring to the cyameluric nucleus as "sym-heptazine" for the seven nitrogen atoms it contained. In 1962, Schroeder and Kober reported on a series of new cyameluric derivatives via reactions of disubstituted amines, alcohols, and benzene derivatives with cyameluric chloride.[86] In 1982, Leonard and coworkers reported the first crystal structure of a cyameluric derivative, after successfully synthesizing the unsubstituted cyamelurine, or tri-s-triazine molecule, $C_6N_7H_3$.[87] The crystal structure showed a coplanar arrangement of three fused triazine which featured bond lengths equivalent to those that Pauling had predicted 45 years earlier. Since then, a series of molecular heptazines have been synthesized and characterized, which will be discussed further in detail.[88-90]

More recently, Tamikuni Komatsu reinvestigated some of the work that Liebig pursued by reexamining the synthesis of melon and some hydromelonate salts.[91-94] He considered these heptazine derivatives to be precursors and intermediates of g-C_3N_4 and attempted to thermally decompose them into the desired carbon nitride material. Komatsu's work was one of the first to discuss the idea of a heptazine-based g-C_3N_4. Heptazine-based precursors have also been utilized in several other recent carbon nitride

network-forming reactions.[95,96] Several thorough thermolysis studies by Schnick and co-workers have convincingly shown that the solid-state thermolysis of small-molecule cyanamides and triazines can also structurally rearrange to form more stable heptazine structures at elevated temperatures (~400-600 °C).[90,97-103]

It is the focus of this dissertation to explore heptazine and carbon nitride chemistry through the study of the synthesis and characterization of new heptazine-based carbon nitrides and other light-element materials. In Chapter II, the structure of a heptazine-based CN_x material synthesized from the thermal decomposition of the precursor, trichloromelamine (TCM), will be explored. Chapter III will outline the modifications to the thermal decomposition of TCM in order to generate new, porous morphologies. Chapter IV will discuss a novel modification of the TCM decomposition using sodium borohydride ($NaBH_4$) to generate a new boron-containing CN_x material. In Chapter V, metal coordinating systems using the heptazine-based cyamelurate ($C_6N_7O_3$) anion will be explored. Chapter VI will cover the synthesis and properties of some luminescent heptazine molecular systems. In Chapter VII, polymeric materials synthesized from trichloroheptazine ($C_6N_7Cl_3$) will be studied. Finally, in Chapter VIII, carbon-rich CN_x materials as conducting metal catalyst supports will be briefly discussed.

CHAPTER II

FROM TRIAZINES TO HEPTAZINES: DECIPHERING THE LOCAL STRUCTURE OF AMORPHOUS NITROGEN-RICH CARBON NITRIDE MATERIALS

Introduction

Over the past few years, there is resurgent interest in study of larger conjugated C-N molecules, particularly those with planar heptazine (C_6N_7) core structures (Figure 2.1b), as opposed to the more commonly proposed triazine cores (Figure 2.1a). As discussed in Chapter I, the heptazine structure has a colorful chemical and structural history, dating back to the days of Pauling[70,71,104] and even further back to syntheses by Liebig.[63,69] Several heptazine molecular and anionic structures have been synthetically targeted for their structural coordination and optical emission interest.[86-89,91,92,94,105-113] Heptazine-based precursors have been utilized in several recent carbon nitride network forming reactions.[91,92,94,95,113,114] Several thorough thermolysis studies by Schnick and co-workers have convincingly shown that the solid-state thermolysis of small molecule cyanamides and triazines can structurally rearrange to more stable heptazine structures at elevated temperatures (~400 - 600 °C).[90,97-103] Generally, polymeric materials form higher temperature thermolysis studies (~550 - 800 °C), though near these temperatures high-nitrogen content CN_xH_y materials decompose into volatile gaseous species.

It has been frequently proposed that triazine precursor derived nitrogen-rich carbon nitride products retain the triazine structural fragment in the extended network structure (Figure 2.1c), but recent studies indicate that this may not generally be the case,

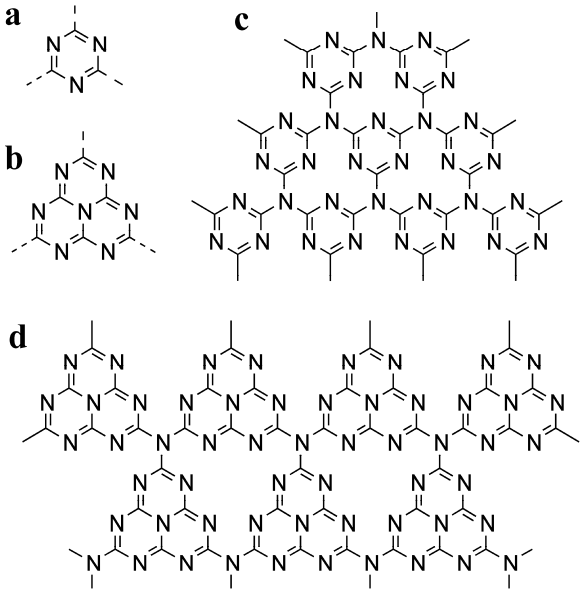

Figure 2.1 - Structures for the a) triazine and b) heptazine precursor cores and postulated planar C_3N_4 extended structures formed from c) triazine and d) heptazine building blocks.

structural reinvestigation of carbon nitride structures, particularly those formed by linked which calls for a (Figure 2.1d).[102] One recent triazine precursor thermolysis study concluded that their analytical data on the amorphous carbon nitride product could be fit to a triazine or heptazine extended network.[115] Extended carbon nitride structures and molecular products that contain larger conjugated heptazine building blocks have been formed under forcing solid-state triazine thermolysis conditions[90,97-103] and the first crystallographically characterized heptazine, tri-s-triazine ($C_6N_7H_3$), was produced via the flash vacuum pyrolysis of a reactive triazine precursor at 400 °C.[87,105,106] Theoretical studies also indicate that the heptazine structure should be thermodynamically more stable than corresponding triazine arrangements.[88,116]

The intractable nature of most nitrogen-rich CN_xH_y network materials limits structural analyses to spectroscopic (e.g, X-ray photoelectron, IR, and solid-state NMR methods), mass spectrometric (in special cases), and compositional analyses. Komatsu and co-workers employed boiling aqueous KOH as a useful chemical "deconstruction method" in the analysis of carbon nitrides derived from heptazine precursor thermolysis at 550°C[91] and from triazine precursor condensation at 650 °C.[93] These studies showed that cyameluric acid [$C_6N_7(OH)_3$] was extracted from CN_xH_y products from heptazine precursors, while cyanuric acid [$C_3N_3(OH)_3$] was obtained from products formed using triazine precursors. This type of base hydrolysis has also been successfully utilized Kroke and co-workers to isolate heptazine anions [$C_6N_7O_3^{3-}$] from melon/heptazine polymers derived from the thermal decomposition of thiocyanates[88,89,111,112] and its utility was noted in early heptazine structural studies.[104] This deconstruction technique in conjunction with other analytical methods produces a more consistent and complete picture of the local structures present in disordered nitrogen-rich CN_xH_y network materials.

In light of recent heterocyclic C-N structural studies, we reexamined the local structure of nitrogen-rich CN_xH_y network materials synthesized in our laboratory via a rapid (in seconds) and exothermic decomposition of a commercially available triazine precursor, trichloromelamine (TCM), $C_3N_3(NHCl)_3$.[55] In addition to residual gas mass spectrometry and solid-state NMR and IR analysis, we utilized base hydrolysis reactions to clearly determine that the local structure of TCM-derived carbon nitride materials contain larger, more stable heptazine fragments. Thus rapid self-propagating exothermic TCM decomposition represents a facile method to grow thermally stable heptazine-based

network structures. A clear picture of true CN_xH_y local structures will greatly aid in their application as functional optical or coordination materials. These triazine to heptazine results are likely applicable to many prior CN_xH_y syntheses involving thermal conversion of triazine precursors to nitrogen-rich carbon nitride products at temperatures above ~400 °C.

Experimental

Reagents

The following reagents were purchased from Aldrich: trichloromelamine (TCM, $C_3N_3(NHCl)_3$, 98%), melamine ($C_3N_3(NH_2)_3$, 99+%), cyanuric acid ($C_3N_3(OH)_3$, 98 %). Potassium hydroxide (KOH, Certified ACS) was purchased from Fisher Scientific. Ethanol (C_2H_5OH, Absolute 200 proof) was purchased from Pharmco-Aaper.

Thermal decomposition of trichloromelamine (TCM)

The synthesis of CN_xH_y materials via exothermic and self-propagating TCM decomposition has been previously reported in detail.[55] Typically, 3.0 g (13.1 mmol) of trichloromelamine (Aldrich, 98+%) was placed inside a 125 mL steel Parr reactor inside an argon atmosphere glovebox, refilled with 1 atm N_2 and heated rapidly to 250 °C. After about 45 min, the internal temperature reached ~165 °C and a rapid jump in the internal temperature was observed, accompanied with an increase in pressure to approximately 300 psi. The yellow-tan solid product was isolated in air, rinsed with 15 mL acetone, and then dried overnight in air. Bulk CHN analysis of the CN_xH_y used in this experiment had the following composition (wt %): C 34.17, H 2.23, N 58.55. This is close to prior analyses of similar products (C 34.21, H 1.56, N 60.01, Cl 0.60),[55] but

demonstrates that there is product composition variability from experiment to experiment for these amorphous CN_xH_y structures. The above exothermic reaction rapidly releases hot gases, including HCl and CN species, so care should be taken to perform this decomposition reaction in a ventilated hood and using a reactor with a pressure release valve.

Base hydrolysis of TCM-derived carbon nitride (CN_xH_y) powder

In a typical reaction, 400 mg of the CN_xH_y product was placed in a 50 ml round bottom flask with 15 ml of a 3M aqueous KOH solution (KOH Fisher ACS grade diluted in 18 MΩ deionized water) and a Teflon-coated stir bar. All manipulations were carried out in the air. The flask was fitted with a reflux condenser containing an internal thermocouple and heated with a heating mantle to an internal temperature of 102 °C, at which point the solution with the suspended carbon nitride powder began to reflux. After 45 minutes at refluxing conditions, the tan-orange CN_xH_y suspension had fully disappeared, leaving a clear, amber colored solution. The solution was refluxed for 4 hours and then it was cooled to room temperature. Long pale yellow needles slowly formed upon cooling to ambient temperature over the course of several hours. The needles were isolated by vacuum filtration, rinsed with 2x15 ml of ethanol and 10 ml of diethyl ether, and air dried overnight. Chemical analysis of the final product was (wt %): C 18.75, H 1.44, N 24.84, K (ICP-AE) 31.96 (calc. for $K_3C_6N_7O_3 \cdot 3H_2O$: C 18.50, H 1.55, N 25.18, K 30.12). The yield assuming production of $K_3C_6N_7O_3 \cdot 3H_2O$ from the CN_xH_y starting powder was 82 % (based on wt % carbon) after reducing the filtrate volume to recover additional hydrolysis product.

Base hydrolysis of molecular triazines

To separate 50 ml round bottom flasks were added 0.5g (3.8 mmol) cyanuric acid and 0.5 g (4.0 mmol) melamine. 15 ml of a 3M aqueous KOH solution (KOH Fisher ACS grade diluted in 18 MΩ deionized water) was added long with a Teflon-coated stir bar. All manipulations were carried out in the air. The flask was fitted with a reflux condenser containing an internal thermocouple and heated with a heating mantle to an internal temperature of 102 °C, at which point the suspensions began to reflux. The suspension were refluxed for 4 hours; cyanuric acid dissolved after 10 minutes, while melamine dissolved after 45 minutes. After cooling to room temperature, no solids crashed out, so the volume was reduced by slow evaporation in a hot water bath. White solids were collected after reducing the volume by half. The solids were washed with ethanol, and diethyl ether. A mass of 0.36 g was recovered from hydrolyzed cyanuric acid. A mass of 0.15 g was recovered from hydrolyzed melamine.

Instrumentation

Thermogravimetric-differential analysis (TG-DTA) was performed on a Seiko ExStar 6300 system under flowing argon. FT-IR absorption spectra were taken with a Nicolet Nexus 670 spectrometer using KBr pellets. Elemental analyses were performed on a Perkin Elmer 2400 CHN/O Analyzer using ultra light weight tin capsules or obtained from Desert Analytics (www.desertanalytics.com). Semi-quantitative energy dispersive spectroscopy (20 kV, 20 μA) was run on a field emission Hitachi S4000 microscope using an IXRF X-ray microanalysis system to examine alkali metal content. Metal contents were determined quantitatively by inductively-coupled plasma atomic emission (ICP-AE) spectroscopy using a Perkin Elmer 400 Emission Spectrometer.

Powder X-ray diffraction was performed on a Siemens D5000 X-ray diffractometer using Cu K_α radiation on samples mounted on glass slides. Solution ^{13}C NMR was collected on a Bruker DRX-400 spectrometer using D_2O with a small amount of CH_3OH as the solvent. Solid state ^{13}C MAS NMR was obtained on a Bruker wide-bore MSL 300 using a CP-MAS sequence mode (20000 scans, 10s delay). The samples were loaded into 4 mm ZrO_2 rotors and spun at 8 kHz, and data referenced to hexamethylbenzene.

Evolved gas analysis was performed using a Stanford Research Systems QMS 300 Residual Gas Analyzer. TCM (3.0 g) was placed in the Parr reactor and tightly sealed under argon. The reactor was connected to a 500 ml three-neck gas collection flask via a gas inlet adapter and PVC tubing. The center neck was connected to the RGA-MS capillary with a sidearm connection to an argon gas Schlenk line and third neck was connected to an oil bubbler. The flask underwent three cycles of evacuation (~200 mtorr) and backfilling with argon. The valve to the reactor was then opened and three more cycles of evacuation and backfilling were performed. Three spectra of this atmosphere were recorded as background blanks. The reactor was then placed in a heating mantle and the temperature controller was set to 300 °C and the TCM rapidly decomposed near its decomposition temperature of 165 °C. After decomposition, the steel reactor was removed from the mantle and cooled to room temperature. The gas collection flask was continuously purged with argon through the oil bubbler while the decomposition took place in the attached Parr reactor. When the reactor reached ~35 °C, the sampling, the argon purge was stopped and the reactor was *slowly* opened to allow the byproduct gases to escape into the glass collection flask and out the bubbler. After flushing the flask with gases for a short period of time, three spectra were recorded in the 1-100 amu range. A

fourth survey of 1-300 amu showed no evidence of volatile species beyond the 100 amu range.

Crystals of the CN_xH_y base hydrolysis product used for X-ray structure analysis were recrystallized from a 1:1 water/acetone mixture. A colorless needle of approximately 0.31 x 0.065 x 0.035 mm in size was mounted on a glass capillary and cooled under a N_2 gas stream (200 K). The data was collected on a Nonius KappaCCD diffractometer using Mo Ka radiation with a graphite monochromator and 21714 total reflections (5665 unique reflections) were obtained. Lorentz and polarization corrections were applied to the data, as well as an absorption correction using the multi-scan technique. The structure was solved by direct methods using the ShelXTL v6.1 XS program. Least-squares refinement of the model versus the data was performed using the XL software. All non-hydrogen atoms were refined with anisotropic thermal parameters. Hydrogen atoms were found by difference Fourier maps, geometrically constrained, and refined with isotropic thermal parameters.

Results and Discussion

Carbon nitride synthesis via the self-propagating thermal decomposition of TCM

Initial studies on exothermic trichloromelamine decomposition indicated that TCM converted to CN_xH_y materials as noted in Equation 1.[55] The absence of chlorine by elemental analysis along with HCl detected by gas phase IR and AgCl precipitation supported this initial proposed reaction (for $x \geq 1.33$).

$$C_3N_3(NHCl)_3 \rightarrow \mathbf{3\ CN_x} + 3\ HCl + (3 - 1.5x)\ N_2 \qquad \text{(Equation 2.1)}$$

Since bulk elemental analysis showed that hydrogen remained in the product, forming a CN_xH_y material, chlorine gas or chloramine elimination byproducts may also form during the exothermic TCM decomposition ($T_{dec} \geq 400$ °C in seconds). The identity of evolved gases from the exothermic TCM decomposition was determined using a residual gas analysis mass spectrometer (RGA-MS). The background blank and spectrum of evolved gases from rapid TCM decomposition are shown in Figure 2.2. Two expected species were identified, namely HCl and N_2, however several other cyanide-based signals were also detected, namely HCN, $(CN)_2$, ClCN, and possibly formamidine ($HN=CH-NH_2$).

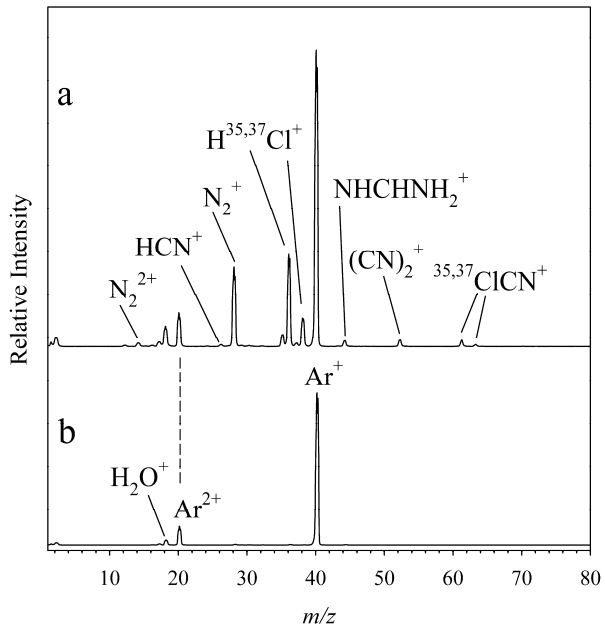

Figure 2.2 - RGA-MS data for (a) TCM decomposition product gases and (b) an argon background blank.

While some Cl_2 gas was observed in small scale (~500 mg) TCM decomposition experiments, the large scale decomposition RGA-MS data did not show evidence of Cl_2. The detection of CN-containing gases is our first direct evidence that the rapid, self-propagating, and exothermic TCM decomposition process involves some degree of triazine ring fragmentation. Without quantifying the relative amounts of evolved gases, a revised (unbalanced) equation for TCM decomposition is shown in Equation 2.2.

$C_3N_3(NHCl)_3 \rightarrow 3\ \mathbf{CN_xH_y} + HCl + N_2 + \textit{HCN} + \textit{(CN)}_2 + \textit{ClCN} + \textit{NHCHNH}_2$

(Equation 2.2)

The new byproducts versus those in Equation 2.1 are in italics and will lead to carbon and nitrogen removal from the TCM, consistent with overall chemical yields that are ~ 62% for CN_xH_y from TCM (based on carbon).[55] The carbon nitride solid from TCM decomposition will be referred to as TCM-CN_xH_y.

The TCM-CN_xH_y product is insoluble in common organic solvents, acids and bases, and is amorphous by powder X-ray diffraction analysis (broad peak near 3.3 Å),[55] consistent with related disordered nitrogen-rich carbon nitride materials synthesized by others.[1,3,5-10,22,41-49,91-95,113,114,117] As noted in the introduction, bulk CHN compositions of CN_xH_y materials are variable and dependent on the precursor choice and synthetic conditions. The TCM-CN_xH_y material used in this study had an overall composition of $CN_{1.47}H_{0.78}$ (or $C_3N_{4.4}H_{2.3}$) and was thermally stable to ~ 600°C under inert conditions before decomposing to gaseous byproducts.

Solid-state IR and NMR analysis of TCM-CN_x powders

The disordered nature of the TCM-CN_xH_y products makes unambiguous IR assignments difficult. In comparing the TCM precursor with the carbon nitride product, it is seen that both solids have major absorption bands in the 1200-1700 cm^{-1} C=N region and show a characteristic triazine ring bending mode near 800 cm^{-1} (Figure 2.3). The TCM-CN_xH_y product has broader peaks and increased absorption in 1000-1300 cm^{-1} region that might be due to new C-N stretching vibrations associated with a cross-linked structure. A band near 3200 cm^{-1} is related to N-H and O-H residues arising from precursor or air exposure. These hydrogen centered vibrations are seen in a majority of

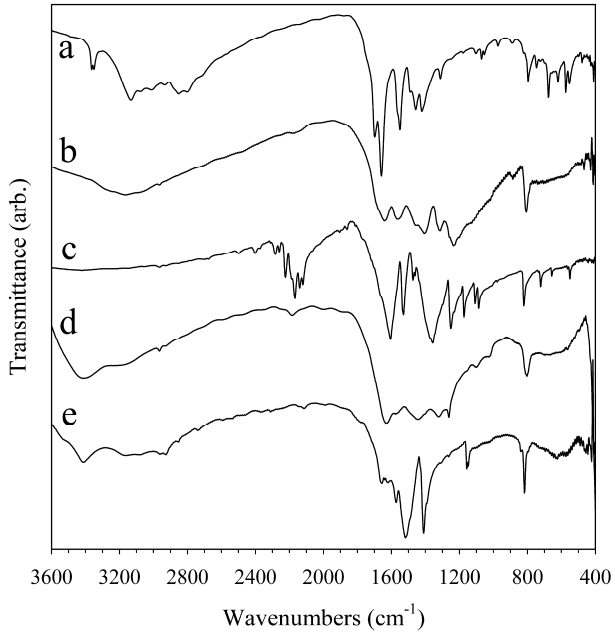

Figure 2.3 - FT-IR spectra for (a) the trichloromelamine precursor, (b) TCM-CN_xH_y decomposition product, (c) triazidoheptazine (TAH), (d) TAH-CN_xH_y product, and (e) crystalline product from KOH base hydrolysis of TCM-CN_xH_y.

nitrogen-rich CN_xH_y materials,even ones that propose triazine extended structure models that do not include hydrogen.[21,22,41-49,93,117]

Our recent results on the thermal decomposition of triazidoheptazine, $C_6N_7(N_3)_3$, revealed striking similarities between the IR spectra of its heptazine-based CN_xH_y product and the IR spectrum of TCM-CN_xH_y (Figure 2.3c,d).[60,61] Both disordered carbon nitride structures show similarities in the ring breathing and C=N bonding regions. Previous XPS analysis showed that nitrogen in TCM-CN_xH_y may be present in an sp^2 hybridized graphite-like environment.[55] Solid-state magic angle spinning (MAS) NMR data also showed a broad peak centered at 156 ppm with a small shoulder at 163 ppm. Clear structural interpretations of the local C-N bonding environments in disordered TCM-CN_xH_y based on previous data were limited.

Cross polarization MAS (CP-MAS) ^{13}C NMR of TCM-CN_xH_y clearly resolved two separate peaks at 157 and 165 ppm. This NMR result more definitively shows that two different carbon chemical environments are present in the carbon nitride product. A comparison of this ^{13}C NMR data with those from other solid-state and solution studies on heptazine molecules and extended structures is shown in Table 2.1. The ^{13}C peak positions for the TCM-CN_xH_y disordered network are similar to most of the heptazine structures. For comparison, N-substituted triazines have ^{13}C chemical shifts near ~163-168 ppm,[50-54,59] while internal heptazine carbons (junctional - bonded to central nitrogen and two nitrogens on the ring periphery) are found below 160 ppm. These NMR data are in reasonable agreement with recent theoretical NMR calculations.[103] The surprising similarity of IR and NMR of the TCM-CN_xH_y product with heptazines, makes it clear

that a re-examination of the proposed local structure of the TCM-derived carbon nitride networks was necessary.

Table 2.1 - Comparison of solution state and solid state ^{13}C NMR for various heptazine structures.

$C_6N_7X_3$	C (internal)	C (external)	Reference
X, for solution state NMR			
H	159.7	171.6	[87,105]
Cl	158.2	175.0	[88]
N_3	158.7	171.4	[60]
O^-M^+; M = Li, Na, K, Rb, Cs	159.1 - 161.0	169.3 - 171.5	[111]
$OSi(CH_3)_3$	158.9	169.5	[112]
$N(Et)_2$	155.0	162.4	[109]
solid-state CP-MAS NMR			
CN_xH_y from TCM	156.6	164.6	Ch. II,[118]
$C_6N_7(NH_2)_3$	155.1, 156.0	164.3, 166.4	[90]
CN_xH_y from $C_6N_7(N_3)_3$	156.0	163.7	[61]
melon (heptazine polymer)	157.0	164.0	[102]

Base hydrolysis of TCM-CN_xH_y

In the absence of long-range crystallographic order, it is difficult to unambiguously determine if there is a local repeat structure in the amorphous and insoluble TCM-CN_xH_y product. Spectroscopic data indicates that the triazine precursor may convert to an extended structure based on predominantly heptazine-like fragments. We embarked on a structural "unzipping" strategy to directly probe the nature of local repeat structures in these materials. This approach was pioneered in studies on triazine

and heptazine precursor approaches to extended C-N solids where intractable solids were boiled in aqueous KOH and molecular decomposition products were isolated.[88,89,91,93,111,112] This deconstruction method can essentially carve stable molecular fragments or building blocks out of the polymeric carbon nitride structure.

The stability of the orange-tan TCM-CN_xH_y was examined in 3M aqueous KOH. While this solid is unreactive in KOH at room temperature, upon heating to reflux temperatures (~102 °C) for several hours, the powder completely dissolved/decomposed to form a dark orange solution. RGA-MS data collected from the gaseous headspace above the boiling KOH solution showed that ammonia (*m/z* = 17) is evolved during the hydrolysis. After cooling the solution to room temperature, long needle-like crystals formed. The IR spectrum of the hydrolyzed product shows the disappearance C-N stretches in the ~1100 - 1300 cm^{-1} region that may be related to broken extended network connections (Figure 2.3e). Chemical analysis and solution ^{13}C NMR of the needles (159 and 169.4 ppm) is consistent with a heptazine salt with the formula of $K_3C_6N_7O_3 \cdot 3H_2O$, which was previously synthesized, fully characterized, and crystallographically studied by Kroke and co-workers.[89,111] They produced a series of related anionic heptazine compounds by metal hydroxide hydrolysis of a heptazine-based polymer (melon) synthesized from NH_4SCN decomposition at ~300 °C. The crude solution mixture from our KOH hydrolysis experiment was evaporated to dryness under vacuum and solution ^{13}C NMR of the isolated solid still showed only two peaks at 159 and 169 ppm, indicating that only heptazine-like species are present after hydrolysis. For reference, the ^{13}C NMR shift for the triazine analogue, $C_3N_3O_3^{3-}$, has a single resonance at 166.9 ppm.[119]

The needle-like solid from TCM-CN_xH_y base hydrolysis exhibits thermal properties consistent with larger conjugated rings versus triazines. These crystals irreversibly lost mass around 75 °C, corresponding to three moles of water (assuming a $K_3C_6N_7O_3$ formula), and decomposed at 550 °C. For comparison, triazine analogs generally decompose at lower temperatures (~380 °C for $K_3C_3N_3O_3$).[120] Further support that the base hydrolysis product is related to a previously structurally characterized heptazine compound, $K_3C_6N_7O_3{\cdot}3H_2O$, is found in strong similarities in the powder X-ray diffraction (XRD) pattern shown by both potassium salts (Figure 2.4). The amorphous

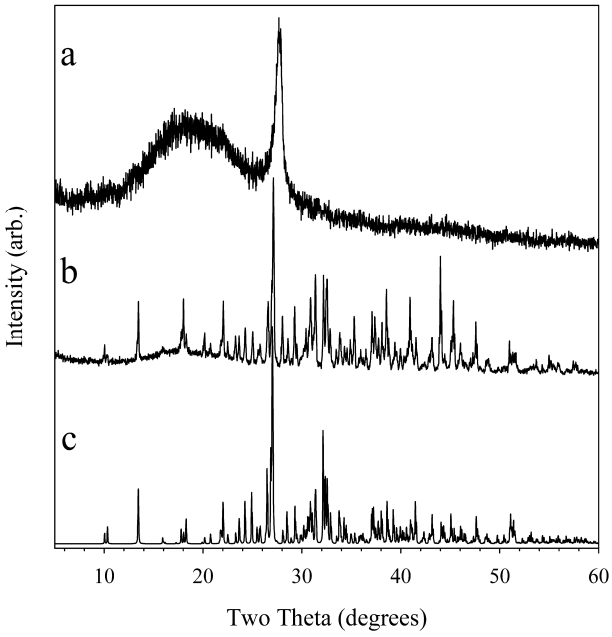

Figure 2.4. - Powder X-ray diffraction patterns for (a) TCM-CN_xH_y product, (b) the product from KOH base hydrolysis of TCM-CN_xH_y, and (c) $K_3C_6N_7O_3{\cdot}3H_2O$ derived from single crystal data.[111]

XRD pattern for the starting TCM-CN_xH_y materials is also shown for reference. The powder XRD data for $K_3C_6N_7O_3{\cdot}3H_2O$ was generated using single-crystal structural data.[111]

The powder XRD structural similarities were verified using single-crystal X-ray structural analysis on the isolated needles from the TCM-CN_xH_y base hydrolysis. Their structure was identical to that described by Kroke and coworkers for $K_3O_3C_6N_7{\cdot}3H_2O$ (Figure 2.5).[111] This result confirms that heptazine structural building blocks were isolated from base hydrolyzed amorphous nitrogen-rich TCM-CN_xH_y material.

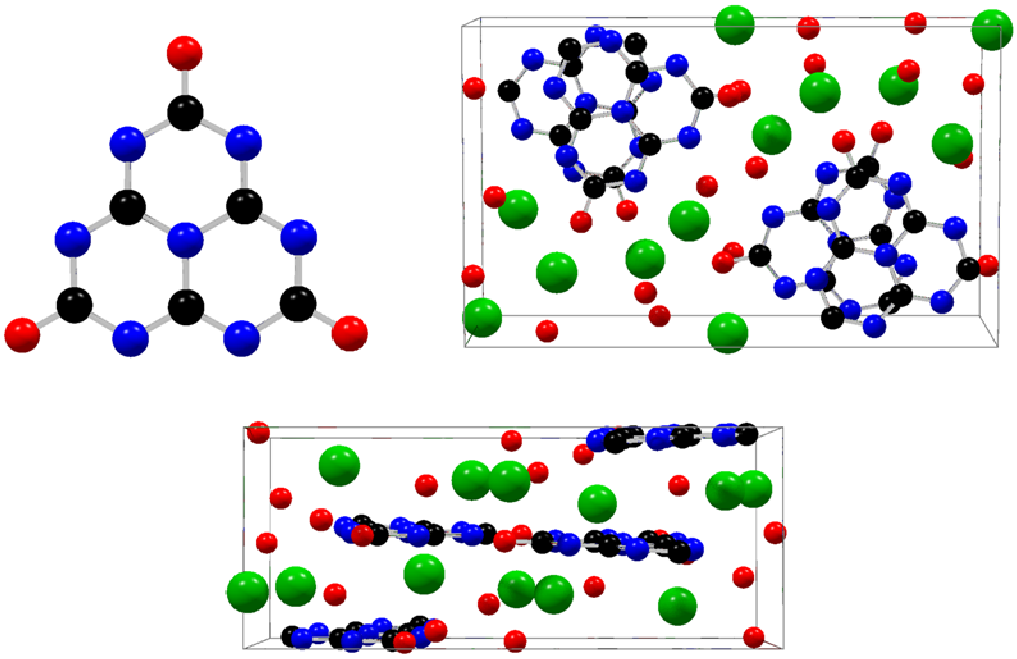

Figure 2.5 - Heptazine oxyanion $C_6N_7O_3^{3-}$ structure and two views of crystal packing arrangements from single crystal structural analysis of $K_3C_6N_7O_3{\cdot}3H_2O$ produced by KOH hydrolysis of TCM-CN_xH_y. Structure agrees with single crystal analysis reported by Kroke and co-workers.[111] Legend: C (black), N (blue), O (red), K(green).

Base hydrolysis of molecular triazines

The KOH base hydrolysis results show that heptazine building blocks were either extracted from the amorphous TCM-CN_xH_y starting material or possibly may form during the hydrolysis process. While prior studies have shown that triazine and heptazine anions have been extracted intact from their respective polymeric starting materials,[91,93,111] two control experiments were conducted to show that triazines do not convert to heptazines under our base hydrolysis conditions. A molecular

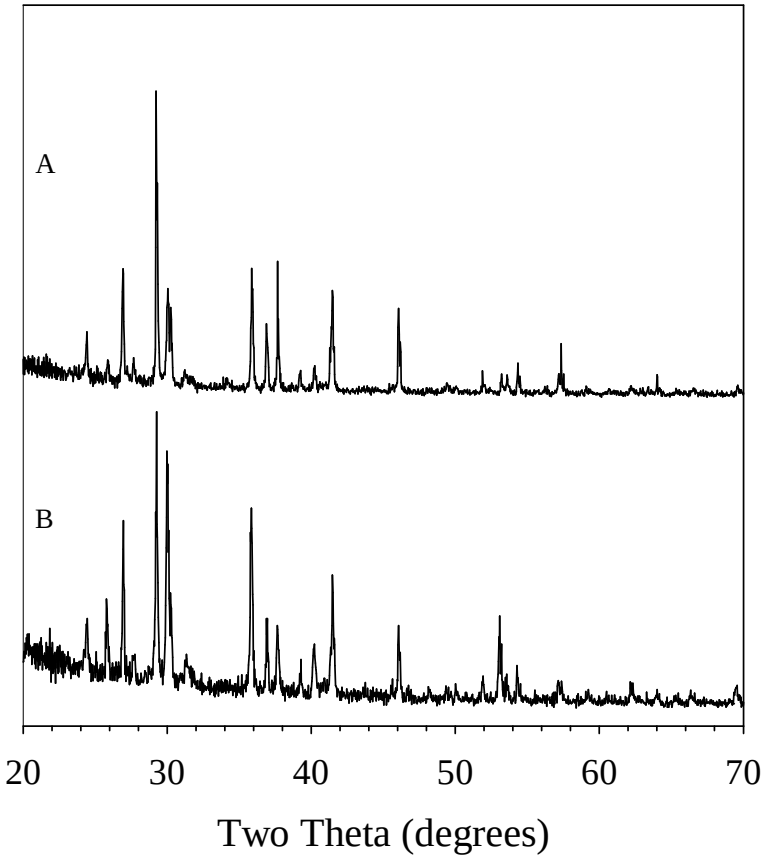

Figure 2.6 - Powder X-ray diffraction patterns of A) cyanuric acid ($C_3N_3(OH)_3$) hydrolyzed in KOH; B) melamine ($C_3N_3(NH_2)_3$ hydrolyzed in KOH.

triaminotriazine, $C_3N_3(NH_2)_3$, was dissolved by boiling KOH under the same conditions as those for TCM-CN_xH_y hydrolysis. The isolated white crystalline powders from this experiment were not needles and had one ^{13}C NMR peak at 161.5 ppm, which is consistent with symmetric substitution on carbon of a triazine ring, suggesting uniform hydrolysis occurs under these forcing conditions, as has been observed by others.[93] A second KOH boiling experiment with cyanuric acid, $C_3N_3(OH)_3$, produced a solid with one ^{13}C NMR peak at 165.5 ppm. The powder XRD of the two triazine products from KOH hydrolysis have very similar powder XRD patterns as shown in Figure 2.6.

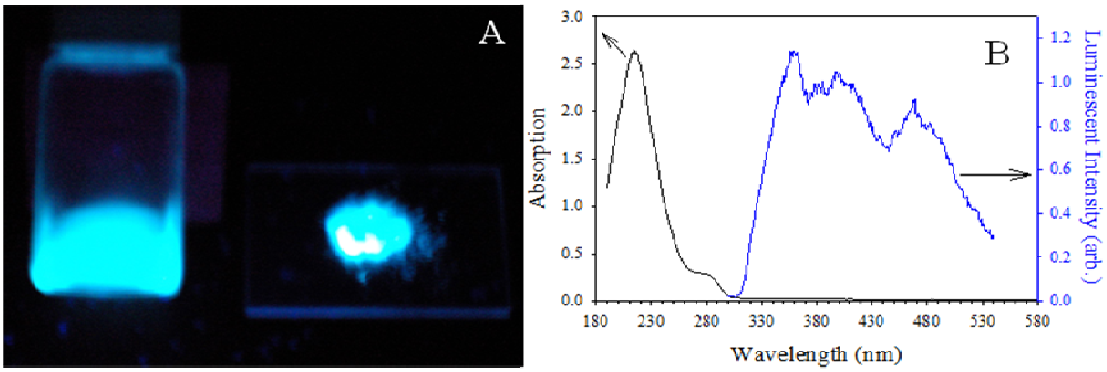

Figure 2.7 - Optical properties of $K_3C_6N_7O_3 \cdot 3H_2O$: A) emission in aqueous solution and in solid state under a UV lamp and B) solution UV-Vis spectra (black) and photoluminescent spectra (blue).

Luminescent support for heptazine components in TCM-CN_xH_y

Solid and aqueous solutions of $K_3C_6N_7O_3 \cdot 3H_2O$ and related materials are intensely emissive in the UV-violet region (~250 - 280 nm) with emission tails reaching well into the blue-green region near 550 nm (Figure 2.7B).[60,111] Triazine precursors

(solid or solution) examined in our group do not show appreciable visible luminescence under illumination with a handheld UV lamp (Figure 2.7A). In contrast, several TCM-CN_xH_y powders and sublimation products exhibit a clear greenish emission that is visible to the naked eye.[55-59] Thus, the optical emission properties of CN_xH_y disordered solids support that conjugated ring structures are present in solids produced from triazine precursor decomposition.

Revised local structure of CN_xH_y materials from rapid, exothermic TCM decomposition

The IR and NMR of the amorphous TCM-CN_xH_y solid indicate that heptazine (C_6N_7) units are present and this is clearly supported by X-ray analysis of base hydrolysis products. Solid-state triazine thermolysis to heptazines has been previously demonstrated in certain cases, and these conversion processes occur in the 400-550 °C range,[86,87,90,97-103,105-110] which is very near the temperatures recorded during the exothermic and self-propagating TCM decomposition processes (~ 420 °C).[55] Note that these temperatures are also near the decomposition of most nitrogen-rich carbon nitride materials. Theoretical thermochemical studies on triazines and heptazines show that the heptazine structure is thermodynamically stable relative to the triazine structure due to enhanced π conjugation,[116] so reactive triazine intermediates may rearrange and convert to more thermodynamically stable heptazine-based structures. In the case of exothermic TCM decomposition, these rearrangements may be facilitated by nitrile elimination, nitrene or imide formation, or HCl vapor interactions that lead to heptazine-based nitrogen-rich CN_xH_y products in seconds. A summary reaction based on the experimental data discussed above is shown in Figure 2.8.

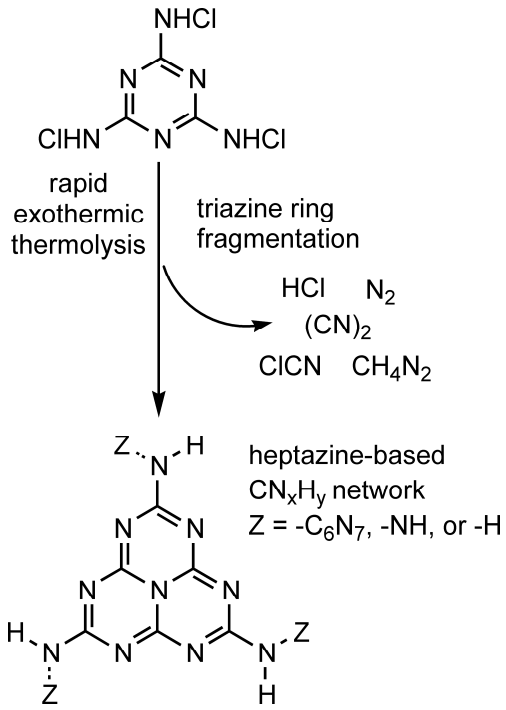

Figure 2.8 - Reaction scheme for TCM decomposition reaction and TCM-CN_xH_y product.

Since hydrogen is present in the bulk carbon nitride product, the structural connectivity of the external nitrogen attached to the heptazine core probably contains some combination of NH bonds and connections to other heptazine units. This material bears structural similarities to other melon-type polymeric systems. There is also recent structural evidence that under some conditions, hydrogenation of nitrogen sites on the heptazine ring also occurs.[112] Given the disordered nature of these products, it is too speculative to definitively propose long-range structural connections for TCM-CN_xH_y. Many triazine precursor decompositions and solvothermal carbon nitride syntheses are performed at temperatures in excess of 400 °C and yield materials with very similar IR data to our TCM-CN_xH_y products, but products are described by triazine-based structural

models. For example, a high pressure synthesis study produced a carbon nitride material from triazine precursors that was described as an extended triazine structure. The ^{13}C NMR of this material showed two peaks, one of which was near 157 ppm, consistent with the internal carbon of the heptazine unit, so alternate structures based on heptazine units may be applicable.[121] Another study utilized solid-state triazine thermolysis to produce a ~C_3N_4 carbon nitride product with ^{13}C NMR peaks at 157 and 165 ppm, also consistent with heptazine linkages versus a proposed linked triazine structure.[122] It is likely that many previously postulated triazine-based CN_xH_y amorphous network structures actually contain heptazine-based local environments, which could be detected by solid-state NMR analysis and base hydrolysis studies similar to those described above. Recent proposals along these lines by other researchers are timely and correct.[88-90,97-103,111,112]

Conclusions

Spurred on by recent triazine to heptazine conversion studies, a structural examination was performed on an amorphous nitrogen-rich carbon nitride material formed via the rapid and exothermic self-propagating decomposition of a triazine (C_3N_3) precursor, trichloromelamine. The thermally stable and insoluble CN_xH_y product was determined to be built up of heptazine (C_6N_7) repeat units that were formed via the thermally induced triazine degradation and conversion. The case for heptazine building blocks was supported by ^{13}C solid state NMR and isolation of stable heptazine molecular anions after corrosive base hydrolysis (structural deconstruction) of the CN_xH_y network material. These results provide strong reinforcement to recent calls for a reexamination of popular triazine-based carbon nitride structural models for disordered extended CN_xH_y materials produced from triazine thermolysis reactions. This study concludes that the

rapid decomposition of a commercially available triazine precursor is a convenient method for the production of a heptazine based nitrogen-rich CN_xH_y extended solid. The base hydrolysis of this TCM-CN_xH_y solid is also a facile method to produce heptazine oxyanions. A more chemically accurate view of disordered carbon nitride networks will aid in their use as optically emissive materials and as metal and non-metal coordination structures.

CHAPTER III

MODIFICATIONS TO TRICHLOROMELAMINE DECOMPOSITION REACTIONS

Introduction

In the previous chapter, it was found that a heptazine-based carbon nitride (CN_xH_y) material can be synthesized from the thermal decomposition of trichloromelamine (TCM). Moving beyond this type of material, the next challenge was to determine whether the morphology of the material can be modified with the introduction of additional components during the decomposition step of TCM. Specifically, the focus was to increase the surface area of these materials via the addition of hard templates or through the addition of gas-forming additives, *i.e.* blowing agents.

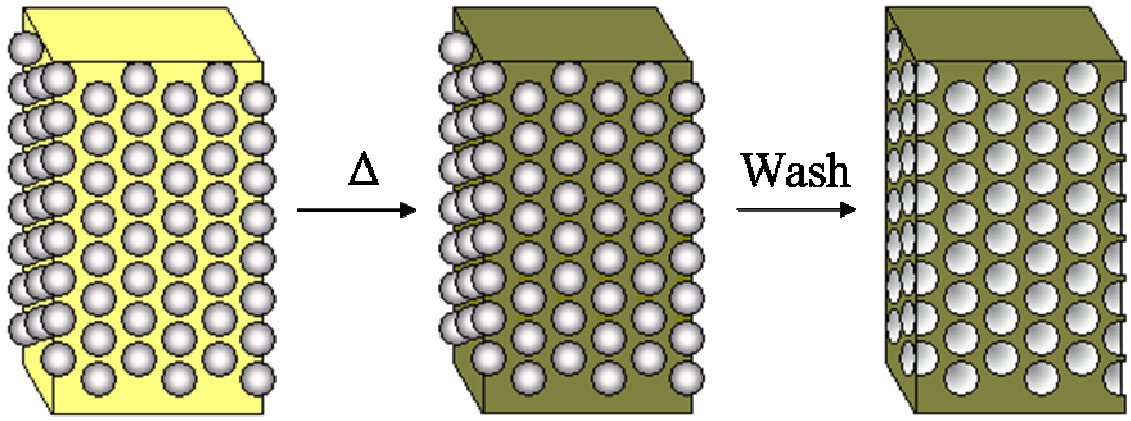

Figure 3.1 - Preparation of porous organic polymers. A mixture of a hard template (spheres) is mixed with the precursor(s) (yellow), then subsequently reacted to form a polymer network (brown) around the template. Upon removal of templates through washing, void spaces are formed, yielding a porous material.

Materials with large surface areas have been around for a very long time. The ancient Egyptians first described using charcoal for medicinal purposes, and in the 1800's, sugar makers began using carbon to purify their products.[123] From these origins, activated carbon has become ubiquitous as a gas adsorbent and catalyst support, among many other uses. Another type of material is porous silicas, which also enjoy uses as an adsorbent, desiccant, and in chromatographic separations.[124] Recently, many high surface area organic polymer materials have been synthesized, with applications towards separations, chemical sensing, catalysis, fuel cells and gas storage.[125-127]

The method for forming porous polymers that is the focus of this chapter is called endotemplating.[125] This involves the incorporation of the organic precursor (or monomer) with a hard, inorganic template followed by polymerization through chemical, thermal, or photochemical means. The template is then removed through washing, leaving a three dimensional negative image of the template imprinted on the remaining polymeric material. Therefore, the type of template will dictate the final form of the polymer. There are two types of inorganic templates commonly used: silica (SiO_2) nanoparticles[128,129] and colloidal crystals.[130-133] Templating can also occur in the reverse manner, called exotemplating, whereby a precursor solution is incorporated into a mesoporous silica monolith and reacted. The formation of the polymer is confined to the mesopores of the monolith, and once the template is removed, leading to polymer nanoparticles.

These templating methods have been recently applied to the synthesis of mesoporous CN_x materials, as well as CN_x nanoparticles. Antonietti, *et. al.* reported the synthesis of a graphitic carbon nitride nanoparticles mesoporous silica host matrices.[5] A

liquid precursor, cyanamide (H_2N-C≡N) was infiltrated into the pores of a mesoporous silica monolith, then reacted by heating at 550 °C for 3 hours. The template was removed with aqueous HF, yielding ~60 nm C_3N_4 nanoparticles. Shortly thereafter, it was reported by the same group, that suspending different amounts of silica nanoparticles in the same precursor, followed by heat treatment and template removal.[4] This resulted in mesoporous graphitic CN_x powders with surface areas of 136, 190, or 440 m^2/g; depending on the amount of template used. This material was subsequently used as an organocatalyst to catalyze Friedel-Crafts reactions,[3] conversion of benzene to phenol through CO_2 activation[1] and trimerization of nitriles.[134] Since then, there have been two reports of new CN_x type materials synthesized by templates of colloidal crystals.[6,135] These highly ordered porous materials were employed for use as a catalyst support in a direct methanol fuel cell (DMFC). This new CN_x material showed a 73-83% higher power density over the commercially available carbon black material, XC-72. This chapter will discuss the various methods used in attempting to increase the surface area of carbon nitride materials derived from trichloromelamine. The FT-IR properties of these materials will be examined and discussed. The structures of these materials will be examined through powder X-ray diffraction and scanning electron microscopy.

Experimental

Reagents

All reagents were used as received, unless otherwise stated. The following reagents were purchased from Aldrich Chemical Co.: trichloromelamine ($C_3N_3(NHCl)_3$, 98%), silica gel (SiO_2, 5-25um, 28,857-8), and ammonium bromide (NH_4Br, 99.99%). Sodium chloride (NaCl, 99%) and ammonium chloride (NH_4Cl, 99.8%) were purchased

from EM Science. The following reagents were purchased from Fisher: sodium bicarbonate ($NaHCO_3$, ACS grade), sodium bromide (NaBr), and methanol (CH_3OH, ACS grade). Sodium azide (NaN_3, 99.5%) was purchased from Sigma.

Inert Additives: Solution incorporation of NaCl and SiO_2 with trichloromelamine precursor and subsequent decomposition

The different reactant ratios used can be found in Table 3.1. The following reactions were performed in a nitrogen gas atmosphere. The manipulation of the trichloromelamine was done in an Ar atmosphere glovebox. In a Schlenk flask, the desired amounts of sodium chloride and trichloromelamine (TCM) were dissolved in the minimum amount of methanol (approximately 120 mL per gram of NaCl). Once all solids were completely dissolved by slight heating in a warm water bath, the solvent was removed by reduced pressure. Once the solvent was removed, the flask was returned to the glovebox. The TCM/NaCl mixture was weighed and placed in a Parr reactor (as described in Chapter I). The reactor was capped with a septum and removed from the glovebox. Once removed, the reactor was hand sealed under a flow of N_2 with the reactor head, then further tightened on the vise. The reactor was placed in a custom Glas-Col heating mantle. The temperature was set to heat to an external temperature of 300 °C. The reactor was heated until an internal temperature of 200 °C was reached in order to ensure that the reaction was complete. Once reached, the reactor was removed from the mantle and cooled to room temperature. Once cooled, the reactor was opened to ambient atmosphere and the crude product was weighed, then washed in 18 MΩ water. Then suspensions were then centrifuged to separate tan or brown products. After

decanting water, the products were then sonicated in methanol, then centrifuged once more. After decanting, the products were vacuum-dried at 45 °C for 4 days.

Using a similar method, silica gel and TCM were suspended in methanol in the ratios described in Table 3.1. After stirring for two hours under N_2 gas, the methanol was removed by reduced pressure. Once the solvent was removed, the flask was returned to the glovebox, where the crude mixture was weighed and placed into a custom reactor or the Parr reactor described in Chapter II. The reactor was a 60 ml custom calorimeter style steel reactor in the glovebox (screw top, inner 5 cm depth × 3.8 cm width and cap fitted with two posts connected to a coiled Nichrome wire that was in contact with reaction mixture). Once the top was screwed shut, the reactor was removed from the glovebox and placed inside a fume hood and connected to a Variac. The reaction was initiated by heating the wire with the Variac at 12V for five seconds. Gaseous

Table 3.1 - Summary of experiments performed with inert additives to trichloromelamine (TCM) decomposition.

Additive	**Mass TCM (g)**	**Molar ratio Add:TCM**	**Appearance**	**Heating Method**
NaCl	0.5	39:1	brown	Parr
NaCl	0.5	20:1	brown	Parr
NaCl	1.0	10:1	brown	Parr
NaCl	1.0	4:1	tan	Parr
NaCl	1.0	0:1	tan	Parr
NaCl	3.0	2.6:1	no rxn	Filament
NaCl	3.0	1.3:1	no rxn	Filament
SiO_2	1.0	7.6:1	brown	Parr
SiO_2	1.0	2.5:1	brown	Filament

byproducts were seen to escape. The crude products from the Parr reaction or the filament-initiated reaction were then washed in 6M NaOH. The products were further washed with water and acetone, and finally vacuum filtered to collect the solids.

Reactive Additives: Solution incorporation of NaBr and NaN_3 with trichloromelamine precursor and subsequent decomposition

All reactions were performed under N_2 gas. The different reactant ratios used can be found in Table 3.2. The following reactions were performed in a nitrogen gas atmosphere. The manipulation of the trichloromelamine was done in an Ar atmosphere glovebox. In a Schlenk flask, the desired amounts of sodium bromide or sodium azide and trichloromelamine (TCM) were weighed, then removed from the glovebox and attached to a Schlenk line. The reagents were then dissolved in methanol by stirring. Once the reactants had dissolved and a clear solution had formed, the solvent was removed via reduced pressure. The solid mixtures were then returned to the glovebox to be weighed and reground by mortar and pestle. The solid mixtures were decomposed by rapid heating in a Schlenk flask under flowing N_2 gas. The flask was placed in a Glas-Col mantle, then heated at 150 °C for 1 hour. The mantle temperature was then rapidly ramped to 300 °C to initiate the reaction. After the observed reaction, the flask was then cooled to room temperature. The products were washed in methanol then vacuum filtered. The products were then dried in air overnight. The 1:1 TCM:NaBr reaction was also performed by slow decomposition by heating in tube furnace under flowing N_2 gas. The material was heated at 150 °C for 1h, the slowly ramped to 200 °C at a rate of 0.2

°C/min. Finally, the material was rapidly heated up to 300 °C and held for one hour then cooled to room temperature.

Table 3.2 - Summary of reactions performed with reactive additives sodium bromide and sodium azide.

Reactant	TCM:Reactant Ratio	Mixture Appearance	Heating Method	Decomposition Appearance
NaBr	1:2.2	Yellow	Schlenk	orange-brown
NaBr	1:2.2	Yellow	Slow heating	orange-brown
NaBr	1:3	Yellow	Schlenk	Light brown
NaN_3	1:3	Pink	Schlenk	tan

Solid state NH_4Cl/NaN_3 and $NaHCO_3$ incorporation into trichloromelamine decomposition: Gas-forming additives

The amounts of TCM, NH_4Cl, and NaN_3 used can be found in Table 3.3. All reagents were manipulated in an Ar atmosphere glovebox. Typically, the reagents were stirred together with a spatula in a ceramic mortar for about one minute. The white mixture was then ground together into a flour-like powder over the course of 5 minutes. The mixture was weighed and placed into Parr reactor. The reactor was capped with a septum and removed from the glovebox. Once removed, the reactor was hand sealed under a flow of N_2 with the reactor head, then further tightened on the vise. The reactor was placed in a custom Glas-Col heating mantle. In order to heat, the temperature was set to 300 °C and allowed to rapidly rise to the decomposition temperature. Once the temperature was noted to rapidly rise or a pressure increase was noted, the reactor was

Table 3.3 - Summary of reactions with gas-forming additives NH_4Cl/NaN_3 or $NaHCO_3$.

Reactant(s) R1/R2	**Mass TCM (g)**	**Molar Ratio TCM:R1:R2**	**Heating Method**	**Appearance**
NH_4Cl/NaN_3	1.0	1:1:1	Parr	brown
NH_4Cl/NaN_3	1.0	1:2:2	Parr	light tan
NH_4Cl/NaN_3	1.0	1:3:3	Parr	tan
NH_4Cl/NaN_3	1.0	1:0:3	Filament	brown
$NaHCO_3$	1.0	1:3	Filament	no reaction
$NaHCO_3$	1.0	1:1	Filament	no reaction
$NaHCO_3$	3.0	1:3	Parr	yellow
NH_4Cl/NaN_3	1.0	1:0.65:0.65	Filament	orange-brown
NH_4Cl/NaN_3	1.0	1:1.94:1.94	Filament	tan
NH_4Cl/NaN_3	1.0	1:2.93:2.93	Filament	brown
NH_4Cl/NaN_3	1.0	1:1.94:0	Filament	tan
NH_4Cl/NaN_3	1.0	1:0:1.94	Filament	brown
NH_4Br/NaN_3	1.0	1:1.41:1.41	Filament	brown

Note: R1 and R2 refer to reactant 1 and reactant 2 if a mixture is used.

further heated for 5-15 minutes then cooled to room temperature. Once cooled, the reactor was vented to release the generated gases in the hood then was disassembled in ambient atmosphere. A mottled brown/yellow/white/gray solid was present on the bottom of the reactor while a white solid was present on the top walls of the reactor. The products were washed in methanol and then vacuum filtered. In the case of larger scale reactions, a second washing in 18 MΩ H_2O was required. While on the filter paper, the products were rinsed with a small amount of acetone then dried in air overnight.

Instrumentation

Thermogravimetric-differential analysis (TG-DTA) was performed on a Seiko ExStar 6300 system under flowing argon. FT-IR absorption spectra were taken with a Nicolet Nexus 670 spectrometer using KBr pellets. Elemental analyses were performed on a Perkin Elmer 2400 CHN/O Analyzer using ultra light weight, ultra clean tin capsules. Powder X-ray diffraction was performed on a Siemens D5000 X-ray diffractometer, using Cu K_α radiation on samples mounted on glass slides with double-sided tape. Scanning electron microscopy (SEM) was performed on a Hitachi S-4800 SEM with samples mounted on Al stubs and coated with Au-Pd alloy. ^{13}C and ^{1}H NMR was performed on an Avance 400 spectrometer.

Results and Discussion

Inert Additives: Solution incorporation of NaCl and SiO_2 with trichloromelamine precursor and subsequent decomposition

This series of experiments was designed to employ the idea of endotemplating in the synthesis of TCM-CN_x.[125] In this case, the inorganic templates used were sodium chloride (NaCl) and commercial silica gel (SiO_2). These templates were added to the TCM powder and then co-dissolved, or suspended (in the case of SiO_2), into a hot methanol solution. It was thought that this would be the best method for forming the most intimate mixture of precursor and template. In the previously reported syntheses of mesoporous graphitic CN_x, the precursor was liquid and could simply mixed directly with the templates.[4,6,135] However, in this case, the TCM had to be dissolved into solution to get the best mixing. The nature of the templates was somewhat different, in that NaCl

was soluble in methanol, while the SiO_2 was not. The silica was reported to be 5-25 μm in diameter, while the size of the NaCl would be dictated by the rate at which the particles precipitated from solution. Given that the rate of solvent loss from methanol solutions was approximately steady, it was assumed particle sizes were roughly the same size. Once the solid mixture was recovered and dried, the reactions could be performed in either a Parr or filament reactor.

The results for the reactions can be found in Table 3.4. What becomes readily apparent is the rapid decline in CN_x yields with increasing NaCl template amounts. It had been previously reported by our group that the inclusion of NaCl in solid state metathesis reactions in the filament reactor can produce lower reaction temperatures, allowing access to metastable phases.[136] It is possible that inclusion of the NaCl in the reaction mixture is preventing the reaction from fully propagating. From the previous chapter, it is known that the reaction reaches temperatures of around 400 ºC, so it is

Table 3.4 - Results of the NaCl:TCM reactions.

Additive	**Mass TCM (g)**	**Molar ratio Add:TCM**	**Mass Yield (%)[a]**
NaCl	0.5	39:1	2.7
NaCl	0.5	20:1	7.0
NaCl	1.0	10:1	7.2
NaCl	1.0	4:1	33
NaCl	1.0	0:1	25
NaCl	3.0	2.6:1	0[c]
NaCl	3.0	1.3:1	0[c]

[a] – Reactions performed in filament reactor.

[b] – Mass yield determined by final mass / initial mass TCM x 100.

possible that the presence of excess NaCl reduces the reaction temperature to the point where it cannot sustain any propagation. This can also be seen in the difference of reactors that are used. Using the Parr reactions resulted in at least some partial reaction, but using the filament reactor resulted in a small amount of recovered CN_x material. This could be explained by the fact that filament reactor only has the wire to heat the reaction, and the temperature rapidly decreases as one move away from the filament. Couple this with the presence of a heat sink like NaCl, and this could disrupt network formation. In the case of the Parr reactor, the wall and floor of the reactor act as multiple, continuously heated initiation sites for the reaction.

Reactions involving the silica template were only performed with the filament reactor. Using a fairly dilute mixture of SiO_2 and TCM, it was found that filament reactions would occur with similar molar ratios. This resulted in mass yield of 6.6% for the 7.6:1 reaction and 30% for the 2.5:1 reaction. The materials appeared to be more of a light brown color, versus the orange-tan of the TCM-CN_x in Chapter II.

Powder X-ray diffraction of the crude products clearly showed the presence of the cubic pattern of NaCl in the crude products (Figure 3.2a). Washing in methanol for 90 minutes, was able to remove the excess NaCl from the crude products. The various NaCl /TCM washed products can be found in Figure 3.2b-f. Unfortunately, silica templates are not soluble in regular solvents, but can be etched away with aqueous HF solutions. Rather than use this dangerous acidic reagent, it was thought a sufficiently concentrated aqueous solution of sodium hydroxide would be able to dissolve the particles enough to remove them from the CN_x network. It was found that stirring just silica particles in a 6M NaOH solution for nine hours at room temperature could effectively remove the

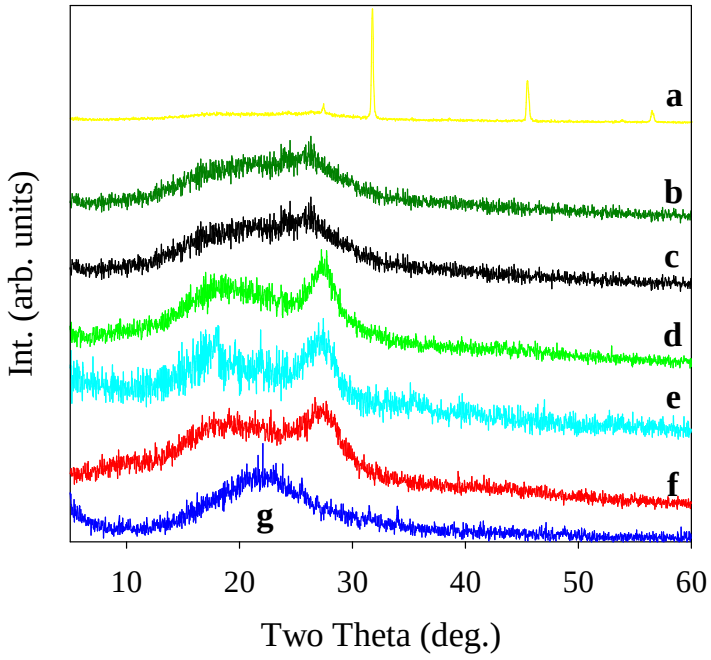

Figure 3.2 - Powder X-ray diffraction patterns for a) TCM-CN_x, b) 10:1 NaCl:TCM washed product, c) 2.5:1 NaCl:TCM washed product, d) 0:1 NaCl:TCM washed product, e) 7.6:1 SiO_2:TCM washed product, f) 2.5 SiO_2:TCM washed product, g) SiO_2 template.

material. This method was monitored by FTIR spectroscopy, as the SiO_2 template is amorphous by XRD (Figure 3.2g). The washed products for the SiO_2 reactions (Figure 3.2e,f) showed a broad peak at 27°, as did a control reaction of TCM dissolved in methanol (Figure 3.2d). As mentioned in the previous chapter, this is indicative of graphite-like layered ordering. The NaCl/TCM reactions did not show this broad peak in the washed products.

The FT-IR spectra of the NaCl:TCM reactions show some similarities in peak positions, though with different band intensities. The peaks from 3100-3500 cm^{-1} are from N-H stretching modes associated with amine bridges. The 39:1 NaCl:TCM reaction

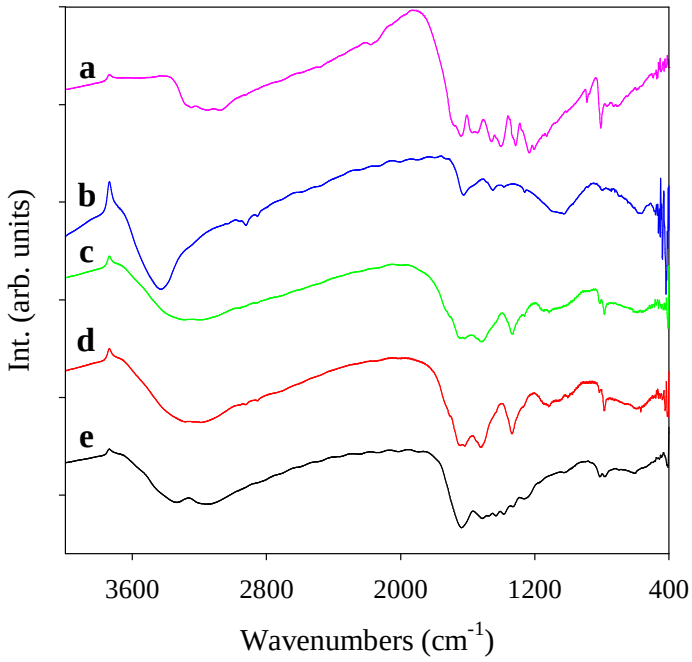

Figure 3.3 - FT-IR spectra for a) TCM-CN_x, b) 39:1 NaCl:TCM washed product, c) 20:1 NaCl:TCM washed product, d) 10:1 NaCl:TCM washed product, and e) 4:1 NaCl:TCM washed product.

(Figure 3.3b) also exhibits a rather large peak at 3500 cm^{-1} which suggests the presence of water in the material. As mentioned previously, a peak near 800 cm^{-1} indicates the presence of either the triazine or heptazine heterocycle. However, in the case of the 39:1 NaCl:TCM reaction, only a very small peak occurs there, while the other materials exhibit two peaks of varying intensity at 807 and 783 cm^{-1}. This suggests the presence of two slightly different ring systems, and that the heptazine and triazine rings are both present in the material. As the TCM-CN_x material has been characterized as having the heptazine ring present near 807 cm^{-1}, this suggests the triazine ring is indicated by the peak at 783 cm^{-1}. More triazine retention in product is consistent with NaCl acting as a heat sink and lowering the reaction temperature. The majority of the peaks occur in the

1100-1650 cm^{-1} region, which is in the region for C-N, C=N, C-C bonding modes. There are strong resonances near 1300 cm-1 region for the 20:1 and 10:1 NaCl:TCM materials (Figures 3.3c and 3.3d), which are indicative of aromatic C-N stretches. The increased intensity here may suggest an increased amount of primary amine endcaps, in the structure, perhaps for a less polymerized type of material.

The FT-IR spectra of the SiO_2:TCM reactions are exhibited in Figure 3.4. As mentioned previously, the removal of SiO_2 template (Figure 3.4b) could be monitored by FT-IR. The peaks at 1100, 800 and 470 cm^{-1} are Si-O bonding vibrations, and clearly

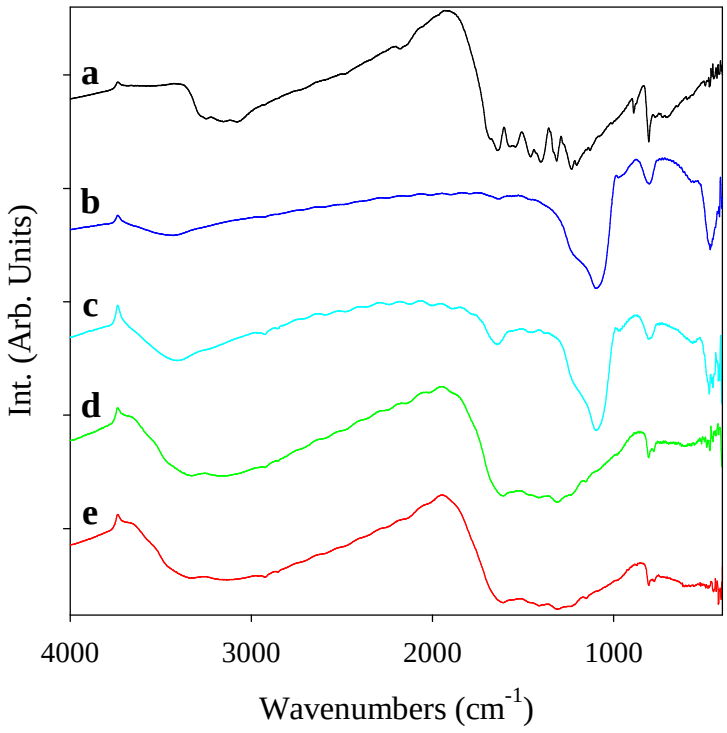

Figure 3.4 - FT-IR spectra for a) TCM-CN_x, b) 7.6:1 SiO_2:TCM crude product, c) 2.5:1 SiO_2:TCM crude product, d) 7.6:1 SiO_2:TCM washed product, and e) 2.5:1 SiO_2:TCM washed product.

disappeared from the washed product spectra with the aforementioned NaOH solutions. The CN_x-type peaks are present in the washed products, with similar relative intensities; however, they appear broader in these materials. This suggests that despite the presence of a template, the TCM was able to decompose to CN_x in the presence of the silica without as much impedance as the presence of NaCl. These broader features are reminiscent of products synthesized from slow decomposition of triazidotriazine, $C_3N_3(N_3)_3$.

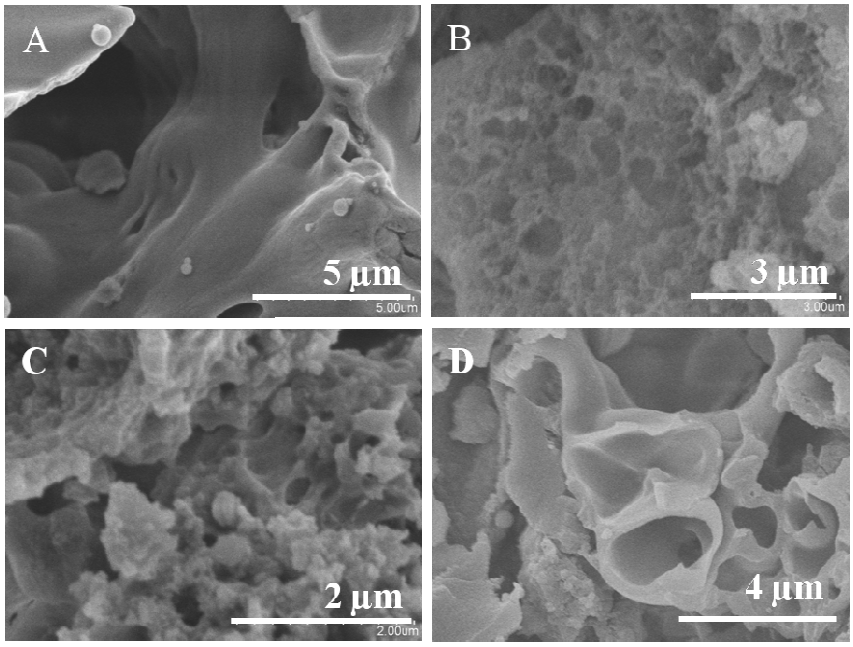

Figure 3.5 - Scanning electron micrographs of A) 0:1 NaCl:TCM washed product, B) 4:1 NaCl:TCM washed product, C) 10:1 washed product, and D) 7.6:1 SiO_2:TCM washed product.

The morphology of the templated materials was explored via scanning electron microscopy. What immediately becomes apparent is the difference of the materials from TCM-CN_x. Whereas TCM-CN_x exhibits a rather smooth, glassy-like appearance, the template materials exhibit a much rougher surface type. This would expected, as the template forces the TCM to decompose around it. Once removed, a negative imprint of the template is left upon the TCM-CN_x material. In Figure 3.5A, the lack of a template leads the TCM to form a smooth material, while in Figures 3.5B-D, the materials appear with external pockets on its surface. These pockets suggest that a template was originally present there, then subsequently removed post-reaction.

Reactive addition of NaBr and NaN_3 to trichloromelamine

In the previous reaction sets, intimate salt mixtures could be made by dissolving NaCl and TCM in methanol. Unfortunately, it required about 120 mL of methanol per gram NaCl to dissolve the template. It was thought that a more soluble salt could be used in lieu of NaCl, so sodium bromide, NaBr, was obtained as a suitable replacement. Using the previous procedure as before, it was found that when the NaBr solution was added to the TCM solution, a bright yellow solution was formed. Once the solvent was removed, a pale yellow solid was collected; this was much different from the off-white material collected from TCM/NaCl mixtures. An XRD pattern of the yellow material revealed that in addition to NaBr being present in the material, there were also peaks that matched NaCl (Figure 3.6a). Since this was before the decomposition step, this suggested a portion of the chlorine atoms of the TCM were being exchanged with bromine atoms. This material was subsequently thermally decomposed to explore what occurred when halogen exchange occurred. Under flowing N_2 gas, the mixture was rapidly heated to

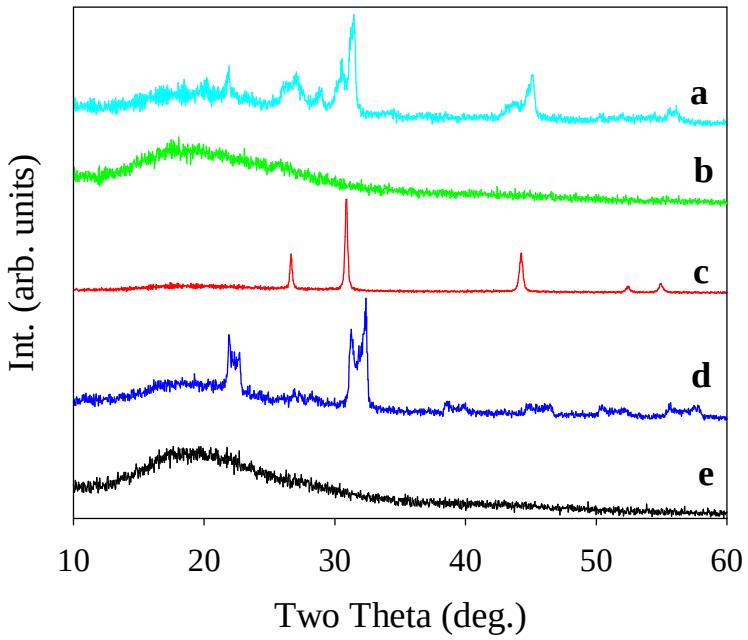

Figure 3.6 - Powder X-ray diffraction patterns of a) 2.2:1 NaBr:TCM mixture, b) washed decomposition product of a), c) crude slow decomposition product of 2.2:1 NaBr:TCM, d) transport material from slow NaBr:TCM decomposition, and E) washed slow NaBr:TCM decomposition product.

300 °C in a Schlenk flask. At ~225 ºC, an orange vapor began to form in the flask and continued to form for 10-15 seconds, leaving a brown solid remaining after decomposition. Some white transport material also began forming from the purge needle of the reaction flask. The orange vapor suggests that formation of HBr gas is occurring, which is analogous to the decomposition route of TCH in the previous chapter. Washing the material in methanol revealed a completely amorphous product (Figure 3.6b). A small portion of the NaBr/TCM mixture was also slowly decomposed by heating under N_2 to 300 °C in a programmable furnace. A dark brown solid was obtained, as was a white transport material. The dark brown solid only contained crystalline NaCl in the product, while the transport product contained a spectrum of ammonium halide salts of

the type $NH_4Cl_xBr_{(1-x)}$, where x = 0-1, as shown in Figure 3.6d. Once again, the washed product was completely amorphous by XRD, as shown in Figure 3.6e.

Given this evidence of halogen exchange, it was thought that other sodium salts could be exchanged with the Cl atoms of TCM in order to form new molecular species. These new species may have different decomposition characteristics from the parent TCM molecule. In particular, an exchange with three molar equivalents of sodium bromide or sodium azide could form and interesting precursors, $C_3N_3(NHBr)_3$ and $C_3N_3(NHN_3)_3$, respectively. In the previous experiment, it was apparent that partial exchange of the bromines had occurred, so complete exchange was required to form the tribromomelamine derivative (TBM). By exchanging with the pertinent amount of sodium azide, a triazidomelamine (TAM) precursor, may be used to form a porous

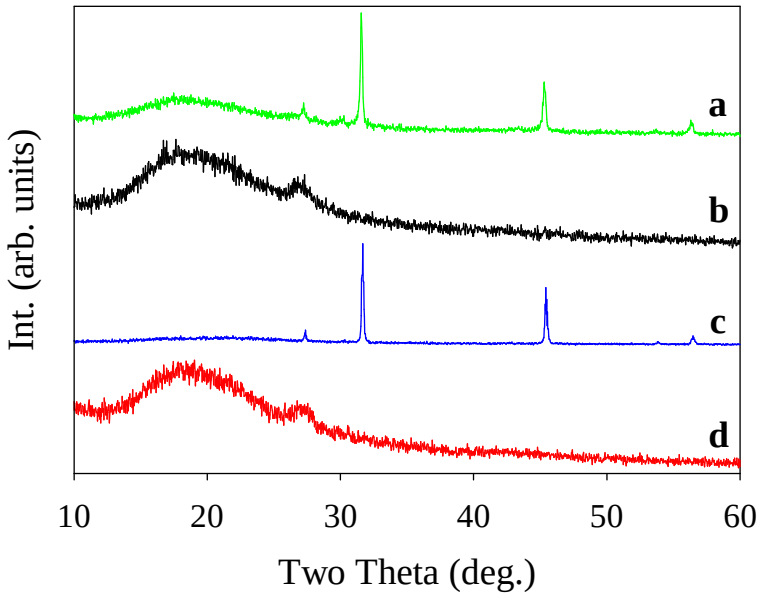

Figure 3.7 - Powder X-ray diffraction patterns for a) 3:1 NaBr:TCM crude precursor product, b) 3:1 NaBr:TCM washed decomposition product, c) 3:1 NaN_3:TCM decomposition reaction product, and d) 3:1 NaN_3:TCM washed product.

material via decomposition and formation of gaseous byproducts. The precursors were synthesized by combining methanol solutions of TCM and with a slight excess of sodium bromide or sodium azide. A bright yellow solid formed in the case of TBM and a pale pink solid was formed in the case of TAM. Powder XRD analysis of this pink solid showed only the presence of NaCl in the crude materials, indicating the expected salt formation via exchange (Figure 3.7a,c).

The purification of the precursor materials proved to be a problem. Much like TCM, it was found that these materials were only soluble in methanol and DMF. However, since the byproduct NaCl was also soluble in these solvents, it could not be separated. ^{1}H and ^{13}C NMR was performed on the crude materials in deuterated

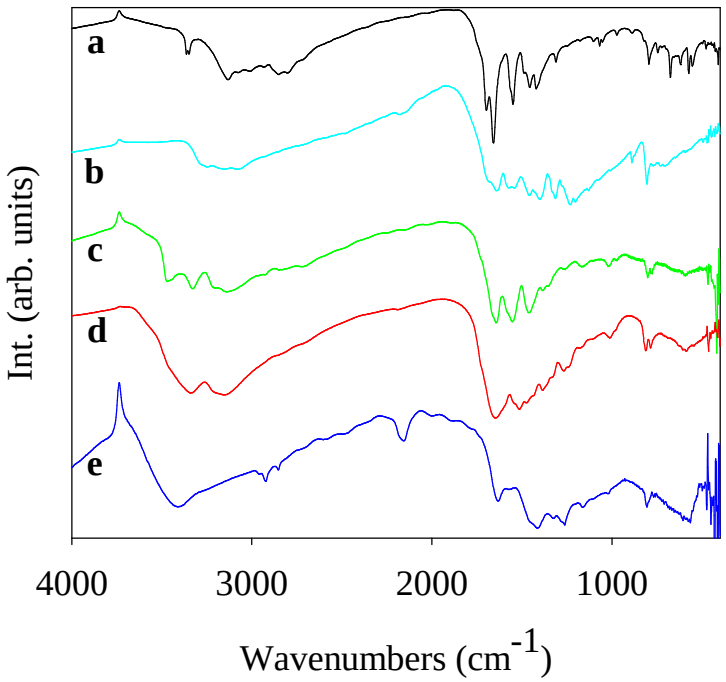

Figure 3.8 - FT-IR spectra of a) TCM, b) TCM-CN_x, c) crude tribromomelamine (TBM), d) washed TBM decomposition product, and e) crude triazidomelamine product.

methanol-d_4. No clear signals could be determined in the crude TAM products, but a broad peak at 7.05 ppm was found in the crude TBM product, suggesting that this could the secondary amine hydrogen. No peaks were found in the ^{13}C NMR spectra.

The crude TBM and TAM precursor mixtures with NaCl byproducts were subject to decomposition reactions. As mentioned previously, the crude TBM showed detonation at a higher temperature than TCM (225 ºC versus 165 ºC). Surprisingly, crude TAM did not show any strongly exothermic decompositions upon heating in a Schlenk flask and further work will be necessary to explain this phenomenon. The IR spectra of the reactive precursor additives and their decomposition products are shown in Figure 3.8. If we compare the spectra of TCM (Figure 3.8a) and crude TBM (Figure 3.8c), we see that there are some broad similarities in peak position. Namely, there are two peaks in the 3300-3500 cm^{-1} region corresponding to N-H stretches. The N-Br stretches are most likely too weak to be observed in the spectra. TBM also features peaks at 1660, 1550, 1460, and 800 cm^{-1}, which correspond well with those heterocyclic vibrations of the triazine ring in TCM. The TBM decomposition product shows retention of vibrational modes, but also with an increase in the 1260 cm^{-1} region, which is in the C-N, N-N region. This suggests that there is some polymerization occurring during decomposition. The TAM material (Figure 3.8e) also displays some of those same characteristic triazine frequencies, although there is increased intensity in the 1250 cm^{-1} region. This could suggest the presence of N-N stretching from the attached azide group. More work will be necessary to uncover the decomposition processes of these materials.

Gas-forming additive incorporation into trichloromelamine decomposition

An additional concept of developing porous CN_x material was the use of a blowing agent to develop porous materials.[124] These blowing agents are materials that will decompose to gaseous byproducts, and are used to make polymer foam structures. A similar strategy was employed in the decomposition of TCM. Solid mixtures of TCM and a gas-forming additive were decomposed to alter the morphology of the TCM-CN_x. The gas forming additive mixtures involved a molar mixture of ammonium chloride and sodium azide (NH_4Cl/NaN_3). It was proposed that the decomposition of the mixtures would produce gaseous byproducts as exhibited in Equation 3.1. Sodium azide has a thermal decomposition temperature of 275 ºC, while ammonium chloride decomposes to NH_3 and HCl at 338 ºC. It is possible that the NH_4Cl and NaN_3 react together the form NaCl and an unstable ammonium azide intermediate (NH_4N_3). This would disproportionate to N_2 and NH_3 gas, which could subsequent react with HCl generated by TCM to reform the byproduct NH_4Cl. A few exploratory reactions were performed with sodium bicarbonate ($NaHCO_3$) which begins to slowly decompose at temperatures in excess of 60 ºC (Equation 3.2). Rather than mixing the materials together in solution, the precursors were mixed together in the solid state using a mortar and pestle. Decomposition of the materials was performed in either Parr or filament reactors. The results of the reactions of TCM with gas-forming additives can be found in Table 3.5.

$$NaN_3 + NH_4Cl \rightarrow NH_4N_3 + NaCl \rightarrow 4/3NH_3 + 4/3N2 \quad \text{(Equation 3.1)}$$

$$2NaHCO_3 \rightarrow Na_2CO_3 + CO_2 + H_2O \quad \text{(Equation 3.2)}$$

Table 3.5 - Results of the reactions of TCM with gas-forming additives.

Reactant(s) R1/R2	**Mass TCM (g)**	**Molar Ratio TCM:R1:R2**	**Heating Method**	**% Mass Yield[a]**
NH_4Cl/NaN_3	1.0	1:1:1	Parr	19
NH_4Cl/NaN_3	1.0	1:2:2	Parr	18
NH_4Cl/NaN_3	1.0	1:3:3	Parr	16
NH_4Cl/NaN_3	1.0	1:0:3	Filament	0.6
$NaHCO_3$	1.0	1:3	Filament	0
$NaHCO_3$	1.0	1:1	Filament	0
$NaHCO_3$	3.0	1:3	Parr	22
NH_4Cl/NaN_3	1.0	1:0.65:0.65	Filament	23
NH_4Cl/NaN_3	1.0	1:1.94:1.94	Filament	21
NH_4Cl/NaN_3	1.0	1:2.93:2.93	Filament	8
NH_4Cl/NaN_3	1.0	1:1.94:0	Filament	30
NH_4Cl/NaN_3	1.0	1:0:1.94	Filament	1
NH_4Br/NaN_3	1.0	1:1.41:1.41	Filament	6

[a] – Mass Yield determined by Final mass /Initial mass TCM x 100.

When the reactions were performed in the filament reactor, detonation was accompanied by the production of a large amount of vapor from the top of the reactor. This was to be expected from the idea that reaction is producing a large amount of gaseous byproducts. A pale brown product was recovered from the bottom of the reactor, while a white byproduct was coating the walls of the reactor. The materials were explored by powder XRD, as exhibited in Figure 3.9. The material recovered from the reactor showed two crystalline components in the pattern: NaCl and NH_4Cl. Judging by relative intensity, NaCl appears to be the predominant crystalline material in the material

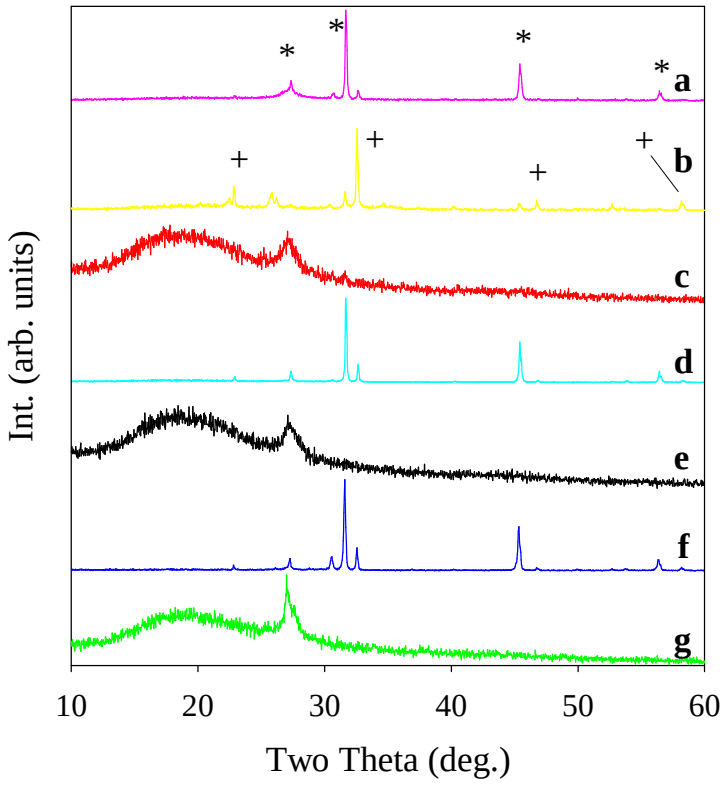

Figure 3.9 - Powder X-ray diffraction patterns of the products a) 1:0.65:0.65 TCM:NH_4Cl:NaN_3 crude, b) 1:0.65:0.65 TCM:NH_4Cl:NaN_3 white byproduct from reactor walls, c) washed 1:0.65:0.65 TCM:NH_4Cl:NaN_3 product, d) 1:1.94:1.94 TCM:NH_4Cl:NaN_3 crude product, e) 1:1.94:1.94 TCM:NH_4Cl:NaN_3 washed product, f) 1:2.93:2.93 TCM:NH_4Cl:NaN_3 crude product, and g) 1:2.93:2.93 TCM:NH_4Cl:NaN_3 washed product. The (*) represents NaCl and (+) represents NH_4Cl.

recovered from the bottom of the reactor, while NH_4Cl predominates the material recovered from the surfaces of the wall. This suggests that upon initiation of the reaction, NH_4Cl is decomposed to to ammonia and HCl gases, then recondense as NH_4Cl on the surface of the cooler reactor walls. The formation of NaCl also suggests a metathesis reaction is occurring between NaN_3 and either the Cl atoms of TCM or that of NH_4Cl. This salt formation may also help to drive the reaction forward, and is one of tenets of

solid state metathesis reactions (SSM).[136] The washed products also exhibited layered, graphite-like ordering, indicated by the broad peak at 27º.

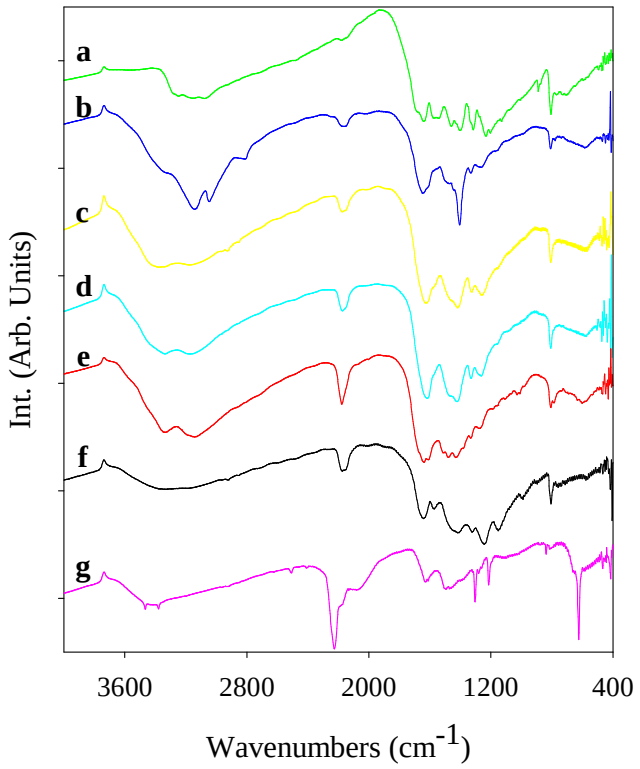

Figure 3.10 - FT-IR spectra of a) TCM-CN_x, b) 1:1.94:1:94 TCM:NH_4Cl:NaN_3 crude product, c) 1:0.65:0.65 TCM:NH_4Cl:NaN_3 washed product, d) 1:1.94:1:94 TCM:NH_4Cl:NaN_3 washed product, e) 1:2.93:2:93 TCM:NH_4Cl:NaN_3 washed product, f) 1:1.94:1:94 TCM:NH_4Cl:NaN_3 annealed product, and g) 1:2.93:2:93 TCM:NH_4Cl:NaN_3 annealed product.

The gas-forming additive reactions were characterized by FT-IR spectroscopy. An example of the crude product (Figure 3.10b) clearly shows the presence of residual NH_4Cl by peaks at 1400, 3050, and 3150 cm^{-1}. The washed products (Figure 3.10c-e) show similarities to TCM-CN_x (Figure 3.10a). They show the bands associated with

heterocyclic vibrations of heptazine, including that of 800 cm^{-1}. This suggests that heptazine based material is still forming. The new peak at 2100-2200 cm^{-1} suggests the presence of a nitrile, C≡N, or a carbodiimide, -N=C=N-, group. The washed materials from the 1:2.93:2.93 and 1:1.94:1.94 TCM:NH_4Cl:NaN_3 reactions were also annealed for 12 h at 450 ºC and characterized as well. No apparent change was observed for the 1:1.94:1.94 reaction, but the 1:2.93:2.93 reaction turned a dark brown color. The annealed products show an increase in the relative intensity of this diimide peak, as well, as an increase in intensity in the 1100-1300 cm^{-1} region. This suggests increased aromatic C-N connectivity, perhaps by –N=C=N- groups. Overall, the extra peak in the spectra suggests that the during the decomposition reaction, either the triazine rings are not fully condensing to the heptazine ring or the triazine rings are breaking open to form carbodiimides during the violent decomposition step or during annealing.

A series of control experiments were performed to probe the reaction of the gas-forming additive. The reactions were performed with only one of the components present, as well as with ammonium bromide, NH_4Br. The filament decomposition reaction was also performed in a crucible, in order to determine if improved heat retention would affect the reaction propagation. These materials were initially characterized by powder XRD. When the reaction is performed with just sodium azide (Figure 3.11b,c), the only crystalline product to appear was NaCl, although the peak had an odd peak shape. When the reaction is performed with NH_4Cl (Figure 3.11d), the only crystalline component is NH_4Cl. If NH_4Cl is replaced with NH_4Br (Figure 3.11e), then the crystalline components consist of mostly NaCl, NaBr, or NH_4Br. This suggests that salt formation is occurring from sodium azide and the chloride from TCM, and not

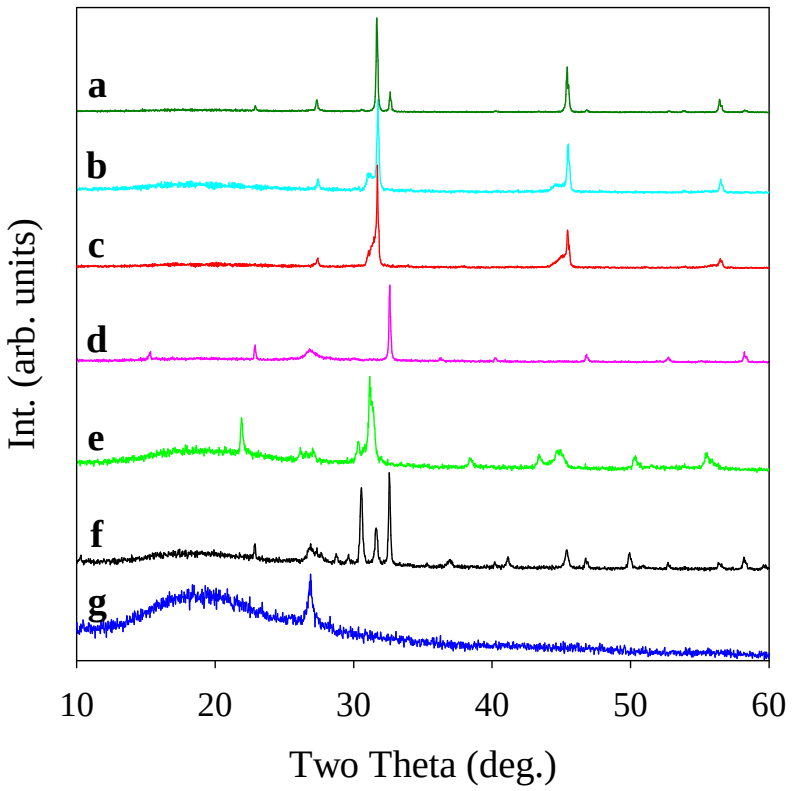

Figure 3.11 - Powder X-ray diffraction patterns for a) 1:1.94:1.94 TCM:NH_4Cl:NaN_3 crude product, b) 1:1.94 TCM:NaN_3 crude product, c) 1:3 TCM:NaN_3 crude product, d) 1:1.94 TCM:NH_4Cl crude product, e) 1:1.41:1:41 TCM:NH_4Br:NaN_3 crude product, f) 1:1.94:1.94 TCM:NH_4Cl:NaN_3 crude product from crucible, and g)1:1.94:1:94 TCM:NH_4Cl:NaN_3 washed product from crucible.

NH_4Cl. Oddly, the reaction performed in a heat-retaining crucible, showed residual NaN_3, as well as NaCl and NH_4Cl. It was thought that a crucible would aid in sodium azide decomposition by maintaining higher reaction temperatures for longer times. The washed product from this reaction shows a much sharper peak at 27 ˚two theta than without using the crucible.

The control reactions were also characterized by FT-IR spectroscopy (Figure 3.12). The peaks of the control reactions were compared with the original

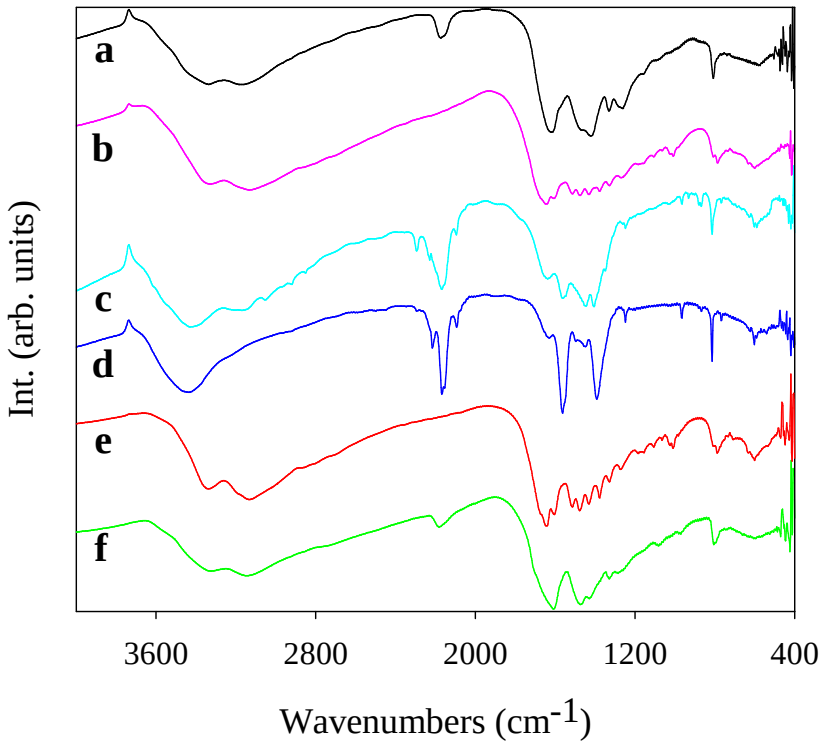

Figure 3.12 - Powder X-ray diffraction patterns for a) 1:1.94:1.94 TCM:NH_4Cl:NaN_3 washed product, b) 1:1.94 TCM:NH_4Cl washed product, c) 1:1.94 TCM:NaN_3 washed product, d) 1:3 TCM:NaN_3 crude product, e) 1:1.41:1:41 TCM:NH_4Br:NaN_3 crude product, and f)1:1.94:1:94 TCM:NH_4Cl:NaN_3 washed product from crucible.

reaction of 1:1.94:1.94 TCM:NH_4Cl:NaN_3 (Figure 3.12a). It was found that the 1:1.94 TCM:NH_4Cl reaction had similar vibrations to the original material, primarily the bands for the heptazine/triazine materials. This was also true of the material derived from the crucible reaction. The reaction without NaN_3 did not show any peaks in the 2100-2200 cm^{-1}, but the materials synthesized from just TCM and NaN_3 (Figures 3.12c,d) clearly show the patterns for cumulated bond stretches, such as azides, nitriles, or carbodiimides. This is also true of the NH_4Br reaction (Figure 3.12f), which contained NaN_3 in the gas-forming additive. This suggests that sodium azide contributes to formation of more these

functionalities from the 2100-200 cm^{-1}. More work is necessary to understand how these vibrations contribute to the overall structure.

The gas-forming reactions were also performed on within Parr reactors. It was reasoned that from the previous experiences with inert additives, that yields may be approved with use of them. It was found that yields did seem to improve for higher dilutions (near 1:3:3 TCM:NH_4Cl:NaN_3), where the Parr reactions were yield twice as much material. This could be expected due to longer heating within the Parr reactors. Structurally speaking, the materials exhibited the same broad peak at 27° as the filament

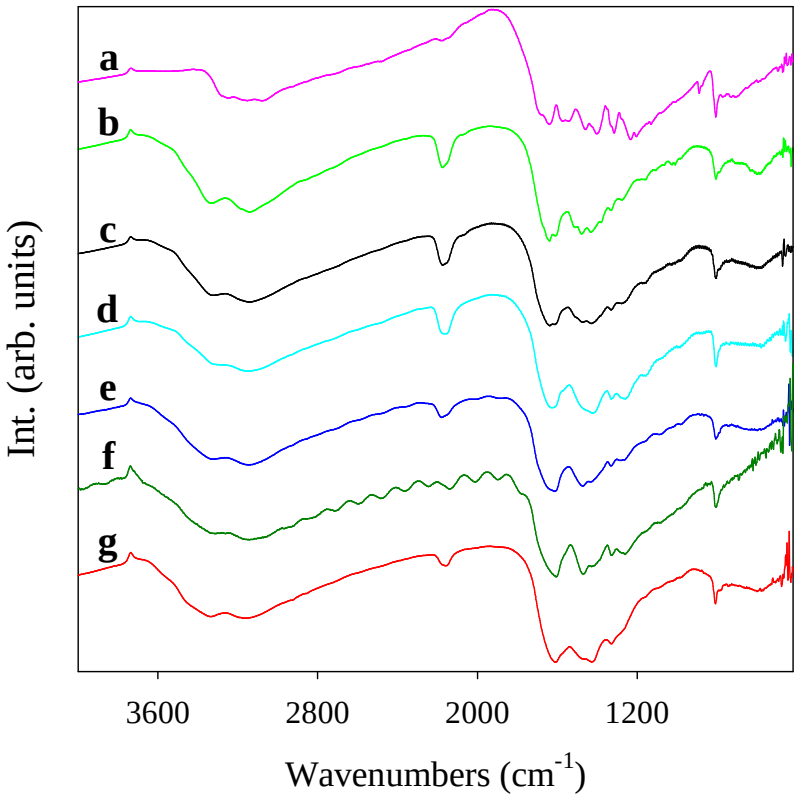

Figure 3.13 - FT-IR spectra of Parr reactions a) TCM-CN_x, b) 1:1:1 TCM:NH_4Cl:NaN_3 washed, c) 1:2:2 TCM:NH_4Cl:NaN_3 washed, d) 1:3:3 TCM:NH_4Cl:NaN_3 washed, e) 1:2:2 TCM:NH_4Cl:NaN_3 upscale, f) 1:3 TCM:$NaHCO_3$ crude, and g) 1:3 TCM:$NaHCO_3$ washed reaction.

reaction. The materials also exhibited very similar FT-IR spectra (See Figure 3.13b-e). These materials exhibited characteristic heterocyclic vibrations (especially near 800 cm^{-1}), as well as the peak near 2150 cm^{-1} from the incorporation of the previous mentioned azide, nitrile, or carbodiimide stretches. An additional reaction of 1:3 TCM:$NaHCO_3$ was performed in the Parr reactor. A yellow solid was generated, and it too, showed the same IR vibrations as the NH_4Cl:NaN_3 reactions (Figures 3.13f,g). These reactions were also attempted with the filament reaction, but no reaction occurred. It is thought that Parr reactions may be a more useful route for TCM reactions with higher concentrations of additives.

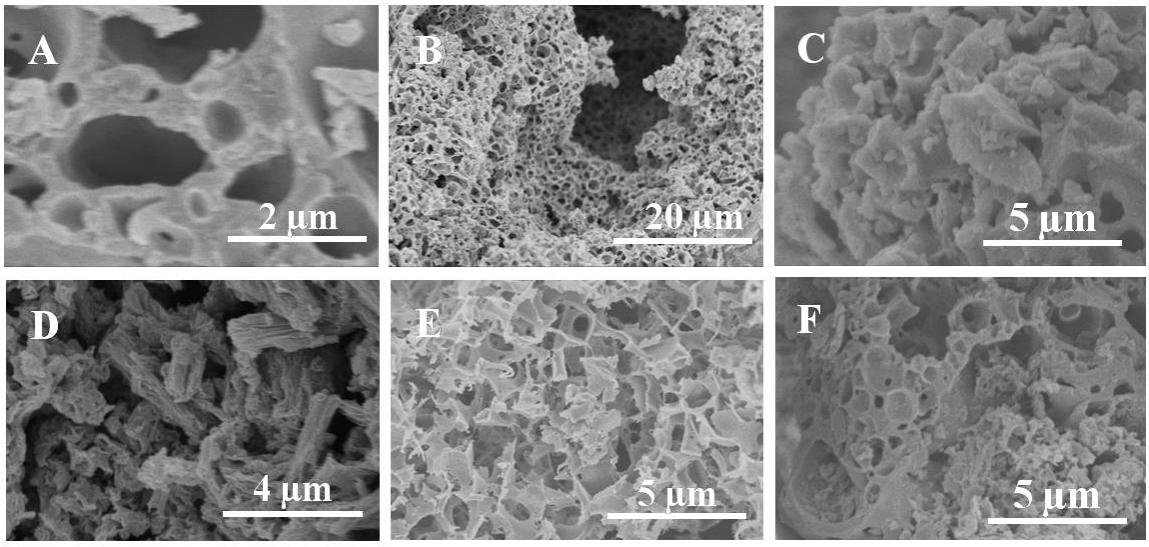

Figure 3.14 - Scanning electron micrographs of washed decomposition products A) 1:1:1 TCM:NH_4Cl:NaN_3 filament decomposition product, B) 1:2:2 TCM:NH_4Cl:NaN_3 filament decomposition product, C) 1:3:3 TCM:NH_4Cl:NaN_3 filament decomposition product, D) 1:3 TCM:NaBr, Schlenk line decomposition, E) 1:2:2 TCM:NH_4Cl:NaN_3 filament decomposition product, annealed, and F) 1:3 TCM:$NaHCO_3$ Parr decomposition product.

The morphology of some of the materials was also explored by scanning electron microscopy. Some of the images can be found in Figure 3.14. The reactions formed with the gas forming additives are found in Figures 3.14A-C. When comparing the smooth glassy morphology of TCM-CN_x, it becomes readily apparent that a change occurs to these materials. They appear to be filled with pockets, in particularly the 1:2:2 filament reaction. Annealing the material at 450 °C (Figure 3.14E) shows that the wall thickness of these pockets appears to decrease. The reaction of TCM with $NaHCO_3$ also shows a bubbled appearance (Figure 3.14F), as well. When comparing these materials with one of the 1:3 TCM:NaBr reaction (Figure 3.14D), it appears that although the salt inclusion changes the smooth morphology of TCM-CN_x, the surface just does not show the deep pocketing of the gas-forming additives. Further surface area measurements of these materials will be very useful in quantifying these changes to structure.

Conclusions

Methods to modify the decomposition of TCM were presented in this Chapter. The introduction of a solid template led to an increase in the roughness of the TCM-CN_x product, as evidenced by scanning electron micrographs. However, increasing the dilution of TCM with NaCl also led to problems with decomposition propagation. It was found that the sodium salts NaBr and NaN_3 led to chloride exchange with TCM. Possible exploration of the new precursor molecules was suggested. The use of a chemical mixture of NH_4Cl and NaN_3 as a blowing agent showed clear changes to the morphology of the material, while only leading to slight changes in the IR vibrations of the material. Preliminary results suggested that sodium bicarbonate ($NaHCO_3$) might also act as an interesting gas-forming additive.

CHAPTER IV

SYNTHESIS OF BORON CARBON NITRIDE MATERIALS FROM TRICHLOROMELAMINE DECOMPOSITION

Introduction

The previous chapters detailed the study of the TCM-CN_x material and structural elucidation of the material, then modifying the morphology of the material without altering its structure on a molecular level. The next phase involved trying to modify these carbon nitride materials with reactive components in order to generate novel materials. As previously mentioned in Chapter I, certain theoretical phases of carbon nitride (C_3N_4) are predicted to have a hardness only less than that of diamond and boron nitride (BN). These three materials present highly interesting mechanical properties on their own, but what would happen if a ternary material was made that featured boron, carbon and nitrogen?

To the left and right of carbon on the periodic table are boron and nitrogen. When combined in a 1:1 ratio, they form BN, or boron nitride, which is isoelectronic to C. The major difference between these materials is the bond polarity that occurs in the B-N bond. In the carbon allotropes, the electrons are shared equally within the C-C bond, but in boron nitride, the nitrogen atom donates its electrons to the deficient boron atom and leads to a slight charge separation within the bond. Like graphite, BN forms a layered structure with fused B_3N_3 rings, called hexagonal boron nitride, or h-BN.[137] Due to the aforementioned bond polarity, the boron atoms of one layer are found directly below the nitrogen atoms of the next layer. The bond polarity results in diminished conductivity and a higher band gap (3.8 eV) when compared to graphite, and this translates to a white

appearance for h-BN. Hexagonal boron nitride also has lubricating properties, and is able to function at high temperatures in air (up to 1000 °C), whereas graphite begins to decompose by ~500 °C. Like graphite, h-BN can be heated under intense pressure (up to 18 GPa) and temperature (1730-3230 °C) to generate cubic boron nitride (c-BN), also called borazon. The structure is isomorphous to that of diamond, and it too is used in cutting and grinding applications, though much more resistant in oxidative conditions.[138] Recent efforts have also sought to synthesize BN-type nanotubes.[139]

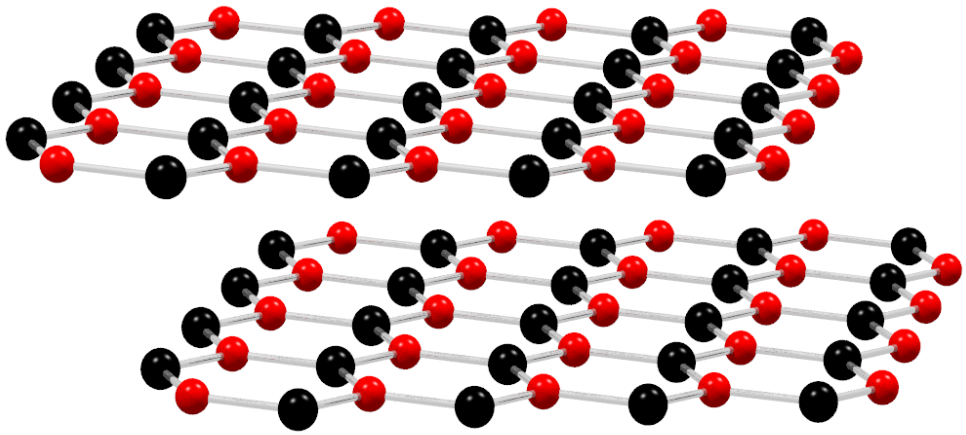

Figure 4.1 - Layered structure of hexagonal boron nitride (h-BN).

It is expected that a ternary material contain B, C, and N should possess the intermediate characteristics depending on the relative amounts of each atom. A planar, layered BCN material should possess semiconducting properties if it is intermediate between h-BN and graphite.[140,141] By substituting a certain amount of carbon atoms in graphite with either boron or nitrogen, a graphite-like network might show better

electrical conducting properties because the electron deficiency of the boron atoms could create holes (positive change carriers) or might have semiconducting properties owing to the localization of lone-pair electrons at the nitrogen atoms. BCN materials could definitely have applications in light-emitting applications[142] or intercalation compounds for electrodes.[143]

In their pioneering approach to BCN materials, Kosolapova, *et al.* simply heated boron and carbon at high temperatures in the presence of either nitrogen or ammonia.[144] Such products, however, were not well characterized. The easier and probably more effective approach to these hybrid materials using chemical vapor deposition (CVD) was first applied by Badzian, *et al.* using chlorides of carbon and boron in combination with hydrogen and nitrogen, but again at a rather high temperature.[145,146] In their first investigations, Kaner *et al.* prepared a BCN hybrid film on either quartz or a pyrolytic boron nitride substrate by the CVD.[140,141] They showed by ESCA measurements that the BCN deposit on the quartz substrate was not simply a mixture of graphite and h-BN. The first attempts to synthesize stoichiometric BCN compounds by Kouvetakis *et al.* and Sasaki *et al.* led to the preparation of BC_3, BC_2N, and C_5N.[147-149] Using a polymeric precursor, Kawaguchi and Kawashima have prepared ordered BC_3N, by the interaction of poly(acrylonitrile) with BCl_3 at low temperature 400 °C, followed by heat-treatment at 1000 °C.[150] In light of these trends to synthesize BCN materials by CVD methods, there have been no reported syntheses by filament-initiated solid state metathesis pathways or by rapid decomposition of precursor materials. Either of these approaches eliminates the need for high temperature or high pressure conditions.

As was previously reported by our group, trichloromelamine can be used as a precursor to form graphitic CN_x type materials. By preparing mixtures of this precursor with sodium borohydride ($NaBH_4$), novel BCN materials can be synthesized by tandem solid state metathesis (SSM) and precursor decomposition. The tan to gray-brown products were analyzed by a series of techniques. It has been determined that a extended layered structure with the formula of approximately $B_{3.2}CN_{3.0}$ is formed and is thermally stable up to at least 1000 °C.

Experimental

Reagents

All reagents were used as received and stored in an argon atmosphere glovebox. The following reagents were purchased from Aldrich: trichloromelamine, ($C_3N_3(NHCl)_3$, Aldrich, 98+%) and sodium borohydride ($NaBH_4$, Aldrich, reagent grade ≥98.5%). Methanol (CH_3OH, ACS grade) was purchased from Fisher Scientific.

Solid state incorporation of sodium borohydride into trichloromelamine decomposition

Sample preparation involved working in an argon glovebox and grinding the sodium borohydride together with the trichloromelamine in a ceramic mortar and pestle. The white mixture was heated by two different methods that are similar to the methods described in Chapter II. The attempted reaction ratios can be found in Table 4.1.

Method 1: Hot filament ignition in stainless steel reactor

Trichloromelamine (1.00 g, 4.36 mmol) was ground together with sodium borohydride (0.495 g, 13.08 mmol) for five minutes inside an argon atmosphere

glovebox. The reaction mixture was placed in a 60 ml custom calorimeter style steel reactor in the glovebox (screw top, inner 5 cm depth × 3.8 cm width and cap fitted with two posts connected to a coiled Nichrome wire that was in contact with reaction mixture). The reactor was removed from the glovebox and placed inside a fume hood and connected to a Variac. The reaction was initiated by heating the wire with the Variac at 12V for three seconds. A white vapor was observed exiting the top of the reactor and the reaction was complete within a few seconds. The reactor was disassembled in air after cooling down to room temperature. A fused solid was isolated, along with a white solid covering the walls of the reactor. The gray solid was crushed and washed in methanol, filtered, and dried in air overnight. A mass of 325 mg was recovered.

Method 2: Rapid heating in stainless steel autoclave

The reaction mixture was placed inside a 125 mL Parr reactor inside the glovebox. The reactor was capped with a rubber septum and removed from the glovebox where it was sealed under flowing N_2 with a reactor head equipped with an analog pressure gauge and an internal thermocouple. The reactor was placed in a Glas-Col beaker-shaped custom heating mantle and quickly heated by setting the temperature controller to 300 ºC. After ~20 minutes, the internal temperature had reached 120 ºC, when a jump in the temperature was observed (to ~240 ºC), accompanied by an increase in pressure to 100 psi. After decomposition, the reactor was removed from the mantle to cool to room temperature. The reactor valve was slowly opened to vent byproduct gases into the hood, and the reactor disassembled in air. A fused dark gray solid was recovered, ground with a mortar and pestle, and washed in methanol for one hour, filtered, then dried over night in air. A mass of 266 mg was recovered.

Annealing experiment of trichloromelamine-derived boron carbon nitride

A mass of 50 mg of the BCN material derived from Method 2 was placed into a 3/8 inch silica ampule. The ampule was connected to a Cajon valve with a Teflon stopcock attached. The ampule was evacuated to a pressure of 150 mtorr, and sealed with a torch to a length of 10 cm. Once cooled, the sealed ampule was placed in a Lindberg/Blue tube furnace. The ampule was heated to 1000 °C at a rate of 10 °C/min. The ampule was heated at temperature for 12 hours, then cooled ambiently to room temperature. The ampule was opened in air for analysis. A mass of 49 mg was recovered.

Table 4.1 - Summary of attempted experiments performed with trichloromelamine mixtures.

TCM:$NaBH_4$ Mole ratio	**Reaction Method**	**Post wash appearance**	**% mass recovery[a]**	**%C**	**%H**	**%N**
1:1	1	tan	17	16.91	2.23	33.56
1:2	1	gray-brown	19	14.22	2.42	27.54
1:3	1	gray	23	10.53	2.27	23.99
1:3	2	gray	20	8.06	1.01	15.74

[a] Percent recovery based on initial reaction mixture weight. All reactions performed based on 1 g (4.36 mmol) of TCM.

Note: Average elemental analysis of the methanol washed materials are included. Note the low CHN percentages; refactory materials are difficult to completely combust.

Instrumentation

Thermogravimetric-differential analysis (TG-DTA) was performed on a Seiko ExStar 6300 system under flowing argon. FT-IR absorption spectra were taken with a Nicolet Nexus 670 spectrometer using KBr pellets. Elemental analyses were performed on a Perkin Elmer 2400 CHN/O Analyzer using ultra light weight, ultra clean tin capsules. Powder X-ray diffraction was performed on a Siemens D5000 X-ray diffractometer, using Cu K_α radiation on samples mounted on glass slides. Solid state ^{13}C and ^{11}B CP-MAS NMR was obtained on a Bruker wide-bore MSL 300. The samples were loaded into 4 mm ZrO_2 rotors and spun at 8 kHz, and data referenced to hexamethylbenzene for ^{13}C and $BF_3 \cdot OEt_2$ for ^{11}B. Scanning electron microscopy (SEM) was performed on a Hitachi S-4800 SEM with samples mounted on Al stubs and coated with Au-Pd alloy. X-ray photoelectron spectroscopy (XPS) analysis was performed with a Kratos Axis Ultra X-ray photoelectron spectrometer with samples pressed into indium foil. Peak fitting procedures involved constraining peaks to the same full width half maximum during the deconvolution step. Shirley type backgrounds were employed for quantification methods. Evolved gas analysis was performed using a SRS QMS 300 residual gas analyzer using the procedure detailed below.

Residual gas analysis of trichloromelamine-derived boron carbon nitride

After performing the reaction via Method 2, the Parr reactor was connected to a 500 ml three-neck flask via a gas inlet adapter and PVC tubing. The center neck was connected to the RGA-MS capillary with a sidearm connection to an Ar Schlenk line, and the third neck connected to an oil bubbler. The flask was flushed with Ar and the reactor

reopened to the Ar atmosphere and three blank Ar spectra were collected. The reactor was resealed then quickly heated by setting the temperature controller to 300 ºC. After ~20 minutes, the internal temperature had reached 120 ºC where an increase in the temperature (~240 ºC) and pressure (100 mtorr) was observed. Upon decomposition, the reactor was removed from the mantle to cool to room temperature. The Schlenk valve was closed then the reactor valve was slowly opened to flush the reaction gases through the flask. Sampling the flask involved opening the sidearm and drawing the gases into the instrument. Two initial surveys of the 1-265 amu region were performed followed by nine scans of the 1-65 amu region.

Results and Discussion

Boron carbon nitride synthesis

In previous work in our group, Dale Miller reported on an attempt to synthesize a composite material via reaction of sodium borohydride and TCM in a 1:1 molar ratio using a hot filament to initiate reaction.[151] He had reported the formation of an orange material with black specks, A large peak at 1397 cm^{-1} was found to be present within the material. This was consistent with a B-N stretching frequency and suggested the possible formation of a new BCN material, but this research direction was not pursued further.

It was initially postulated that the following reaction between TCM and sodium borohydride would occur:

$$C_3N_3(NHCl)_3 + xNaBH_4 \rightarrow B_xC_3N_{6-y} + xNaCl + (3-x)HCl + y/2N_2 + 6H_2 \quad \text{(Equation 4.1)}$$

The idea was to take advantage of the competing reactions of TCM decomposition and NaCl formation to be the driving forces behind the synthesis of a possible new B-C-N

material. Table 4.1 summarizes the reaction results. One of the most readily apparent indicators that a chemical change is occurring is the appearance of the products. After reaction, a fused mass of gray material is formed around the filament of the reactor. There was tan material that formed around the outermost edges of the fused gray solids and could be found near the walls of the reactor. A second white material could be found on the walls of the reactor when reactions were performed by Method 1, but not by Method 2. This is in contrast to TCM-CN_x synthesis where only an orange-tan product is formed.

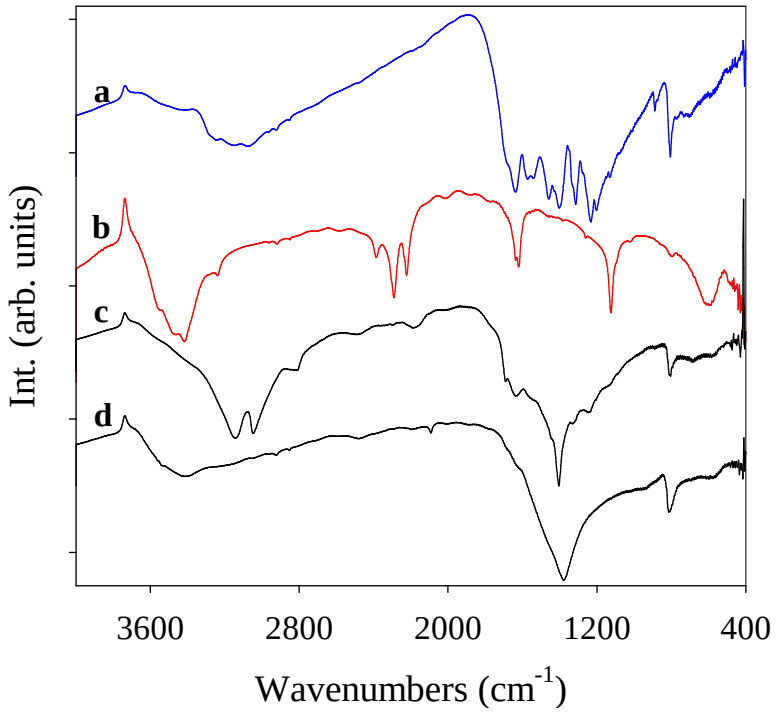

Figure 4.2 - FT-IR spectra for a) trichloromelamine (TCM) decomposed via Method 2, b) sodium borohydride ($NaBH_4$), c) crude product from 1:1 TCM:$NaBH_4$ reaction via Method 1, and d) crude product from 1:3 TCM:NaBH4 reaction via Method 2.

FT-IR spectroscopic data was collected on the crude materials acquired from Method 1, as can be seen in Figure 4.2. There are four major peaks at 3142, 3048, 2812 and 1404 cm^{-1}. These peaks are consistent with N-H stretching and bending modes of ammonium chloride (NH_4Cl), respectively. Additional smaller peaks occur in the 2300-2500 cm^{-1} region and are consistent with B-H stretching modes. For comparison, a spectrum of $NaBH_4$ is shown in Figure 4.2. Another peak of interest is the peak near 800 cm^{-1}; this peak may be consistent with out-of-plane bending modes of triazine or heptazine heterocycles that is present in the TCM-CN_x products. In addition, there a number of shoulders present on the large peak at 1404 cm^{-1}. The spectrum of the crude product synthesized by Method 2 was different, in that there were no peaks that

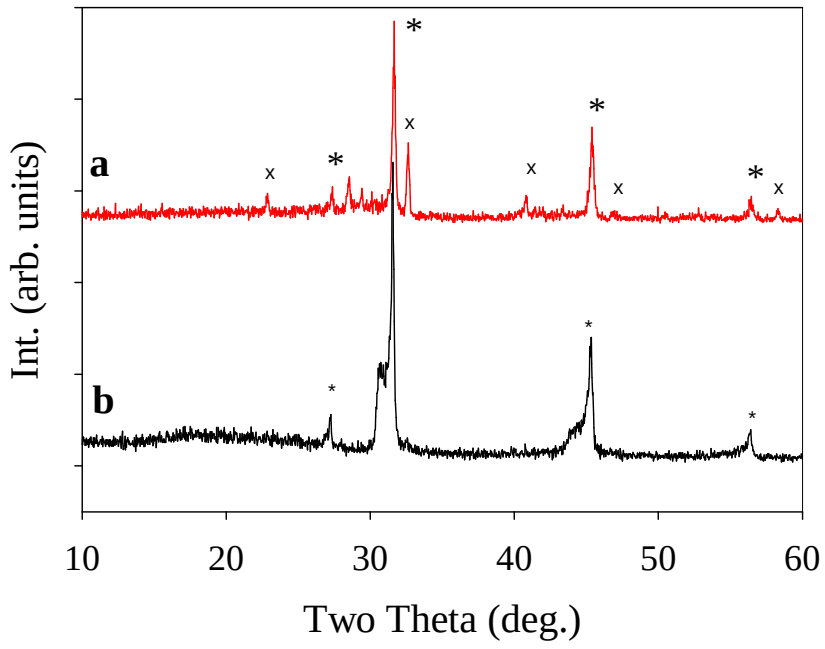

Figure 4.3 - Powder X-ray diffraction patterns of a) typical pattern for crude products formed via Method 1 and b) crude product from Method 2. The pattern for NaCl is denoted by (*) and NH_4Cl is denoted by (x).

corresponded to NH_4Cl. A peak at 3418 cm^{-1} corresponds to N-H stretches, a small broad peak at 2480 cm^{-1} corresponds to some residual B-H stretches; and a peak at 2093 cm^{-1} occurs in the C≡N region. The spectrum is dominated by the two peaks at 1376 and 814 cm^{-1}. These peaks are in the B-N or C-C region and compare very favorable with BCN type materials synthesized by Komatsu.[152]

Powder X-ray diffraction (XRD) data was used to see if the predicted crystalline NaCl was formed during the reactions of $NaBH_4$ with TCM. As can be seen in Figure 4.3, the cubic pattern for NaCl is clearly evident in the materials synthesized by Method 1. In addition, an XRD pattern that is consistent with NH_4Cl. This further confirms the identification in the FT-IR of the crude materials from Method 1. The fact that the white NH_4Cl was found on the walls of the reactor suggests that ammonia (NH_3) and hydrogen chloride (HCl) are possibly forming during the reaction and recondensing as ammonium chloride in a cooler area. The temperature at which ammonium chloride decomposes is 338 °C; this would suggest that the reaction mixture is getting hotter than this temperature. Otherwise, the byproduct ammonium chloride should be found within the reaction mixture and not sequestered to the cold reactor wall. The reaction of 1:3 TCM to $NaBH_4$ by Method 2 showed only peaks that matched the cubic pattern for NaCl. An interesting note about the pattern is that each peak shows a shoulder occurring on the low angle side of the peak. This might suggest that the crystalline NaCl is formed along with some poorly crystallized amount of byproduct salt or closely related NaX salt.

In order to further assess the reaction pathway, a reaction between TCM and $NaBH_4$ in a 1:3 molar ratio was performed using a rapidly heated autoclave (Method 2). The sealed system allows for the analysis of the byproduct gases formed during the

reaction using atmospheric pressure residual gas analysis. The method was similar to the system used in exploring TCM decomposition reaction in Chapter II. The reaction was performed under Ar gas in order to assess the presence of byproduct N_2 gas. The system background blank and spectrum of evolved gases from rapid reaction of $NaBH_4$ and

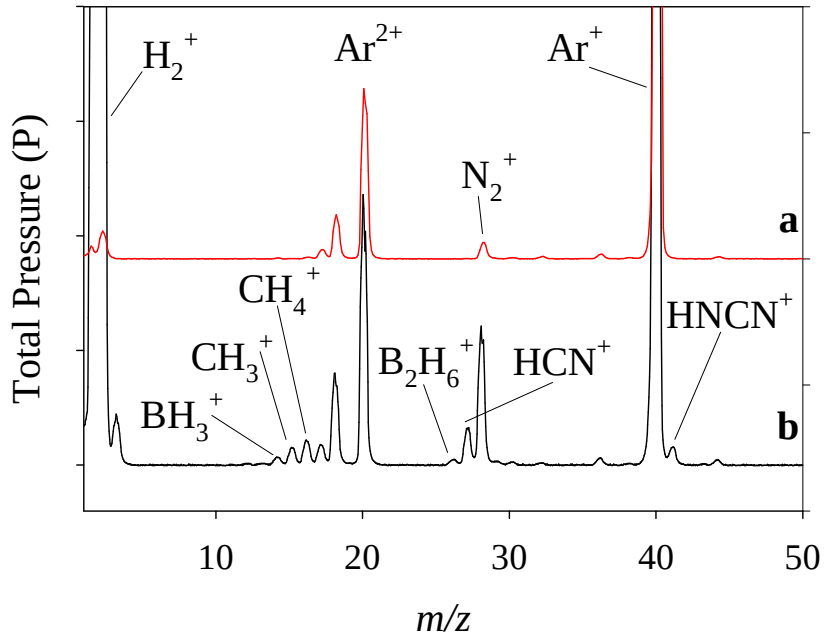

Figure 4.4 - Residual gas analysis (RGA-MS) of 1:3 TCM:$NaBH_4$ reaction performed by Method 2 for a) background spectrum of argon (Ar) atmosphere, b) spectrum of headspace gases after reaction.

TCM are shown in Figure 4.4. There are nine peaks that occur at levels significantly higher than those of the background. The largest peak by far occurs at m/z = 2 and corresponds to H_2 gas. This may be expected due to the fact that sodium borohydride converts to its constituent elements on heating to 500 °C. There are also peaks at m/z = 14, 15, and 16 which could correspond to BH_3^+, CH_3^+, and CH_4^+ species, respectively.

There also peaks at m/z = 26, 27, and 29 that possibly correspond to either some cyanide based species such as HCN (m/z = 27), or a diborane (B_2H_6) species (m/z = 26). A peak at m/z = 41 could correspond to a cyanamide species (H_2N-CN). One thing to note about the byproduct gases, is that there is not much of a similarity with TCM-CN_x decomposition gases. There were no peaks that matched with HCl formation and no real increases at m/z = 28 to note the formation of N_2 gas. This suggests a different pathway is occurring in the reaction of TCM with $NaBH_4$ versus TCM decomposition alone.

The crude products were washed with methanol to remove any unreacted TCM or $NaBH_4$. No efforts were made to dry the methanol prior to use and some efferverscence was noted upon addition of the wash solvent to 1:1 and 1:2 TCM/$NaBH_4$ reactions. It was thought that any unreacted $NaBH_4$ would react with the H_2O in the methanol to form H_2 gas and sodium metaborate ($NaBO_2$). No bubbles were seen to form in the two 1:3 TCM:$NaBH_4$ cases. The washing step recovered approximately 33-40% of the pre-wash mass of crude material, as would be expected since a majority of the weight of crude product comes from the byproduct sodium chloride.

Structural characterization of boron carbon nitrides

Powder XRD of these washed BCN materials revealed no peaks in the pattern. BN materials often require very high annealing temperatures in order to form crystalline phases, but BCN materials usually decompose to BN and C.[137,153] Therefore, an amorphous B-C-N product seems likely. However, if the products are annealed at 1000 °C for 12 hours, some broad peaks begin to appear in the pattern. Two broad peaks occur at 26.8° and 41.6°. This is in good agreement with other hexagonal BCN materials reported, as well as other hexagonal systems such as h-BN and graphite (Figure 4.5d).[154]

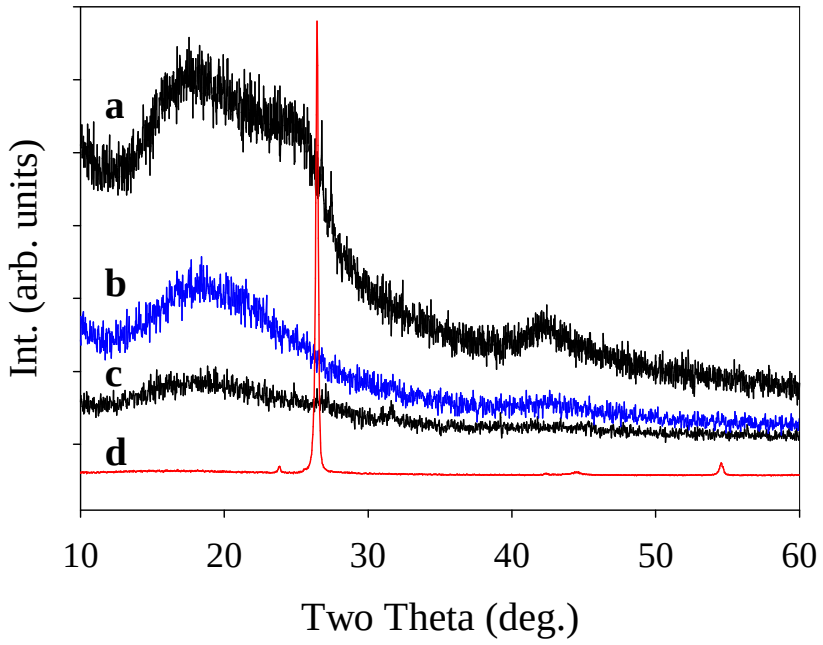

Figure 4.5 - Powder XRD patterns of washed products for a) 1000 °C annealed product from 1:3 TCM:$NaBH_4$ reaction by Method 2, b) Method 2 product from 1:3 TCM:$NaBH_4$ reaction, c) Method 1 product from 1:2 TCM:$NaBH_4$ reaction, and d) synthetic graphite.

The washed BCN materials showed very similar spectra by FT-IR. The IR characteristics of the materials can be seen in Figure 4.6 All four species show five specific bands: from 3150-3450, near 2500, near 1400 cm^{-1}, and near 807 cm^{-1}. The broad peaks seen near 3200 cm^{-1} are NH stretching vibrations likely due to the presence of secondary amines bridges. These peaks are inconsistent with imines (C=NH) or NH_2 groups as these absorb most intensely near 3350 cm^{-1}. Those near 2500 cm^{-1} fit with stretches from B-H bonds. In all the products produced by Method 1, there is a small absorbance at 2170 cm^{-1}; this suggest that very minor C≡N or N=C=N components are generated during TCM:$NaBH_4$ reaction. The bands in the region of 807-808 cm^{-1} indicate out-of-plane bending of fused heterocycles. Similar values occur for both B-N rings and C-N

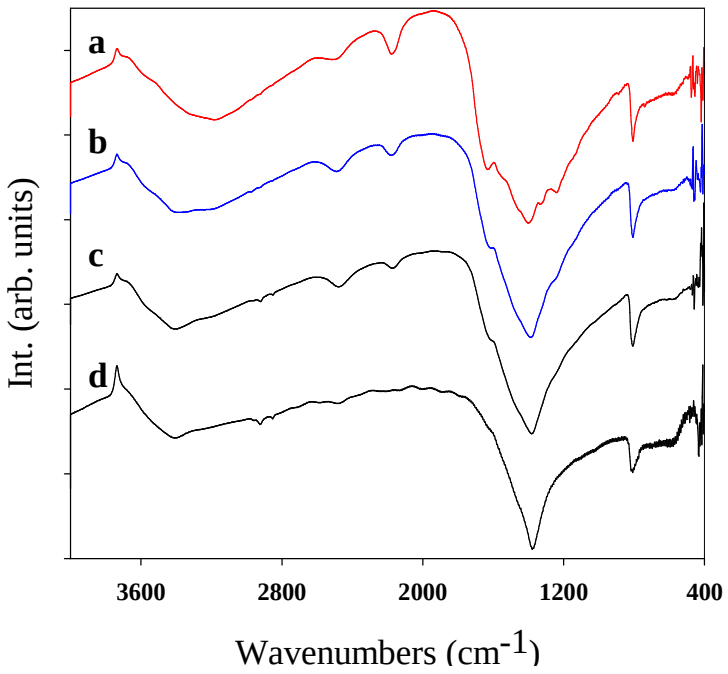

Figure 4.6 - FT-IR spectra of MeOH-washed products a) 1:1 TCM:$NaBH_4$ reaction by Method 1, b) 1:2 TCM:$NaBH_4$ reaction by Method 1, c) 1:3 TCM:$NaBH_4$ reaction by Method 1, and d) 1:3 TCM:$NaBH_4$ reaction by Method 2.

rings.[155,156] The dominant peak near 1400 cm^{-1} is also in the region for B-N or C=C bonds. However, given that the TCM reactant features only C-N bonds, it is more likely that the major peak is from B-N bonds. In his work on graphitic BCN materials, Komatsu suggested that major peak would shift to higher wavenumbers with an decrease in B/N content.[152] This turns out to be the case with the synthesized materials; with an increase in $NaBH_4$ reactant, the major shifts from 1400 cm^{-1} in the 1:1 TCM:$NaBH_4$ reaction to 1378 cm^{-1} in 1:3 TCM:$NaBH_4$ synthesized by Method 2. Therefore, as more B-N bonds are being formed, the ionicity is being increased as carbon content increases and the absorbances shift to a lower wavenumber. This lends credence to the idea that one phase of material is being formed and not a heterogenous mixture of CN_x and BN.

The solid-state ^{13}C CP-MAS NMR spectrum (Figure 4.7a) of the BCN product synthesized by Method 2 has a very broad peak centered at 135 ppm. This region is characteristic of sp^2-bonded carbon in aromatic rings and is consistent with a study performed on pyrolytic carbon blacks,[157] while being slightly higher than that of graphite.[158] This suggests that the carbon environment could be slightly deshielded by

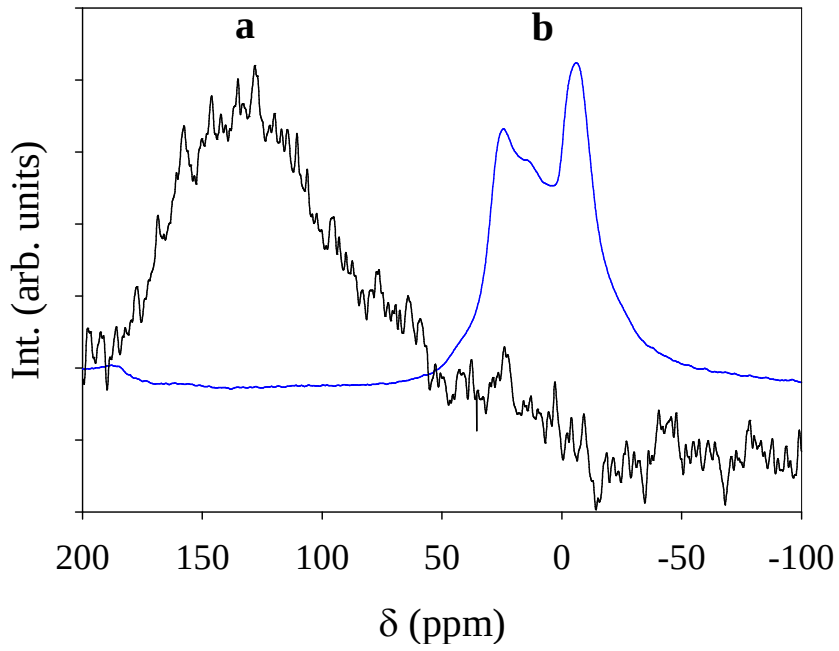

Figure 4.7 - Solid state NMR spectra for 1:3 TCM:$NaBH_4$ reaction by Method 2 a) ^{13}C CP-MAS experiment and b) ^{11}B MAS experiment.

the presence of nearby N atoms and there is carbon incorporation into a BN type structure. The ^{11}B NMR (Figure 4.7b) of the same BCN material shows a pattern that is reminiscent of hexagonal boron nitride.[159] ^{11}B is a nucleus with spin of I=3/2 and possesses a quadrupolar nuclear moment. This means the boron nucleus is very sensitive

to the distortion of the site and that depends on the bonding symmetry of the nucleus. Therefore a MAS experiment can only average part of the quadrupolar interaction for boron in a trigonal planar (such as h-BN) bonding arrangement and this leads to a two-pronged lineshape, whereas boron in a tetrahedral environment (such as c-BN) would lead to a Gaussian lineshape.[160] Chemical shifts also can help determine the bonding environment of boron[161]. The region of 90 to -10 ppm is the observed range for 3-coordinate boron, and 10 to -130 ppm is the observed shift range for tetrahedral boron.[160] The two peaks at 24.3 and -6.2 ppm, as well as the lineshape suggest that the boron environment is a planar, sp^2 arrangement. The fact that the signal is saddled near 0 ppm also suggests that boron is coordinated to carbon and nitrogen. Some boron-doped graphitic materials have been reported as having peaks near zero, whereas h-BN occurs near 30 ppm.[161]

Along with FT-IR and NMR spectroscopic analysis, X-ray photoelectron spectroscopy (XPS) was performed on the products from the 1:3 TCM/$NaBH_4$ reactions synthesized by both Methods 1 and 2. The annealed products were also analyzed by the same method. X-ray photoelectron spectroscopy (XPS) is sensitive to light element chemical environments and has shown utility in investigating carbon nitride structural environments. The technique involves bombardment of the sample with X-ray photons that are high enough in energy to cause ejection of a core electron. It is this core electron that is detected and the energy of the detected electron correlated to a specific element. However, due to scattering of ejected electrons the depth of XPS is limited to 3 nm making this a highly surface sensitive technique. The strength of XPS lies in the fact that it can distinguish different bonding environments for a particular element. It is for this

purpose that the BCN materials were probed, but it can also help to elucidate chemical compositions.

The survey spectra of the four BCN products synthesized by Method 1 and 2, as well as their annealed products are in Figure 4.8. The presence of Na, O, N, C, and B can be found in all four samples. Normally, adventitious carbon is used to calibrate XPS spectra, but since the C 1s region is of interest, the spectra were calibrated to the sodium peak. It was reported that the Na 1s in solid sodium chloride samples is found to occur at a binding energy of 1072 eV.[162] Each element peak was deconvoluted with two peaks, and those two peaks were constrained to have the same FWHM. The calculated percent concentrations and chemical formulas are provided in Table 4.2. Some of the products also were examined by elemental CHN analysis (Table 4.1) and it was found that the N/C ratios were much smaller. There was also 1-3 wt% H residue found within the samples. However, it should be noted that boron nitrides are known for their resistance to oxidation, and do form glassy boron oxides when heated in air. It is quite possible that incomplete combustion could occur and would give false analyses, therefore, the XPS compositions may be closer to the realistic values.

The B 1s, C 1s, and N 1s regions were also scanned for bonding information. In each chemical region were, the peaks selected for deconvolution were constrained to retain the same FWHM as the largest peak. The deconvoluted peaks of the B 1s region are displayed in Figure 4.8 and the C 1s and N 1s regions are in Figure 4.9. In the B 1s region, the peaks were deconvoluted to peaks in four different regions: 187.9-188.1 eV (B1), 188.7-189.1 eV (B2), 190.8-191.2 eV (B3), and 192.1-193.2 (B4). The major peak occurred in the B3 region and was assigned to a BN_3 structure. Given the lower

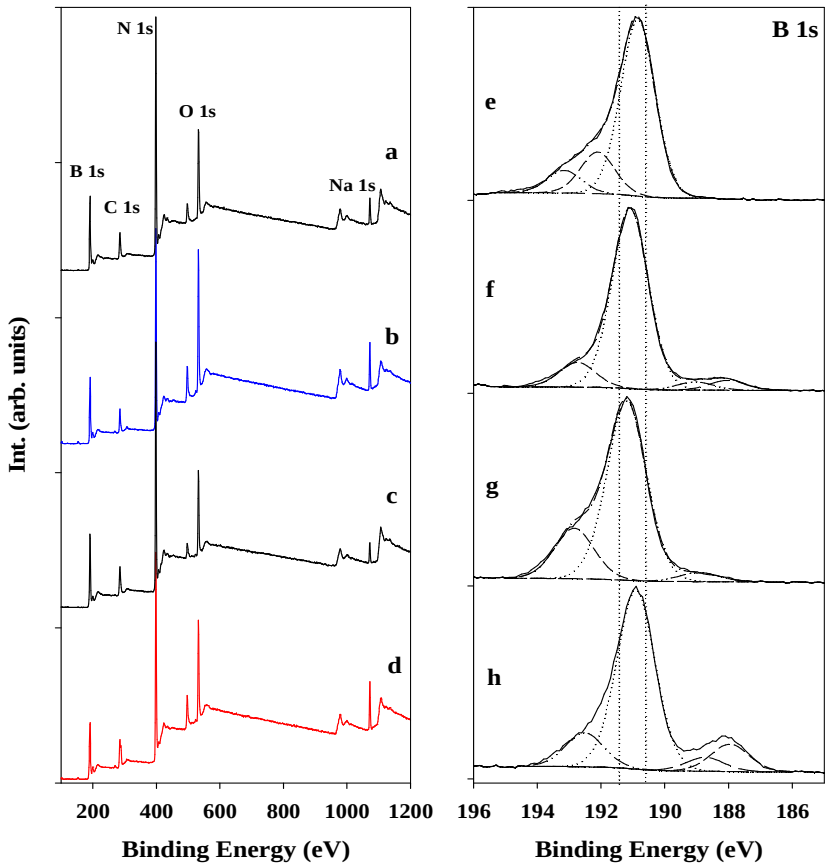

Figure 4.8 - X-ray Photoelectron (XPS) Spectra for a) survey of anneal product from Method 2, b) survey of product from Method 2, c) survey of annealed product from 1:3 $NaBH_4$ reaction by Method 1, d) survey of product from 1:3 $NaBH_4$ reaction by Method 1, e) B 1s spectrum of anneal product from Method 2, f) B1s spectrum of product from Method 2, g) B 1s spectrum of annealed product from 1:3 $NaBH_4$ reaction by Method 1, and h) B 1s spectrum of product from 1:3 $NaBH_4$ reaction by Method 1.

electronegativity difference, it was suggested that B2 could fit well with B-C bonding, and B1 agreed with the values for $NaBH_4$.[163] It is interesting to note that the B1 peaks disappeared in the annealed products. Komatsu reported values for a $B(N\text{-}C)_3$ environment to agree well with region B4.[152] The C 1s region was deconvoluted into five different regions: 283.0-283.3 (C1), 284.9-285.3 (C2), 286.5-286.8 (C3), 287.6-288.2 (C4), and 289.1-290.3 (C5). The C4 and C5 region corresponds well to C-O and C=O

Table 4.2 - Compositional data collected by X-ray photoelectron spectroscopy (XPS).

Element Atomic Percent	1:3 TCM:$NaBH_4$ by Method 1	1:3 TCM:$NaBH_4$ annealed (Method 1)	1:3 TCM:$NaBH_4$ by Method 2	1:3 TCM:$NaBH_4$ annealed (Method 2)
B at. %	36.5	38.4	40.1	39.9
C at. %	14.5	8.6	12.4	10.5
N at. %	35.2	32.9	37.3	37.5
Formula	$B_{2.5}CN_{2.4}$	$B_{4.5}CN_{3.8}$	$B_{3.2}CN_{3.0}$	$B_{3.8}CN_{3.6}$

species.[163] The presence of C1 region can be assigned to some reported C-B bonding environments, and the >C=N- can be a suitable fit for C3. The major peak of C2 was found to be slightly higher than the normal adventitious carbon peak that results from hydrocarbon contamination. Previous reports on BCN materials have shown this to be slightly higher and may be indicative of C-N-B bonds.[152] Three peaks were assigned to the N 1s region: 398.42-398.75 (N1), 399.38-399.55 (N2), 400.59-400.71 (N3). The major peak was N1 and was found to compare well with the work of Komatsu and others on BCN type materials.[155,164] This peak was suggested to be for a B-N-C environment. The N2 peak is in the region for reported nitrile type environments[165,166], and this would agree with the FT-IR data reported for these types of material. The last peak of N3 also agreed with some possible amine (N-H) type environments or possible N-C(O) type environments.[165,166]

Morphological Properties of BCN materials

The BCN materials were imaged by scanning electron microscopy (SEM). It shows that these materials formed by either decomposition method have a glassy

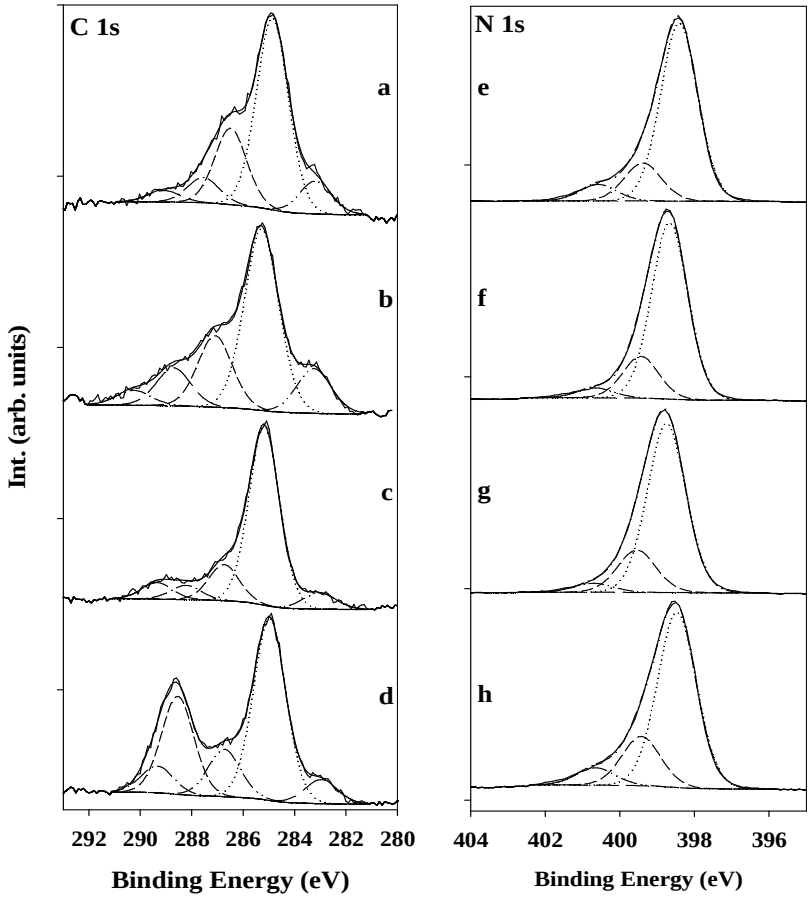

Figure 4.9 - X-ray Photoelectron (XPS) Spectra for a) C 1s spectrum of annealed product from Method 2, b) C 1s spectrum of product from Method 2, c) C 1s spectrum of annealed product from 1:3 $NaBH_4$ reaction by Method 1, d) C 1s spectrum of product from 1:3 $NaBH_4$ reaction by Method 1, e) N 1s spectrum of anneal product from Method 2, f) N 1s spectrum of product from Method 2, g) N 1s spectrum of annealed product from 1:3 $NaBH_4$ reaction by Method 1, and h) N 1s spectrum of product from 1:3 $NaBH_4$ reaction by Method 1.

microstructure with large holes and voids. The structure is reminiscent to that of the TCM decomposition product. On higher magnification, some fused spherical particle morphology is evident on the solid's surfaces (Figure 4.10). The spherical particles range from roughly 100 to 300 nm in diameter. Another type of morphology has a burst vesicle

structure. It appears that some portion of the forming solid burst open, leaving a rough type of opening on the surface. This suggests that gas is indeed being formed and bursting out of the solid. Given the residual gas analysis, it is known that gaseous byproducts are being formed during the reaction. The spherical morphology could be part of the forming solid that bulges but does not burst open.

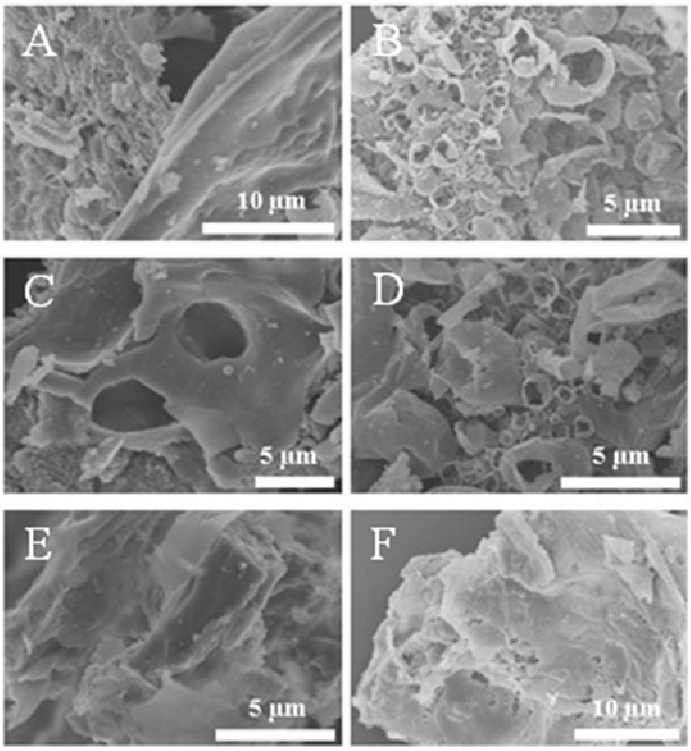

Figure 4.10 - Scanning electron micrographs of A) reaction product from 1:3 TCM:$NaBH_4$ product from Method 1, B) reaction product from 1:3 TCM:$NaBH_4$ product from Method 1, C) reaction product from 1:1 TCM:$NaBH_4$ by Method 1, D) reaction product from 1:2 TCM:$NaBH_4$ product from Method 1, E) annealed reaction product from 1:3 TCM:$NaBH_4$ via Method 2, and F) reaction product from 1:3 TCM:$NaBH_4$ from Method 2.

Thermal stability of the BCN materials

As was noted before, the 1:3 TCM/$NaBH_4$ products were annealed in sealed ampules for 12 hours at 1000 °C with little mass loss. The BCN products are indeed quite thermally stable, but to what extent it is not known. Several experiments were performed via thermogravimetric-differential thermal analysis, by heating under Ar gas at 10 °C/min to 1000 °C. The results are shown in Figure 4.11. For comparison, the TCM-CN_x material completely decomposes near 660 °C (Figure 4.11e). Unfortunately, in all cases, when the products reached approximately 700 °C, they actually began to gain weight. In one case, the experiment actually finished with the sample weighing slightly more than what it started with. This indicated that there may be a small oxygen leak

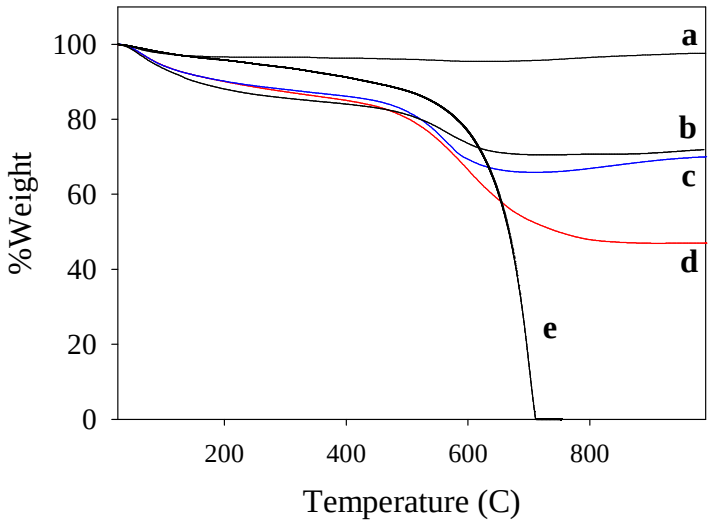

Figure 4.11 - Thermogravimetric analysis (TG-DTA) data for the products a) 1:3 TCM:$NaBH_4$ via Parr reaction, b) 1:3 TCM:$NaBH_4$ via filament reaction, c) 1:2 TCM:$NaBH_4$ via filament reaction, d) 1:1 TCM:$NaBH_4$ via filament reaction, and e) TCM-CNx product via Parr reaction (See Chapter II).

within the system, as the only reason that these types of materials would gain weight is if they are oxidized to form boron oxides. Indeed, when the annealing experiments were performed, weight gain did not occur. When the product from Method 2 was annealed, it showed a very negligible weight loss. This suggests that perhaps the material is "pre-annealed" by the reaction itself. BCN materials require high temperatures or pressures to crystallize, so it is no surprise that the reactions do not yield crystalline products.

Conclusions

This work describes an extremely rapid method to produce boron carbon nitride (BCN) material. The reaction between trichloromelamine and sodium borohydride generates a highly exothermic reaction and results in an amorphous material that begins to crystallize to a graphitic material near temperatures of 1000 °C. XPS analysis showed the material to contains a 2-4 molar excess of B and N when compared to carbon. The decomposition reaction was accomplished by two different methods: rapid heating in an autoclave and rapid initiation by a heated filament. The autoclave method allows for a more sustained reaction and seems to lead to a more annealed product when compared to the filament reaction under the same reactant ratios.

Spectroscopic analysis by XPS, FT-IR, ^{13}C and ^{11}B NMR on the B-C-N products shows data that are consistent with structure containing significant sp^2 bonding character for B,C, and N atoms. XRD also suggests a layered type of structure when the material is annealed at 1000 °C. The annealing process shows negligible weight loss during heating. The morphology of the materials has both smooth and "popped vesicle" structures that may suggest a pathway for the release of H_2 gas that was observed by residual gas analysis.

CHAPTER V

SYNTHESIS OF METAL CYAMELURATES VIA REACTION OF POTASSIUM CYAMELURATE WITH METAL SALTS

Introduction

It was first reported by Redeman and Lucas that the polymer melon [-$C_6N_7(NH_2)(NH)$-]$_n$ would undergo base hydrolysis by aqueous KOH to form the salt, potassium cyamelurate ($K_3C_6N_7O_3$) (Figure 5.1a).[71,104] In Chapter II, it was found that the carbon nitride material synthesized from the decomposition of trichloromelamine (TCM-CN_x) would yield the heptazine based potassium cyamelurate ($K_3C_6N_7O_3$) under base hydrolysis conditions. Kroke et al. reported the synthesis of a series of alkali cyamelurates along with their crystal structures.[111]

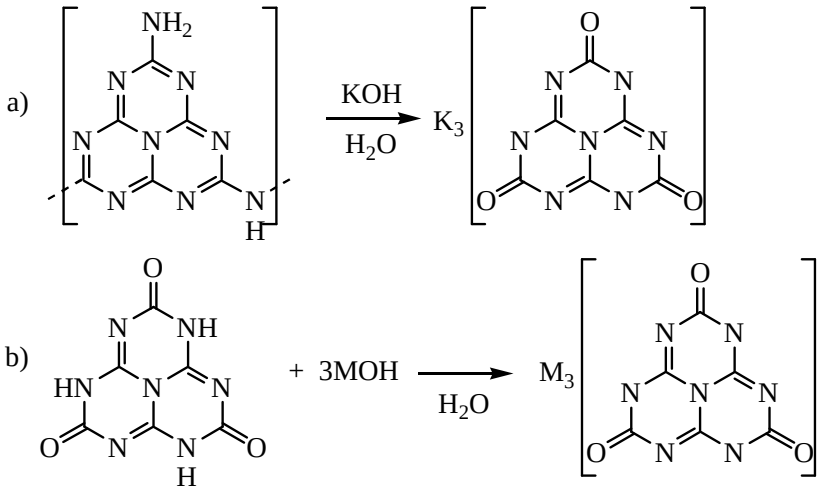

Figure 5.1 - Previously reported synthetic methods of metal cyamelurates. They are formed from a) the with alkali hydrolysis of melon, or b) from reaction of cyameluric acid with alkali hydroxides where M = Li, Na, K, Rb, and Cs.

Kroke formed these new alkali cyamelurates by acidifying the potassium cyamelurate with HCl to form cyameluric acid, then reacting the acid with the corresponding alkali hydroxide, as demonstrated in Figure 5.1b. This family of inorganic heptazines showed high thermal stability as well as interesting optoelectronic properties such as strong absorption in the ultraviolet region (234-307 nm) and high intensity photoluminescence at 369 nm. It was suggested that these materials could act as UV stabilizers in polymeric materials and chemosensor applications.

In the 1970s, Finkel'shtein published some studies on the vibrational spectra of a series cyameluric acid salts with some mono- and bivalent metals (M = K, Na, Ag, Ba, Mg, Pb, Mn, Zn, Co, Fe, Al, Bi, and Cr), as well as their thermal decomposition.[82] These are the only two publications to study cyamelurates containing non-alkali metals. There are several other reported crystal structures of partially hydrogenated alkali cyamelurates, but none involving any other types of metals.[112,167] Therefore, it was hypothesized that the cyamelurate anion might show interesting coordinating properties with transition metals or lanthanides.

This chapter will cover the synthesis of novel metal cyamelurates through a cation exchange reaction with potassium cyamelurate. The FT-IR properties of these materials will be discussed, as well as their thermal properties. An investigation into their composition will be performed through elemental analysis and electron diffraction spectroscopy. The structure of these microcrystalline materials will also be explored through powder X-ray diffraction and a preliminary structure solution of the Cu^{2+} salt elucidated from powder data will be discussed.

Experimental

Reagents

The following reagent were purchased from Alfa Aesar and were used as received: vanadium (III) chloride (VCl_3, anhydrous, 95%), iron (III) chloride ($FeCl_3$, anhydrous, 98%), nickel (II) chloride ($NiCl_2$, anhydrous, 99%), copper (II) chloride ($CuCl_2$, anhydrous, 98%), lanthanum (III) chloride ($LaCl_3$, anhydrous, 99.9%), and cobalt (II) chloride ($CoCl_2$, anhydrous, 99.7%). The following reagents were purchased from Aldrich and were used as received: chromium (III) chloride hexahydrate ($CrCl_3 \cdot 6H_2O$), iron (II) chloride tetrahydrate ($FeCl_2 \cdot 4H_2O$, 99%), zinc (II) chloride ($ZnCl_2$, 98%), copper (II) chloride dihydrate ($CuCl_2 \cdot 2H_2O$, 99+%), zinc (II) nitrate ($Zn(NO_3)_2$), and nickel (II) chloride hexahydrate ($NiCl_2 \cdot 6H_2O$). Manganese (II) chloride ($MnCl_2$, anhydrous, 95%) and cerium (III) chloride ($CeCl_3$, 99.9%) were purchased from Cerac and used as received. Copper (II) nitrate hemipentahydrate ($Cu(NO_3)_2 \cdot 2.5H_2O$, 99%) and nickel (II) nitrate hexahydrate ($Ni(NO_3)_2 \cdot 6H_2O$, 99.9%) were purchased from Strem and used as received. The following were purchased from Sigma-Aldrich and were used as received: ammonium thiocyanate (NH_4SCN, 97.5+%), and acetone (99.5 %,ACS grade). Methanol (ACS grade), pentane (ACS grade), concentrated HCl (37%), sodium hydroxide (NaOH), and potassium hydroxide (KOH) was purchased from Fisher Scientific and were used as received. The remaining reagents were purchased as follows: copper (II) acetate ($Cu(C_2H_3O_2)_2 \cdot 2H_2O$, Mallinckrodt) and 14.8 M ammonium hydroxide (NH_4OH, EM Science).

Synthesis of melon, [-$C_6N_7(NH_2)(NH)$-]$_n$

The following procedure is based on a previously reported synthesis of melon.[91] A large, glazed, ceramic crucible was charged with 400 g (5.26 mol) of NH_4SCN. The colorless crystalline solid was heated to 315 °C via heating mantle for four hours. The solid melted to a pale yellow liquid near 200 °C and began bubbling near 230 °C. A white vapor accompanied the boiling, as well as a sulfurous odor. After approximately 40 minutes, a gummy, yellow solid began forming. The solid began to further harden, so it was broken up with a spatula and the temperature was raised to 325 °C for 18 hours. At this point, no appreciable amounts of white vapor were being generated, so the yellow solid was cooled to room temperature.

Once cooled, the yellow crude melon was crushed into a fine powder with a ceramic mortar and pestle. The solids were aliquoted into two large Schlenk tubes which were fitted with gas inlet adapters and sidearms to accompany any evolved gases. Under a flow of nitrogen, the tubes containing the crude material were annealed at 400 °C for 20 hours. The annealing generated a significant amount of white transport material at the gas outlet, along with a small amount of orange and yellow transport products. Once cooled, the crude melon had turned a yellow-tan color. The purification steps proceeded as follows: the annealed melon was 1) reground and 2) boiled in 500 mL of deionized H_2O for 25 minutes then isolated via vacuum filtration, 3) the wet solid was boiled for 15 minutes in 500 mL of 12 M HCl then filtered, 4) the wet solid was heated at 50 °C for 15 minutes in 500 mL of 3M KOH(aq) solution then filtered, 5) the wet solid was washed in 1000 mL H_2O for 15 minutes then filtered, 6) the solids were rinsed three times with

diethyl ether. The solids were dried in 130 °C oven overnight. A mass of 75.3 g of purified melon was isolated. Yield: 86%

Synthesis of potassium cyamelurate ($K_3C_6N_7O_3$)

A 2000 mL round bottom flask was charged with 74.8 g of purified melon. The melon was suspended in 1000 mL of a 3M KOH solution and boiled in air for 90 minutes. After 1 hour, the suspension had turned a clear amber color. Ten minutes later, a precipitate began forming, so the flask was cooled to room temperature. The pale yellow needles were collected by vacuum filtration, and a second batch of yellow needles formed immediately in the filter flask. The second batch was collected and clear filtrate was concentrated to approximately 50% of its original volume. A third batch of solids was collected upon cooling the concentrated solution.

All three fractions of crude potassium cyamelurate were suspended in 800 mL of hot, deionized H_2O. 5 g of decolorizing charcoal was added and the cloudy mixture was stirred for 30 minutes. After filtering, the resultant pale yellow solution was boiled to reduce the volume. Once a precipitate began to form, more H_2O was added to redissolve it and the clear solution was slowly cooled to room temperature. A large amount of colorless needles formed and were collected by filtration. Three more cycles of concentrating the filtrate and forming crystalline products resulted in four fractions of potassium cyamelurate. The crystalline materials were washed in 300 mL absolute ethanol for two hours. A mass of 62 g of potassium cyamelurate trihydrate ($K_3C_6N_7O_3 \cdot 3H_2O$) was collected in a yield of 51%.

The potassium cyamelurate recovered from the base hydrolysis of melon was recrystallized by the method reported by Kroke.[111] A large amount of the crude material

was dissolved in a minimum amount of deionized water. Acetone was added dropwise to the clear colorless solution until a slightly cloudiness persisted. The cloudy solution was allowed to sit undisturbed overnight. Colorless needles were collected by filtration.

Metal cyamelurates formed via exchange of potassium cyamelurate with metal chlorides

The metal salts were synthesized according to the following general procedure. The metal chloride (1 or 1.5 mmol) was placed in a 100 mL Schlenk flask, and the potassium cyamelurate (0.39 g, 1 mmol) was placed in a 250 mL Schlenk flask. 18 MΩ water was placed in a graduated cylinder and degassed with nitrogen for at least 20 minutes. In the meantime, each flask was attached to the Schlenk flask and purged with nitrogen. Into each flask was placed 50 mL of degassed H_2O. The metal chloride solution was transferred to the clear potassium cyamelurate solution at a rate of 3 drops per minute. The suspensions were stirred for 30 minutes under N_2, then vacuum filtered in air. The filter cakes were rinsed three times with 30 mL of DI H_2O. The recovered products were dried in air for two days. A summary of the reactions performed can be found in Table 5.1.

Metal cyamelurates formed via exchange of potassium cyamelurate with metal nitrate salts

The general procedure for the metal cyamelurate synthesis with non-chloride metal salts was as follows. A mass of 0.13 g (0.32 mmol) potassium cyamelurate was dissolved in 50 mL H_2O in air. The metal nitrate (0.48 mmol) was dissolved in 5 mL H_2O. While stirring, the aqueous metal salt solution was slowly dripped into the

Table 5.1 - Summary of metal chloride reactions with potassium cyamelurate.

Metal Chloride	$K_3C_6N_7O_3$:MC mole ratio	Product Appearance	Recovered amt. (g)
$CrCl_3 \cdot 6H_2O$	1:1	Gray	0.31
VCl_3	1:1	Dark Green	0.29
$MnCl_2$	1:1.5	Cream	0.36
$FeCl_2 \cdot 4H_2O$	1:1.5	Orange	0.36
$NiCl_2$	1:1.5	Pale Green	0.33
$CuCl_2$	1:1.5	Pale Purple	0.38
$LaCl_3$	1:1	White	0.43
$CeCl_3$	1:1	White	0.46
$FeCl_3$	1:1	Reddish Brown	0.18
$CoCl_2$	1:1.5	Gray	0.38
$ZnCl_2$	1:1.5	White	0.37 (scaled)

potassium cyamelurate solution at rates of approximately a drop every 10-15 sec. The suspensions were stirred for at least one hour, followed by vacuum filtration to collect the products. The products were rinsed three times with 10 mL H_2O and dried overnight in air.

Recrystallization attempts of copper and nickel cyamelurate

Attempts were made to recrystallize the nickel and copper cyamelurate precipitates from the previous section by dissolving the precipitates in mixtures of concentrated ammonium hydroxide and slowly precipitating on addition of methanol but not single crystals could be recovered. A second series of recrystallization attempts were made by diffusing methanol vapors into an ammonium hydroxide solution of metal

cyamelurates. Only bluish violet precipitates were obtained for copper and aggregated green needles formed for the nickel salt.

Sample preparation for structure solution of metal cyamelurate

The samples explored were potassium cyamelurate and copper cyamelurate derived from reaction of potassium cyamelurate with copper nitrate. Ten to twenty milligrams of the sample were ground together with a nonpolar solvent, such as pentane or hexanes. An internal standard of lanthanum hexaboride (LaB_6) or silicon (Si) was ground together with the sample. The samples were mounted on a zero background holder with a small smear of grease. In order to ensure a random orientation of the powder, the powders were dropped onto the holder with a spatula. The holder was shaken to remove excess powder. A PXRD step scan (0.01 deg/step) was performed from 5-60 ° two theta. The data was indexed using the profile fitting program, XFIT,[168] in conjunction with the indexing program, Crysfire[169]. The structural model was developed by the FOX program.[170]

Instrumentation

Thermogravimetric-differential analysis (TG-DTA) was performed on a Seiko ExStar 6300 system under flowing argon. FT-IR absorption spectra were taken with a Nicolet Nexus 670 spectrometer using KBr pellets. Elemental analyses were performed on a Perkin Elmer 2400 CHN/O Analyzer using ultra light weight, ultra clean tin capsules. Powder X-ray diffraction was performed on a Siemens D5000 X-ray diffractometer, using Cu K_α radiation on samples mounted on glass slides with double-sided tape. Scanning electron microscopy (SEM) was performed on a Hitachi S-4800

SEM with samples mounted on Al stubs and coated with Au-Pd alloy. Electron diffraction spectroscopy (EDS) was performed on Hitachi S-3400N with samples on Al stubs affixed with carbon tape and coated with carbon.

Results and Discussion

Conversion of ammonium thiocyanate to melon

The chemical transformations occurring during the heating of NH_4SCN involve isomerization of NH_4SCN to form thiourea ($CS(NH_2)_2$) near 170 °C followed by thiourea decomposing into hydrogen sulfide (H_2S), carbon disulfide (CS_2), ammonia (NH_3) and guanidine thiocyanide ($NHC(NH_2)_2 \bullet HSCN$) near 200 °C.[171] The formation of H_2S gave rise to a distinctive rotten egg type odor. At 300 °C guanidine has been shown to cyclize, forming melamine (1,3,5-triamino-*s*-triazine, $C_3N_3(NH_2)_3$).[172] Therefore it is likely that during heating the guanidine thiocyanide intermediate begins to cyclize forming melamine-like intermediates which, upon extended heating at 300 °C and annealing at 400 °C further cyclize and polymerize to form crude melon. As mentioned before in Chapter II, similar chemistry was observed when heating melamine at 450 °C[90] or $H[C_3N_3](N=CH-NH-CN)_2$ at 400 °C[87] producing melem or *s*-heptazine, respectively.

Following the changes in vibrational modes by FT-IR shows readily identifiable functional group transformations as the synthesis moves from NH_4SCN to melon. The spectrum of NH_4SCN shows the sharp bands indicative of a molecular species. Specifically bands are seen at 3131 cm^{-1} (N-H), 2050 cm^{-1} (S=C=N), 1661 cm^{-1} (C=N) and 1403 cm^{-1} (C=S). In contrast, the spectrum of purified melon shows losses of the S-based vibrations followed by the intoduction of two broad bands in the NH stretch region

(3300-3000 cm^{-1}) and the C-N and C=N region (1640-1300 cm^{-1}). This broadening is indicative of the disordered, polymeric nature of the material.

Conversion of melon to potassium cyamelurate

The reaction of melon with $KOH_{(aq)}$ to generate potassium cyamelurate is analogous to reactions performed in Chapter II, and have been previously reported.[88,89,91,93,111-113] There are only two reagents under simple reflux conditions, then once the reaction is complete and slowly cooled beautiful, needle shaped crystals grow directly out of the reaction mixture. The one nuance seems to be related to reaction rate. If KOH concentration is too high (> 2.5M) and/or reflux temperature is too high (> 150 °C) and/or heating time is too long (> 2 hrs) one only generates the triazine species melamine, $C_3N_3(NH_2)_3$. This is similar to the chemistry observed by Rathke when melamine was formed upon heating melem in aqueous ammonia.[173]

Conversion of potassium cyamelurate to metal cyamelurate precipitates

The synthesis of novel metal cyamelurates involved a simple double displacement reaction allowing for the balance of potassium chloride (KCl) formation as the byproduct. The stoichiometric ratios were based on either divalent of trivalent metal chlorides and can be seen in Equation 5.1 and 5.2 respectively. Since the reported alkali cyamelurates showed the inclusion of water molecules into their crystal structures, it was expected that the same would occur for these types of materials. A survey of water-stable first row

$$K_3C_6N_7O_3\text{-}3H_2O + 1.5MCl_2 \rightarrow M_{1.5}C_6N_7O_3\text{-}xH_2O + 3KCl \quad \text{(Equation 5.1)}$$

$$K_3C_6N_7O_3\text{-}3H_2O + MCl_3 \rightarrow MC_6N_7O_3\text{-}xH_2O + 3KCl \quad \text{(Equation 5.2)}$$

transition metal chlorides was performed along with two lanthanides (La and Ce). During the reaction, the mixtures began to turn cloudy once the metal chloride solution was added to the clear potassium cyamelurate solution. In the case of the transition metals, colored precipitates would form out of solution while white precipitates formed from the lanthanides, as well as zinc and manganese. This would make sense from the fact that the transition metal cations, except for zinc, contain unfilled d-orbitals and these tend to show absorbances in the visible region of the spectrum. Lanthanum, cerium and zinc cations all contain filled d-orbitals and no transitions should occur in the visible region. Manganese is normally in a high spin configuration in an octahedral field and gives spin and parity-forbidden transitions, thus accounting for very pale colors.[174] The alkali cyamelurates were all reported as being on soluble in water[111], while these new metal exchanged materials immediately crashed out of an aqueous solution. The filtrates were also tested for pH; all showed neutral values (pH = 7) except for the reaction with $LaCl_3$, which showed a pH of 10. All filtrates were also noted for color; the only colored filtrate was from the reaction with $CrCl_3 \cdot 6H_2O$ and it had a bluish-green tint to it. This filtrate was dried by evaporation and only showed peaks for KCl by powder X-ray diffraction. This is also a proof of concept by showing that the byproduct KCl is forming during the reactions.

Compositional analysis of metal cyamelurate precipitates

The composition of these precipitates was explored by elemental analysis, as well as energy dispersive spectroscopy. A summary of the CHN analysis is shown Table 5.2. Each analysis was performed three times to obtain an average, and a formula was calculated, based on the heptazine ring. According to the calculated values, the metal

cyamelurate precipitates all exhibit the appropriate molar ratio of N/C (1.167) for heptazine, within 2.8% error. If it assumed that all hydrogen content comes from water, an estimate of the amount of hydration can be made about the precipitates. This type of assumption should be approached cautiously, because any protonation of the heptazine would alter the expected amount of hydration.

Table 5.2 - Summary of results from CHN analysis of metal cyamelurates.

Metal	Wt% C	Wt% H	Wt% N	Wt% Diff.	Mol C	Mol H	Mol N	Calc. Formula
Cr(III)	21.94	2.14	29.66	46.26	1.83	2.13	2.12	$C_6N_{6.95}H_{6.98}$
V(III)	19.78	1.83	26.84	51.55	1.65	1.81	1.92	$C_6N_{6.98}H_{6.58}$
Mn(II)	18.03	2.06	24.55	55.36	1.50	2.05	1.75	$C_6N_{7.00}H_{8.20}$
Fe(II)	17.00	2.08	23.20	57.73	1.42	2.06	1.66	$C_6N_{7.01}H_{8.70}$
Ni(II)	16.22	2.97	22.02	58.80	1.35	2.94	1.57	$C_6N_{6.98}H_{13.07}$
Cu(II)	18.05	1.78	24.59	55.58	1.50	1.77	1.76	$C_6N_{7.04}H_{7.08}$
La(III)	14.32	2.46	18.92	64.30	1.19	2.44	1.35	$C_6N_{6.81}H_{12.30}$
Ce(III)	14.37	2.36	19.27	64.00	1.20	2.34	1.38	$C_6N_{6.90}H_{11.70}$
Fe(III)	15.51	2.35	20.76	61.38	1.29	2.33	1.48	$C_6N_{6.88}H_{10.84}$
Co(II)	17.14	2.44	22.88	57.53	1.43	2.42	1.63	$C_6N_{6.84}H_{10.15}$

The metal contents were also explored by energy dispersive spectroscopy; the results are exhibited in Table 5.3. Upon scanning the spectra, it was found that many of the synthesized precipitates showed unusually high amounts of potassium remaining in the solids. The metal-to-potassium molar ratios were then calculated from the data. The precipitates showing the highest amounts of potassium were Cr, Mn, Cu, Fe, and V. This suggests that incomplete cation exchange is occurring for many of the reactions. Another

issue of note is the presence of only small amounts of residual Cl in the structures. Mapping of the materials only showed the elements dispersed throughout the material and were not localized to any particular structures in the material.

Table 5.3 - Summary of results from energy dispersive spectroscopy.

Metal	M wt %	K wt %	O wt %	N wt %	C wt %	Cl wt %	M/K*
Cr(III)	10.01	6.83	36.38	31.91	14.56	0.42	1.10
V(III)	25.72	5.78	25.75	25.72	11.93	0.41	3.41
Mn(II)	20.50	10.50	22.34	20.47	10.39	0.36	1.39
Fe(II)	21.54	6.76	19.33	13.30	10.48	0.32	2.23
Ni(III)	23.63	0.88	39.62	29.57	15.29	0.39	17.82
Cu(II)	31.76	11.14	15.61	15.10	7.36	1.15	1.75
La(III)	27.72	1.55	20.09	19.88	22.39	0.60	5.05
Ce(III)	26.62	1.23	35.88	34.40	16.11	0.35	6.05
Fe(II)	38.29	0.69	38.25	24.74	10.46	0.33	38.67
Co(II)	30.25	0.93	33.98	25.13	11.45	0.39	21.66
Zn(II)	39.06	0.68	28.32	28.73	11.18	0.43	34.17

* calculated metal-to-potassium molar ratio

Thermal stability of metal cyamelurate precipitates

Using the thermogravimetric-differential thermal analysis (TG-DTA), the thermal stability of the metal cyamelurates were probed. Since the reactions were performed in H_2O as a solvent, any low temperature weight loss events that occur should be most likely attributed to the loss of water from the structures. Preliminary studies showed early weight losses to occur below 300 °C. Therefore, precipitates were heated at 300 °C

for 2 hours in the TG-DTA in order to characterize the amount of H_2O present in the precipitates. A second experiment was also performed by heating under an air atmosphere to 1000 °C in order to determine the amount of metal oxide present in the material.

The dehydration experiments showed that all the metal cyamelurate precipitates were dehydrated in the range of 116-263 °C. The two lanthanide cyamelurates (La and Ce) showed the earliest losses, while the early transition metal cyamelurates (Cr and V) showed the highest temperatures of dehydration (263 and 242 °C, respectively). This

Table 5.4 - A summary of the thermal stability of metal cyamelurate precipitates.

Metal	**Dehyd. Temp. (°C)**	**Dehydration Wt % loss**	**Wt % H_2O[a]**	**Dehydrated Color**	**Decomposition Temp (°C)**	**Metal oxide post-TGDTA**
Cr(III)	263	22.0	19.18	blue-gray	477	Cr_2O_3
V(III)	242	20.0	16.31	moss green	512	Mix K-V-O[b]
Mn(II)	133, 194	22.5	18.46	tan	542	$K_{0.5}Mn_2O_4$
Fe(II)	162	23.5	18.56	orange-brown	466	Fe_2O_3
Ni(II)	181	26.0	26.49	tan	519	NiO
Cu(II)	180	21.1	15.94	green-brown	532	CuO
La(III)	135	24.2	21.98	pale yellow	578	La_2O_3
Ce(III)	119	24.0	21.08	white	522	CeO_2
Fe(III)	116	25.2	20.99	dark gray	526	Fe_2O_3
Co(II)	158	21.8	21.80	purple	421	CoO
Zn(II)	133	21.7	N/A	white	471, 696	ZnO

[a] The weight percent H_2O was calculated from CHN analysis.

[b] a mixture of of potassium vanadium oxides were found by XRD.

suggests the water may be more tightly bound to the these early transition metals versus the larger lanthanide metals. Manganese also showed a second dehydration at 194 °C, suggesting that some of the waters present are coordinated more strongly than others. The percentage of water lost for each metal cyamelurate measured from the TG-DTA data was slightly larger than the calculated weight % of H_2O from elemental analysis. This suggests that there may still be a significant amount of adsorbed water on the surfaces of the material. Another matter to address is the color change that occurred during the dehydration processes. For instance, the gray cobalt cyamelurate powder becomes a bright purple color, and the copper material turns a greenish brown color. These changes suggest that the coordination sphere is changing during the dehydration step. Structurally speaking, the water in the precipitates are most likely bound to the metals present.

The decomposition of these materials occurred between 421 and 578 °C in an air atmosphere. Finkel'shtein, *et al.* reported the decomposition of his reported cyameluric acid salts to occur in the 420-540 °C range, so the values reported here are in good agreement.[82] The DTA signals showed very sharply exothermic peaks at the decomposition point, and were accompanied by an oddly shaped TG curve. This suggests that the decomposition is a very violent process, and is generating enough heat to significantly raise the entire sample temperature beyond the normal heating rate.

Powder XRD of the final decomposition products revealed the presence of crystalline metal oxides. The matched patterns of these oxides can be found in Table 5.4. One thing to note is the products recovered from the oxidation of the Mn(II) and V(III) cyamelurates. These species did not generate the most stable metal oxides Mn_3O_4 or

V_2O_5, respectively. Instead, the patterns were matched to potassium-containing metal oxides. This is in agreement with the results of the EDS study, which indicated the presence of siginificant amounts of potassium in the manganese and vanadium cyamelurates. The other cyamelurates with high amounts of potassium may also have it present in the decomposition products; however, the limitation of XRD is that it only reveals crystalline materials. If any K-containing oxides are present, they would have to be amorphous and indeteminate by this method. Since it is known that these precipitates contain potassium, then it is difficult to calculate the weight percent of metal from the decomposition data.

Structural analysis of the metal cyamelurates

The FTIR data of the as-synthesized materials can be found in Figure 5.2. There are several similarities between the spectra of each metal cyamelurate precipitate. Each spectra shows broad peaks in the 3500-3100cm-1 region, a series of absorbances in the 1700-1100 cm-1 region, as well as a sharp peak near 800 cm-1. The higher frequency peaks. Peaks in the 3500-3100 cm-1 region are indicative of either the O-H stretch from the presence of H2O in the structure or from the N-H from a protonated cyameluric core. In order to differentiate between the two types of stretching modes, the dehydrated materials from the thermal stability experiments were subjected to FTIR study. It was found that upon dehydration, the absorbances near 3500 cm-1 were reduced in intensity. This suggests that these absorbances are related to the coordinated waters. Several low frequency peaks (<1000 cm-1) as well as a sharp peak centered at 1150 cm-1 were also reduced in intensity. These are regions associated with the O-H vibrations of reported

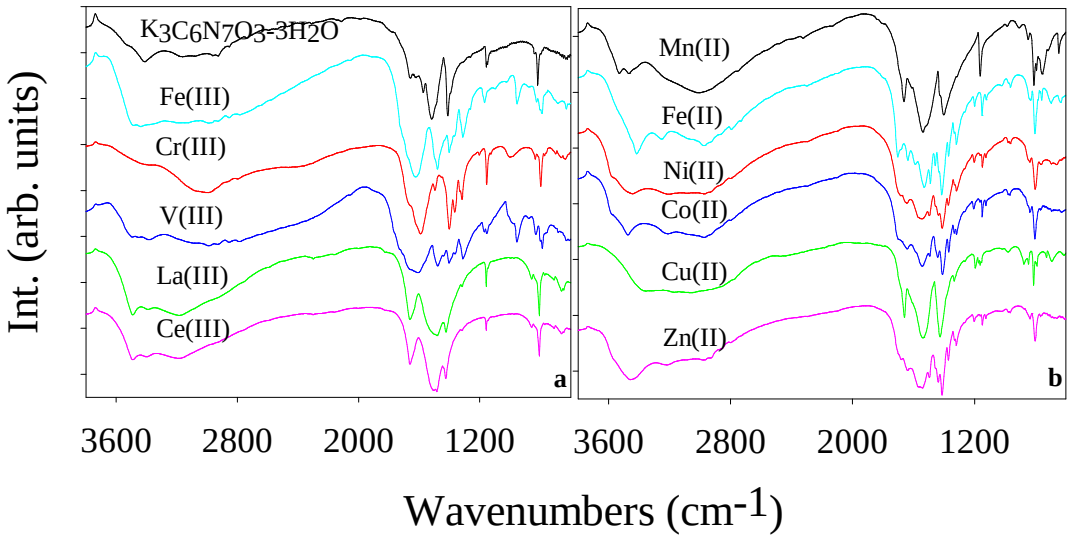

Figure 5.2 - FTIR spectra of a) potassium cyamelurate and trivalent metal cyamelurates, and b) divalent metal cyamelurates.

aquo complexes.[175] In all the dehydrated materials, there was still a broad absorbance near 3200 cm^{-1}; this peak could not be unambiguously assigned to an N-H stretch.

The stretch near 800 cm^{-1} has been described in previous chapters as the out-of-plane bending of the heptazine core. This absorbance indicates the presence of the cyamelurate anion in all the metal precipitates. There also three other major absorbances the agree with the other reported cyamelurates: 1660-1640 cm^{-1}, a peak in the 1540-1480 cm^{-1} region, and a peak in the 1425-1400 cm^{-1} region.[111,112] The presence of any other peaks is somewhat less straightforward. For example, the peaks for vanadium and iron(III) cyamelurate are slightly different from the other spectra; they show peaks at ~1615, 1478, 1400, and 1310 cm^{-1}. The additional peaks could not be identified. In general, when the samples are dehydrated, these three peaks are still present, though some slight shifting of the peak positions does occur.

Powder XRD experiments were also performed on the metal cyamelurate precipitates. The patterns are exhibited in Figure 5.3. It was immediately noticed that the synthesis conditions generated crystalline materials directly from precipitation. These patterns did not show any similarity with the previous reported alkali cyamelurates. Despite this, the patterns did show some self-consistency. For example, some of the metals that were neighbors to each other showed very similar patterns. The patterns for lanthanum and cerium cyamelurate are quite similar, as are the following pairs: Cr(III)/V(III), Ni(II)/Zn(II), and Mn(II)/Fe(II). This would be expected, given that cations should have very similar ionic radii, and the crystal packing would be very similar. With the current configuration of the diffractometer, there has been trouble collecting spectra for Co(II) and Fe(III). It is possible that there is some fluorescence is occurring, leading to higher-than-normal backgrounds in the patterns. It is difficult to tell, but there may be some similar peak position in the Co(II) sample with those of the higher intensity peak in Ni(II) and Zn(II).

The structures of the Cu, Ni, and Zn cyamelurates were also further explored by repeating the syntheses of these materials with different metal salts. It was wondered if there might be any effect on the structure by the anion present in solution. In the case of copper, the reaction was repeated with copper nitrate ($Cu(NO_3)_2 \cdot 2.5H_2O$) and copper acetate ($Cu(O_2CCH_3)_2 \cdot 2H_2O$). The nickel and zinc reactions were repeated with their respective nitrates, $Ni(NO_3)_2 \cdot 6H_2O$ and $Zn(NO_3)_2$. The resulting XRD powder patterns are shown in Figure 5.4. It was found that all of the Cu(II) salts produce very similar powder patterns. The reactions with zinc and nickel nitrate also provided similar patterns as well (See Figure 5.4b). When compared the Zn and Ni cyamelurates as well as the

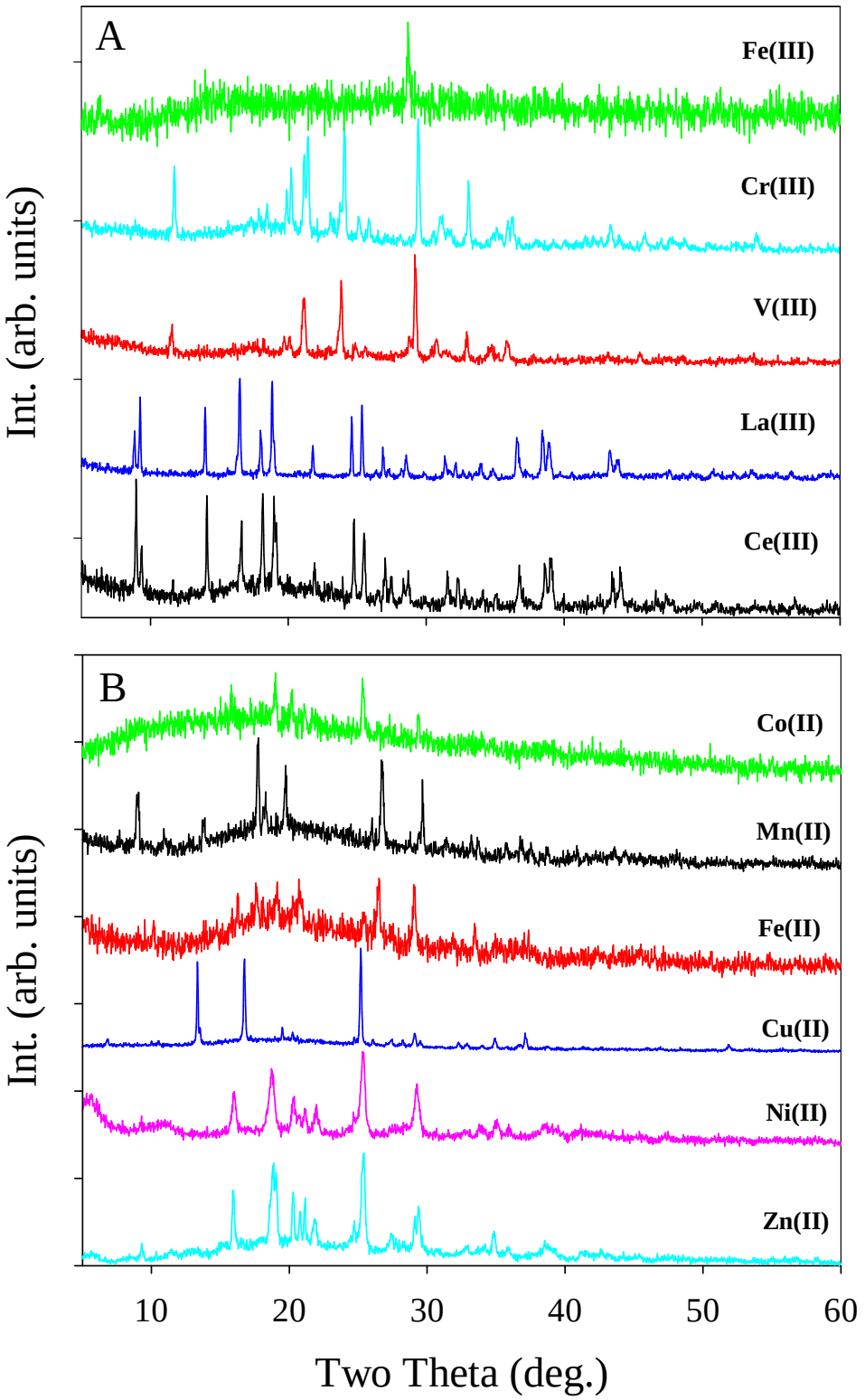

Figure 5.3 - Powder X-ray diffraction patterns for A) trivalent metal cyamelurates and B) divalent metal cyamelurates.

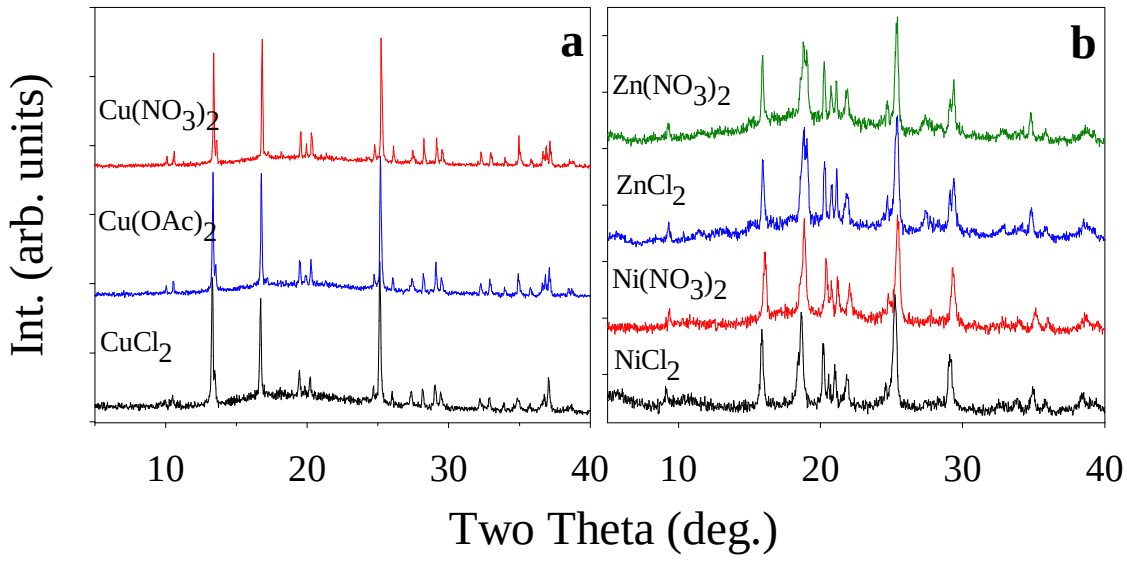

Figure 5.4 - Powder X-ray diffraction patterns of a) reaction products from different Cu(II) salts; b) reaction products from different Zn(II) and Ni(II) salts.

other metal species, the copper cyamelurate species showed very sharp peaks, with a high signal-to-noise ratio; this suggested a very well ordered crystal packing.

There several attempts to recrystallize the Cu and Ni precipitates from aqueous ammonia, THF, and DMF. Unfortunately, no large crystals were available for single crystal analysis. Therefore, attempts were made to solve the structure from powder XRD data. Structure solution from powder data has made many leaps in the past ten years, with the number of structures being solved in this fashion increasing significantly. The general process for solving the structure is as follows: 1) collection of a high quality powder pattern; 2) profile fitting to determine exact peak positions 3) indexing and space group determination to elucidate the lattice parameters of the unit cell; 4) ab initio structure determination using specially design computer algorithms; and 5) refinement of the structure. It was thought that these methods may be amenable to the structure

solution of the copper cyamelurate for the sole reason that cyamelurate anion is, for the most part, a rigid body. The most important factor, then, is determining the appropriate ratio of components in the unit cell, i.e. number of copper cations, number water molecules, etc. It also helps that previous cyamelurate structures have by solved by single crystal data. Therefore, we can take the same material and try to resolve the structure from its powder data, while concurrently trying to solve the unknown copper cyamelurate. The methods will be briefly addressed in a step-by-step manner.

Powder data collection

A high quality data set requires very long scanning times (12-14 hours). This is due to the very short scanning steps (0.01 ° 2θ) and the long scan times at each step (10-

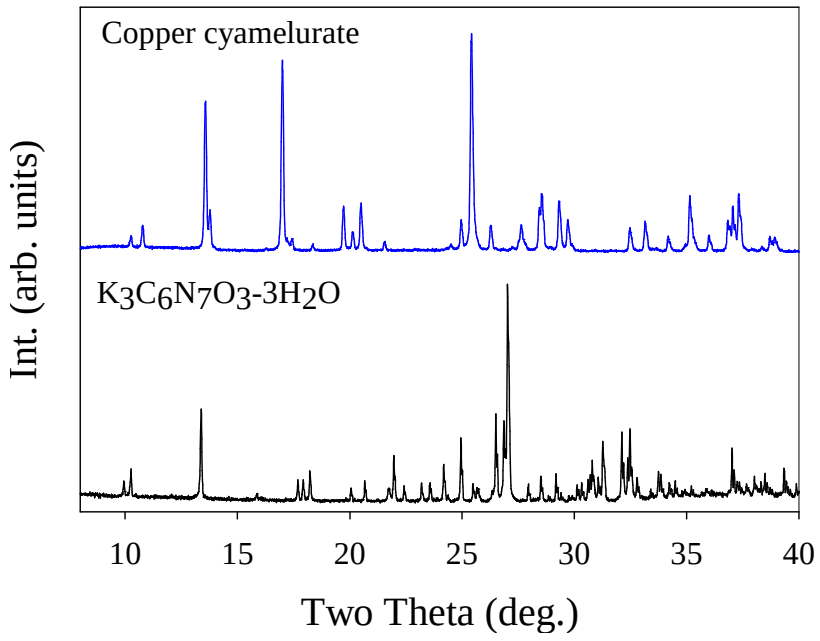

Figure 5.5 - High quality powder patterns of copper cyamelurate and potassium cyamelurate ($K_3C_6N_7O_3 \cdot 3H_2O$).

15 sec). This pattern needs to generate very precise peak positions so a well calibrated system is necessary. If this is a concern, then an internal standard can be used to later calibrate peak positions; the most popular are silicon (Si) or lanthanum hexaboride (LaB_6). Another concern is preferred orientation of the powder. If the powder has either needle-shaped or plate-like crystallites, then they tend to diffract X-rays in a particular direction that alters the intensity of the peak at that particular reflection. Therefore, a completely random orientation of the powder is absolutely necessary. This can be accomplished by grinding the powder in a nonpolar solvent, i.e. wet grinding. This tends to lead to a narrow distribution of particle sizes in a random orientation. In addition to wet grinding and internal standards, a zero background holder (ZBH) was used. The ZBH is a piece of silicon cut along a certain plane and affixed to a standard sample holder. The silicon acts to diffract any X-rays away from the detector, so there is no contribution to background from the sample. This leads to high signal-to-noise ratio in the powder patterns. The results of the collected powder patterns can be found in Figure 5.5.

Profile fitting

Profile fitting of the peaks occurs in the computer program *XFIT*.[168] The program employs curve-fitting procedures to generate precise peak positions. There are several peak shapes that can be used to fit these curves; for example, the curve-fitting procedures in X-ray photoelectron spectroscopy (XPS) employ a Gaussian-Lorentzian peak (as used in Chapter IV). However these often have no experimental basis. One of the peak shapes employed in the *XFIT* program is the fundamental parameters (FP) method.[168] It uses the geometry of the diffractometer to calculate the peak shape. Therefore, if the X-ray

configuration are known for a particular instrument, then a peak shape can be modeled based on that knowledge. Since peak widths can be constrained, deconvolution of overlapping peaks can be elucidated. The Cu Ka radiation can also be modeled to reflect peak splittings that occur at higher 2θ angles. Armed with these computations, a list of peak positions can be generated.

Indexing

A rule of thumb in the art of indexing is that at least 20 peak positions are needed to index a powder pattern to a particular unit cell. The most important peaks are the first lines, which unequivocally describe the unit cell parameters. Therefore, the first 20-25 peak positions from *XFIT* can input into indexing software to calculate possible unit cells. A popular indexing suite is *Crysfire*.[169] This simple program compiles eight different indexing programs into one, and is able to generate a set of possible unit cells matching the provided peak positions. There are two parameters that indicate the quality of a particular solution: the number of indexed lines, and the figure of merit. A good solution will use all the inputted lines and the figure of merit is quantity based on the differences between the calculated and observed peak positions. Therefore, a high figure of merit indicates a possible candidate unit cell. Another observation to note is the presence of repeating unit cells. If different programs are generating the same unit cell, then that may be a good candidate. In the case of the copper cyamelurate, there was one particular lattice parameter that fit all these criteria (See Table 5.5). When a similar process was applied to the potassium cyamelurate, the best candidate was very close to the previously reported lattice parameters (See Table 5.5).[111] The program *Checkcell* can then be used to check systematic absences and propose a likely space group. It was found that the

Table 5.5 - Results of the indexing procedure for potassium and copper cyamelurate.

Cyamelurate	***a* (Å)**	***b* (Å)**	***c* (Å)**	**β (°)**	**Space Group**
Potassium	10.270	17.092	7.072	90.52	$P2_1/c$
Potassium[111]	10.276	17.115	7.145	90.48	$P2_1/c$
Copper	10.541	16.537	7.245	103.71	$P2_1/c$

Note: The unit cell parameters for the previously reported potassium cyamelurate are included for comparison.

space group $P2_1/c$ (No. 14) was the "best" solution for both potassium and copper cyamelurate.

Ab initio structure solution

Using the unit cell parameters, an initial structure solution can be generated. The FOX program uses a parallel tempering algorithm to generate possible structures.[170] The inputs for this program are the unit cell parameters, the powder pattern, and the present molecules. A rigid model of the cyamelurate was generated in the program and input into the unit cell. In the case of potassium cyamelurate, 3 potassium cations were also input, as well as three oxygen atoms. The three oxygen atoms represent the three water molecules reported in the single crystal structure. In the case of copper cyamelurate, two copper atoms, one potassium atom, and four oxygen atoms were imported into the unit cell. These values were based on the compositional data obtained from EDS and CHN analysis (~1.5:1 Cu:K molar ratio and 3.5 H_2O molecules). In FOX, it is best to overestimate the amounts of atoms in the unit cell. The reported structure of potassium cyamelurate was generated by the program. Unfortunately, it was not the most optimized configuration. This is significant because it would hard to justify why one might select

that particular model as the best fit. Likewise, an optimized structure was generated for the copper cyamelurate. The structure is shown in Figure 5.6. The optimized formula of this structure was found to be $KCu[C_6N_7O_3]\cdot 4H_2O$. The 1:1 molar ratio of Cu to K balances the -3 charge of the cyamelurate anion, but EDS data did not indicate that potassium amounts were that high. Further ICP data needs to be collected to establish the proper ratio. Likewise, oxygen analysis might help to reveal the amounts of water present in the copper salt. Since these questions still need to be answered, further refinements of this structure were not made. This may not be actual structure, but the

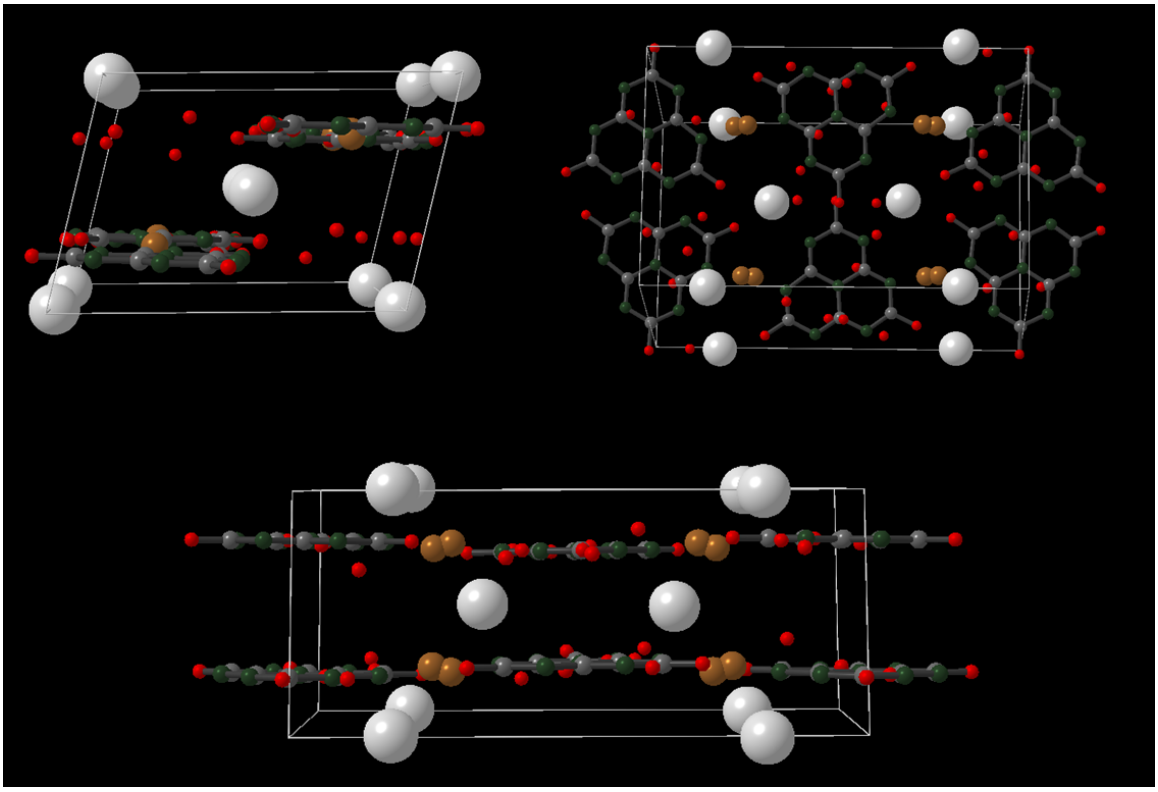

Figure 5.6 - Optimized structure of $KCu[C_6N_7O_3]\cdot 4H_2O$ from different angles. Legend: C(gray), N(green), O(red), Cu(brown), K(white).

arrangement of atoms is very similar other reported cyamelurate structures. Namely, the cyamelurate anions are coplanar to each other, and the potassium cations are found to the side of the anions and between layers. Interestingly, the copper occurs in a linear coordination mode, bound to two cyamelurate anions. This makes sense because the smaller Cu cation should fit between anions much better than the larger potassium cation. The waters from previous structures[111,112,167] were reported to occur both in plane with the cyamelurate anion as well as as between layers, and the same is true within the optimized structure. They appear most closely associated with the potassium cations. If the optimization procedure is repeated with just copper cations, a very similar structure is generated, except, the potassium site is replaced with copper.

Conclusions

A series of metal cyamelurate precipitates were generated by a cation exchange reaction with potassium cyamelurate. Compositional analysis indicated the presence of potassium remaining in the precipitates. Elemental analysis also revealed the presence of H_2O in the structures as well. Thermal analysis in air of the materials showed two major events occurred: a dehydration step in the range of 116-243 °C and a highly exothermic decomposition from 420-540 °C. Analysis of the decomposition products, showed the respective metal oxides, except in the case of Mn and V which showed potassium manganese oxides and potassium vanadates. FTIR analysis of the precipitates revealed the absorbances associated with the cyamelurate anion, as previously reported. Coordinated water vibrations were also present. Powder XRD patterns showed crystalline materials which had similarities for cations of similar size. It was found that the nature of the metal salt used during the reaction had no effect on the crystalline

structure of the precipitates. A structure solution was attempted for the crystalline copper cyamelurate salt. Initial solutions indicate that the structure is for $KCu[C_6N_7O_3]\cdot 4H_2O$, but further work is required to identify the composition of the crystalline material, then refine possible structures.

CHAPTER VI

SYNTHESIS OF NEUTRAL MOLECULAR HEPTAZINES

Introduction

Since the publication of Nelson's first reported crystal structure of the parent heptazine, tri-s-triazine ($C_6N_7H_3$) there have many newly reported heptazine structures.[87,105] These structures can be divided into a two main structure types: ionic and neutral materials. The ionic structures feature several adducts of the triaminoheptazine, melem ($C_6N_7(NH_2)_3$)[176,177] and alkali metal salts of trihydroxyheptazine, cyameluric acid ($C_6N_7O_3H_3$),[111,112,167,178] or the potassium salt of hydromelonic acid, and potassium melonate ($K_3C_6N_7(NCN)_3$).[89] There was also one reported crystal structure of a metal organic framework featuring 2,5,8-tris(p-benzoate)-1,3,4,6,7,8,9,9b-heptaazaphenalenic acid ($C_6N_7(p\text{-}C_6H_4COOH)_3$).[110] There have been seven reported crystal structures of neutral heptazine molecules, including triazido-s-heptazine, which was previously synthesized by our group,[60] and can be found in Table 6.1.

Table 6.1 - Neutral heptazine molecules with reported crystal structures.

Compound	Formula	First year reported
Tri-s-triazine	$C_6N_7H_3$	1982
Trichloro-s-triazine	$C_6N_7Cl_3$	2002
2,5,8-(triamino-tri-s-triazine) (melem)	$C_6N_7(NH_2)_3$	2003
Triazido-s-heptazine	$C_6N_7(N_3)_3$	2004
2,5,8-Tris(diethylamino)-s-heptazine	$C_6N_7(N(C_2H_5)_2)_3$	2004
2,5,8-Triphenoxy-s-heptazine	$C_6N_7(OC_6H_5)_3$	2006
Tris(trimethylsilyl)cyamelurate	$C_6N_7(OSi(CH_3)_3)_3$	2007

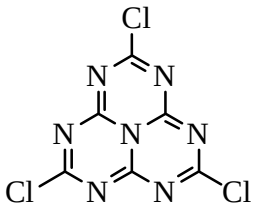

2,5,8-trichloro-s-heptazine

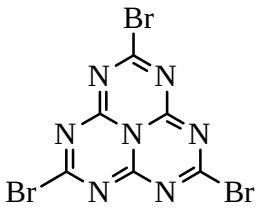

2,5,8-tribromo-s-heptazine

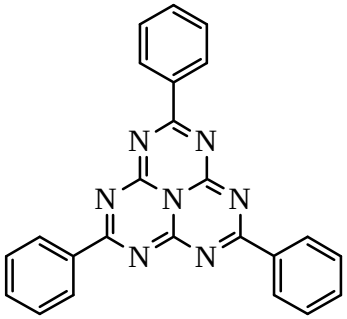

2,5,8-triphenyl-s-heptazine

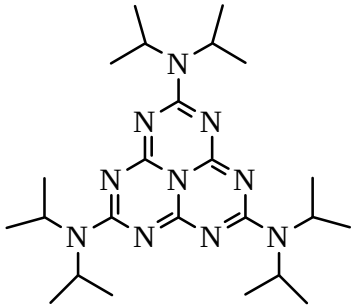

2,5,8-tris(diisopropylamino)-s-heptazine

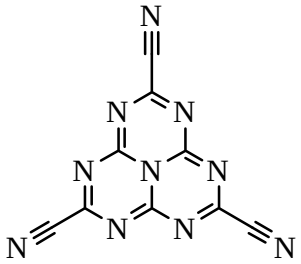

2,5,8-tricyano-s-heptazine

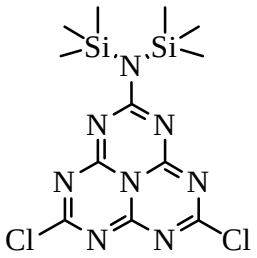

2-bis(trimethylsilylamido)-5,8-dichloro-s-heptazine

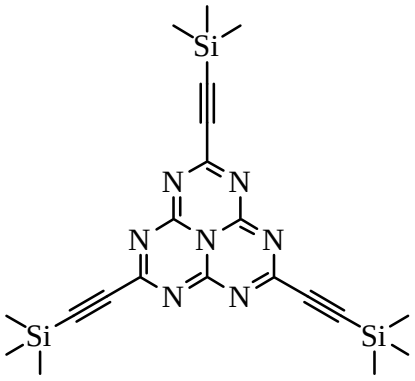

2,5,8-tris(trimethylsilylethynyl-s-heptazine

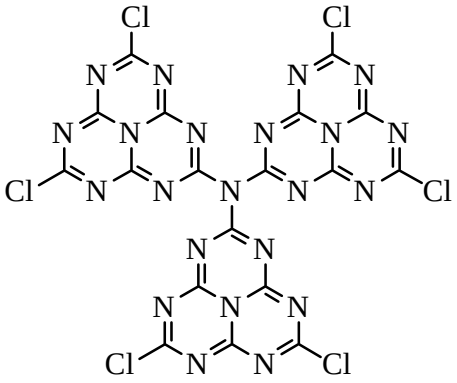

Tris(2,5-dichloroheptazinyl)amine

Figure 6.1 - Target molecular heptazines for synthesis.

This chapter describes the synthesis and characterization of neutral organic heptazine molecules. The molecules of interest can be found in Figure 6.1 and include trisubstituted derivatives with Cl, Br, $N(^{i}Pr)_2$, C_6H_5, CN, and $C{\equiv}CSi(CH_3)_3$ substituents as well as a monosubstituted species ($C_6N_7Cl_2(N(SiMe_3)_2)$) and three heptazine bounds to a central nitrogen $N(C_6N_7Cl_2)_3$.

Experimental

Reagents

Phosphorus pentachloride (PCl_5, 98%) was purchased from Alfa Aesar and stored in argon atmosphere glovebox. Toluene (distilled from Na/benzophenone), tetrahydrofuran, (THF, distilled from Na/benzophenone), and benzene was purchased from Fisher. Phosphorus pentabromide (PBr_5) was obtained from Aldrich, and sublimed under N_2 gas at 80 °C. Other reagents include aluminum chloride($AlCl_3$, 99%), diisopropylamine ($HN(C_3H_7)_2$, 99%), sodium hexamethyldisilazane ($NaN(Si(CH_3)_3)_2$, 97%), sodium cyanide (NaCN), trimethylsilylcyanide ($(H_3C)_3SiCN$, 98%), trimethylsilylacetylene ($(H_3C)_3SiC{\equiv}CH$, 98%), copper iodide (CuI), palladium acetate ($Pd(O_2CCH_3)_2$, 98%), triphenylphosphine ($P(C_6H_5)_3$), lithium nitride (Li_3N), and magnesium sulfate ($MgSO_4$, EM Science).

Synthesis of 2,5,8-trichloro-s-heptazine ($C_6N_7Cl_3$)

The synthesis of trichloroheptazine (TCH) was previous reported by Kroke[88], as well as Schroeder and Kober.[86] All manipulations were performed in an Ar atmosphere glovebox or under a nitrogen gas blanket. Potassium cyamelurate ($K_3C_6N_7O_3$-$3H_2O$) was synthesize according to the method from Chapter V and was first dried overnight in a 130

°C drying oven, then heated under vacuum for eight hours at 150 °C. In the glovebox, 40 g (0.12 moles) of dried potassium cyamelurate ($K_3C_6N_7O_3$) were mixed with 90 g (0.43 moles) phosphorus pentachloride (PCl_5) in a ceramic mortar and pestle. A 1000 mL round bottom flask was charged with the mixture and capped with a gas inlet adapter. The apparatus was removed from the glovebox and attached to a Schlenk line. The pale yellow mixture was then slowly heated to a mantle temperature of 200 °C and held for one hour. The bright yellow product was then cooled to room temperature and returned to the glovebox. A mass of 77 g of crude yellow product was recovered. The crude product was then purified directly by Soxhlet extraction in dry toluene. The bright yellow crystalline solid was collected by removing the solvent and drying under vacuum. Yield: 33 g, 92%.

Synthesis of 2,5,8-tribromo-s-heptazine ($C_6N_7Br_3$)

All manipulations were performed in an argon atmosphere glovebox. To a ceramic mortar and pestle, was added 1.01 g dried potassium cyamelurate ($K_3C_6N_7O_3$) and 4.49 g sublimed phosphorus pentabromide (PBr_5). The two solids were ground together to form a bright yellow solid mixture. The solid mixture was divided into two aliquots and added to two predried pyrex ampules. The ampules were attached to the Schlenk line via a Cajon valve and filled with N_2 gas. The end of the ampule was placed in a liquid nitrogen bath to freeze the solid mixture, then a vacuum was applied. The ampules were evacuated to a pressure of 100 mtorr and sealed to lengths of 13 cm. The ampules were placed side-by-side in the center of a clamshell furnace with the ends plugged with glass cloth. The furnace was programmed to heat to 100 °C at a rate of 1 °C/min. The programmed heated the ampules at 100 °C for 96 hours, after which the

ampules were cooled back to room temperature at 1 °C/min. An orange-yellow solid was obtained in a mass of 5.0 g. The crude mixture was placed in 1-inch pyrex tube fitted with a Cajon type valve and attached to the Schlenk line. Under dynamic vacuum, the crude mixture was heated to 200 °C at 5 °C/min and a bright yellow solid sublimed out the hot zone of the tube. Yield: 0.56 g, 46%.

Synthesis of 2,5,8-triphenyl-s-heptazine ($C_6N_7(C_6H_5)_3$)

The following procedure was based on a procedure by Zhou et. al. to synthesize 2,5,8-tris(p-tolyl)-s-heptazine ($C_6N_7(p\text{-}C_6H_4CH_3)_3$.[110] All manipulations were performed in an argon atmosphere glovebox. Benzene was dried by bubbling over calcium chloride for 20 minutes. A dried 100 mL Schlenk flask was charged with 1.2 g (9 mmol) $AlCl_3$. A mass of 0.553 g (2 mmol) TCH was weighed out and set aside in the glovebox. The flask was removed from the glovebox and attached to a Schlenk line. To the flask was added 15 mL of benzene via canula. Under stirring, the suspension of $AlCl_3$ was heated at a mantle temperature of 70 °C for 25 minutes. TCH was retrieved from the glovebox and slowly added to the reaction flask with a spatula over the course of 30 minutes. Once added, the red suspension was stirred at 70 °C for five hours. After cooling to room temperature, 40 mL of 18MΩ H2O was added to the flask and the mantle temperature was raised to 150 °C. The red suspension was boiled for five minutes and turned a bright yellow color. The yellow solid was collected by vacuum filtration while the suspension was still hot. The crude material was recrystallized from a large amount (~250 mL) of hot m-xylene. Yield: 90 mg, 11%.

Synthesis of 2,5,8-tris(diisopropylamino)-s-heptazine

($C_6N_7(N(C_3H_7)_2)_3$)

The following procedure is similar to those laid out by Schroeder and Kober and more recently by Traber, *et. al.*[109] The manipulations were performed under N_2 gas or in an argon atmosphere glovebox. To a dried 100 mL Schlenk flask was added 0.25 g (0.9 mmol) TCH. The flask was capped and removed from the glovebox and attached to the Schlenk line. Under flowing N_2, a reflux condenser was attached to the flask. 10 mL of degassed diisopropylamine was added to the flask via canula. While stirring, the flask was slowly heated to reflux at a mantle temperature of 120 °C. The flask was maintained at reflux for three days. The flask was cooled to room temperature. Toluene (30 mL) was added to the reaction and the contents were transferred to a separatory funnel. The organic layer was washed three times with a concentrated NaCl solution, then dried over magnesium sulfate. The toluene was then filtered and removed by reduced pressure to yield a cream-colored product. The product was further purified by vacuum sublimation up to 165 °C, then by column chromatography (SiO_2, in ethyl acetate). Yield: 0.17 g, 40%.

Synthesis of 2-bis(trimethylsilylamido)-5,8-dichloro-s-

heptazine ($C_6N_7Cl_2(N(Si(CH_3)_3)_2)$) (DCAH)

The synthesis of this molecule was briefly reported by Horvath-Bordon in her dissertation.[179] The reaction took place under N_2 gas and all reactants were handled in an argon atmosphere glovebox. A mass of 0.73 g (4 mmol) sodium hexamethyldisilazane (NaHMDS) was added to a 50 ml Schlenk flask, then 1.11 g (4 mmol) TCH was added to a 100 mL Schlenk flask. Both flasks were capped and removed from the glovebox and

attached to Schlenk line. TCH was dissolved in 30 mL dry THF and the NaHMDS was dissolved in 15 mL THF. After stirring each solution for five minutes, the NaHMDS solution was slowly added to the TCH solution via canula over the course of 5 minutes. The clear yellow TCH solution turned a cloudy, golden brown color. The suspension was stirred for 19 hours at room temperature under N_2 gas. The contents were transferred to a N_2 flushed centrifuge tube by canula and centrifuged for 15 minutes. The supernatant was transferred to a clean, dry Schlenk flask and the solvent removed under reduced pressure. A reddish brown solid was recovered and subsequently washed in toluene. The resulting orange suspension was again centrifuged in N_2-flushed centrifuge tubes. The supernatant was removed and the remaining solid was collected in the glovebox and vacuum dried. Yield: 0.63 g, 39%.

Attempted synthesis of tris(2,5-dichloroheptazinyl)amine

($N(C_6N_7Cl_2)_3$)

Eleven unsuccessful attempts were made towards the synthesis of $N(C_6N_7Cl_2)_3$. The synthesis conditions are summarized in Table 6.2. Two different methods were employed: a) solid state reactions of TCH with lithium nitride and b) solid state and solution reactions of TCH with DCAH. The lithium nitride reactions were performed in sealed ampules and the DCAH reactions were performed under N_2 in Schlenk flask or tubes. Only mixtures of products were observed by FTIR.

Table 6.2 - Summary of attempted syntheses of $N(C_6N_7Cl_2)_3$.

$C_6N_7Cl_3$ + 1/3Li_3N Reactions				
mmol TCH	**mmol Li_3N**	**Temp**	**Ramp Rate**	**Time**
0.89	0.43	350	1	48
0.90	0.37	250	1	48
0.91	0.34	300	1	48
0.91	0.34	400	1	48
0.45	0.14	325	0.1	72
0.45	0.14	350	Soak @ 200 °C	26
$C_6N_7Cl_3$ + 1/2DCAH Reactions				
mmol TCH	**mmol DCAH**	**Solvent**	**Temp (°C)**	**Time**
0.25	0.12	Toluene	160	20
0.25	0.12	None	250	6
0.26	0.12	THF	115	20
0.26	0.12	None	200	15.5
0.26	0.12	THF	115	18

($C_6N_7(C{\equiv}N)_3$)

Ten unsuccessful attempts were made towards the synthesis of $C_6N_7(CN)_3$. The synthesis conditions are summarized in Table 6.3. Reactions were performed with either trimethylsilylcyanide (TMSCN) or sodium cyanide (NaCN). The reactions performed with NaCN followed reported procedures for the synthesis of tricyanotriazine[180] and the reactions with TMSCN followed a similar procedure for the synthesis of triazidoheptazine from $TMSN_3$[60,61] or for the synthesis of hexacyanobenzene.[181] All reactions were performed under N_2 in Schlenk flasks. Only mixtures of products were obtained.

Attempted synthesis of 2,5,8-tris(trimethylsilylethynyl)-s-heptazine ($C_6N_7(C{\equiv}CSi(CH_3)_3)_3$)

Twelve unsuccessful attempts were made towards the synthesis of $C_6N_7(C{\equiv}CSiMe_3)_3$. The synthesis conditions are summarized in Table 6.4. Reactions were performed with either an alkali acetylide formed from the deprotonation of trimethylsilylacetylene or using standard Sonogashira reaction conditions.[182] All reactions were performed under N_2 in Schlenk flasks. Only mixtures of products were obtained in NMR.

Table 6.3 - Summary of attempts to synthesize $C_6N_7(CN)_3$.

Mmol TCH	Cyanide	Solvent	Solvent vol. (mL)	TCH:CN	Temp (°C)	Time	Wash
0.45	TMSCN	None	0	1:5	115	23	CH_2Cl_2
0.45	TMSCN	DMF	15	1:5	115	23.5	CH_2Cl_2
0.45	TMSCN	None	0	1:18	80	2	None
0.45	TMSCN	DMF	10	1:21	80	1	None
0.46	TMSCN	DMF	15	1:5	80	10.5	Toluene
0.45	NaCN	DMF	15	1:3.5	115	10.5	CH_2Cl_2
0.47	NaCN	CH3CN	15	1:3.5	RT	12	Toluene
0.45	TMSCN	CH3CN	15	1:3.5	100	8.5	None
0.50	TMSCN	THF	15	1:7	115	8	None
0.50	TMSCN	None	neat	1:21	85	1.25	Toluene

Instrumentation

Thermogravimetric-differential analysis (TG-DTA) was performed on a Seiko ExStar 6300 system under flowing argon. FT-IR absorption spectra were taken with a

Nicolet Nexus 670 spectrometer using KBr pellets. Elemental analyses were performed on a Perkin Elmer 2400 CHN/O Analyzer using ultra light weight, ultra clean tin capsules. Powder X-ray diffraction was performed on a Siemens D5000 X-ray diffractometer, using Cu K_α radiation on samples mounted on glass slides. ^{13}C and ^{1}H NMR was obtained on a Avance 400 Spectrometer. Solids probe mass spectrometry was

Table 6.4 - Summary of attempts to synthesize $C_6N_7(C{\equiv}CSi(CH_3)_3)_3$.

Alkali Acetylide Reactions							
mmol TCH	**TCH:TMSA**	**Base**	**Acetylide**	**Solvent**	**Solvent vol. (mL)**	**Temp (°C)**	**Time (h)**
0.125	1:3.75	None	$LiC{\equiv}CH{\cdot}en$[a]	THF	25	-94	16
0.125	1:5.0	None	$HC{\equiv}CSi(CH_3)_3$[b]	Neat	0.40	130	20
0.139	1:3.3	$LiNH_2$	$Li\text{-}C{\equiv}CSi(CH_3)_3$	THF	30	Reflux	4
0.139	1:3.3	LDA[c]	$Li\text{-}C{\equiv}CSi(CH_3)_3$	THF	35	-83	10
0.138	1:3.3	$NaNH_2$	$Na\text{-}C{\equiv}CSi(CH_3)_3$	THF	40	25	12
0.138	1:3.3	$NaNH_2$	$Na\text{-}C{\equiv}CSi(CH_3)_3$	THF	25	-74>25	4
Sonogashira Reactions							
mmol TCH	**mmol $Pd(PPh_3)_2Cl_2$**	**mmol CuI**	**mmol TMSA**	**Base**	**Solvent**	**Temp (°C)**	**Time (h)**
0.5	0.075[d]	0.15	4.25	TEA	THF	25	40
0.5	0.05	0.10	3.5	TEA	THF	115	16
0.5	0.05	0.11	5	DIPEA	THF	50	18
0.5	0.05	0.11	5	DIPEA	THF	115	18
1.0	0.085	0.17	6	TEA	None	70	13
1.0	0.085	0.17	6	TEA	THF	70	13

[a] Reaction was performed in sealed autoclave.

[b] $LiC{\equiv}CH{\cdot}en$ = lithium acetylide-ethylenediamine complex

[c] LDA = lithium diisopropylamide

[d] Different palladium catalyst was used; Tetrakis(triphenylphosphine)Palladium(0) $[Pd(PPh_3)_4]$

performed using a VG TRIO-1 quadrupole system. UV-Vis spectra were taken using a Hewlett-Packard 8453 diode array spectrophotometer. Fluorescence spectra were taken using a Jobin-Yova spectrofluorometer.

Results and Discussion

Conversion of potassium cyamelurate to 2,5,8-trichloro-s-heptazine (TCH) and 2,5,8-tribromo-s-heptazine (TBH)

The reaction of potassium cyamelurate with the phosphorus pentahalides is a relatively simple procedure. Our group previously relied on the previously reported syntheses of TCH by Kroke,[88] and Schroeder and Kober.[86] One difference between these previously reported was the synthesis of TCH was performed under a N_2 atmosphere, rather than vacuum. When the reaction was occurring a refluxing liquid could be observed on the walls of the flask. This was presumed to be phosphorus oxychloride, which has a boiling point of 108 °C. Often, it could be observed that the bright yellow solid forming would actually begin to return to a pale yellow color. It was thought that some of the PCl_5 may have been hydrolyzed to phosphoric acid, thereby causing the TCH to hydrolyze to cyameluric acid. Therefore, the reaction times were lowered to one hour versus ten hours. Another problematic issue had been to wash the crude TCH in cold water, in order to remove the KCl byproduct. Often, the TCH would hydrolyze while filtering out the product. It was found that by just performing a Soxhlet extraction on the crude material, the KCl could be separated with the use of nonpolar toluene. Subsequent vacuum drying of the purified product, could remove the remaining $POCl_3$.

$$K_3C_6N_7O_3 + 3PCl_5 \rightarrow C_6N_7Cl_3 + 3POCl_3 + 3\ KCl \qquad \text{(Equation 6.1)}$$

$K_3C_6N_7O_3 + 3PBr_5 \rightarrow C_6N_7Br_3 + 3POBr_3 + 3\ KBr$ (Equation 6.2)

It was thought that a reaction between potassium cyamelurate and PBr_5 could yield tribromoheptazine, as can be seen in Equations 6.1 and 6.2. PBr_5 decomposes to PBr_3 and Br_2 in temperatures in excess of 105 °C, so it was thought that to keep the chemistry analogous, reaction temperatures would need to be maintained below this value. An initial unsuccessful attempt involved heating potassium cyamelurate and PBr_5 in a Schlenk flask. It was quickly discovered that PBr_5 will easily sublime at mantle temperatures of 50 °C. Therefore, the move was made to perform the reaction in sealed ampules. Upon heating the reactants, it was observed that the ampules would fill with reddish vapor and the solid materials would turn a brick red material. It was found that when PBr_5 is heated near the decomposition temperature of 105 °C, it will reversibly disproportionate to PBr_3 and Br_2, which would explain the presence of reddish colored vapors.[183,184] On cooling, the vapors disappear and yellow-orange solid remains. Analysis of the crude product clearly reveals the presence of the expected KBr byproduct. Heating of the crude material at 200 °C under vacuum resulted in the formation of a yellow sublimate. Any incompletely reacted potassium cyamelurate would remain ionic and should not be sublimable.

Initial evidence for the conversion to TBH was seen through the comparison of FT-IR spectra for TCH and TBH, as shown in Figure 6.1. The most prominent feature is the marked similarity between the two spectra. Both spectra contain the out-of-plane bending mode of the heptazine ring at 824 cm^{-1}, but the other absorbances in the 1700-900 cm^{-1} region are slightly shifted to lower wavenumbers for TBH. The largest shift occurs for the lowest peak; the peak shifts from 648 cm^{-1} for TCH to 600 cm^{-1} for TBH.

This suggests that these are primarily C-X stretches, given that halides are the only differences between the two compounds .[108] The heavier Br atom would result in a lower stretching frequency, when compared to the lighter Cl atom.

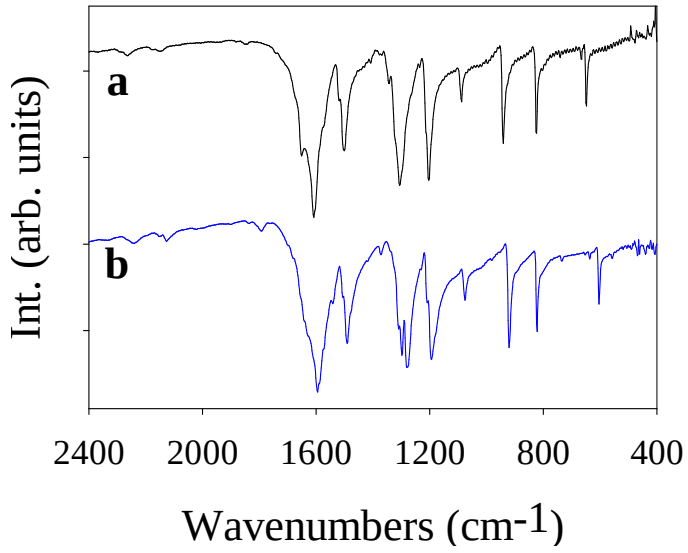

Figure 6.2 - FT-IR spectra of a) trichloroheptazine (TCH) and b) tribromoheptazine (TBH).

Analysis by ^{13}C-NMR showed two resonances for TBH. The signal due to the bridgehead carbon occurs at 158 ppm, which exactly the same as that for TCH. The substituent carbon, bound to Br, showed an upfield shift at 170 ppm compared to TCH at 176 ppm. This indicates that the bromine is less deshielding than the chlorine, and would be in line with what one would expect, considering the difference in electronegativity of the two halides.

Solids probe mass spectrometry of TBH shows the parent at 409 amu along with the distinctive isotope pattern of peaks at 407, 411, and 413 amu that accompanies

polybrominated compounds. The three other peaks result from the presence of ^{79}Br and ^{81}Br in TBH; each isotope has nearly a 50% abundance, making them almost equally likely to occur in the TBH. The pattern also clearly shows peaks from the ion [M]-Br.

The powder XRD patterns of TCH and TBH are also very similar (Figure 6.3). They show a very clear cubic pattern. The peaks for the TBH are shifted to lower two theta angles compared to TCH. If these materials are isomorphous, then this would make sense because the shift to lower two theta angles would equate to a larger unit cell. This would make sense given the presence of the larger bromine atom. These cubic patterns also do not match any of the reported crystal structures for TCH.[88,108]

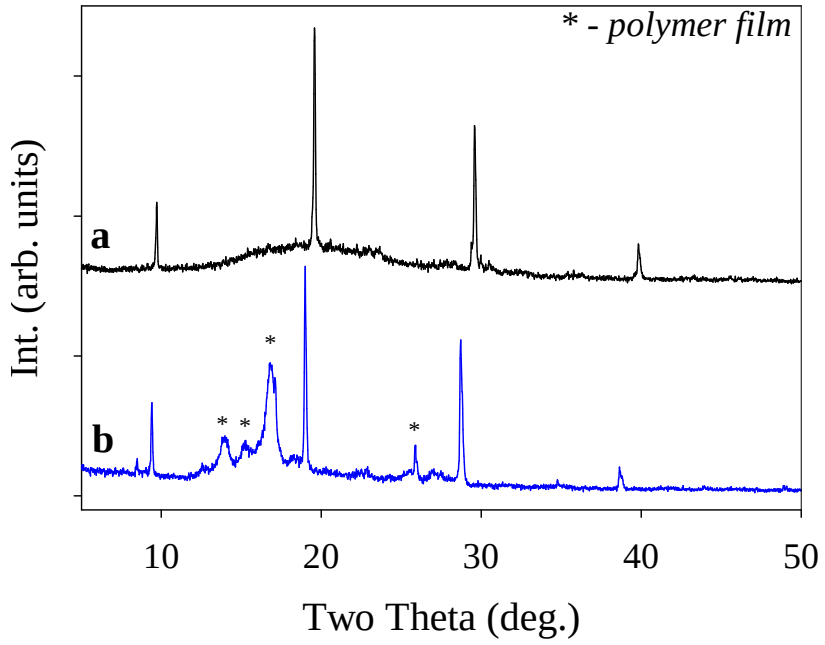

Figure 6.3 - Powder X-ray diffraction patterns of a) TCH and b) TBH.

Conversion of TCH to 2,5,8-triphenyl-s-heptazine (TPH)

The synthesis of triphenylheptazine (TPH) was relatively straightforward Friedel-Crafts reaction. In their early work on heptazine derivatives, Redemann and Lucas, considered TCH to be the acid chloride of cyameluric acid ($C_6N_7O_3H_3$) and would have similar reactivity as other acid chlorides.[71,104] Schroeder and Kober indeed found TCH that would undergo Friedel-Crafts types of reactions with benzene derivatives.[86] The Friedel-Crafts reaction involves the use of a Lewis acid catalyst to induce electrophilic substitution on the benzene derivative. In this case the catalyst is aluminum chloride ($AlCl_3$) and benzene is the aromatic derivative. During the reaction, when TCH was added to the reaction flask containing $AlCl_3$ and benzene, the mixture would turn a brick red color. This suggests that the $AlCl_3$ is forming a complex during the reaction, as would be expected during the reaction. Once water is added to the reaction mixture, the color turns to a bright yellow color and the complex is destroyed. Unreacted $AlCl_3$ and benzene can be separated through filtration. The yield of 11% for TPH was very low. The conditions of the reaction that were followed were for the substitution of toluene and not benzene. Toluene is more active than benzene under Friedel-Crafts reactions; higher temperatures or longer reaction times may improve yields.

Initial evidence for the conversion to TPH was seen through the comparison of FT-IR spectra for TCH and TPH, as shown in Figure 6.4. The most prominent feature is the difference between the two spectra. The major difference is the presence of absorbances near 3000 cm^{-1}, which indicates the presence of C-H stretches due to the presence of phenyl rings. The peaks in the 1700-900 cm^{-1} would represent the vibrations for both the heptazine skeletal vibrations, as well as the aromatic C=C vibrations from the

substituent phenyl rings. A major peak at 697 cm^{-1} is the region for out-of-plane bending of aromatic C-H bonds. Another major difference of note is the reduction of intensity of many of the peaks of the heptazine vibrations. Either of two smaller peaks at 790 and 829 cm^{-1} could represent the out-of-plane bending of the heptazine ring, but it is unclear how much shifting would occur in the vibrational modes due to aromatic substitution.

Analysis of TPH by NMR demonstrated distinct differences between it and the starting material TCH. The ^{1}H-NMR showed a doublet near 8.4 ppm and two triplet peaks between 7.6 and 7.8 ppm. The doublet would indicate protons in the ortho position of the phenyl rings; the ortho proton only has one neighbor. The downfield shift of the peaks may indicate some hydrogen bonding interactions of the hydrogens to the peripheral nitrogens of the heptazine rings. The two triplets would indicate the protons in

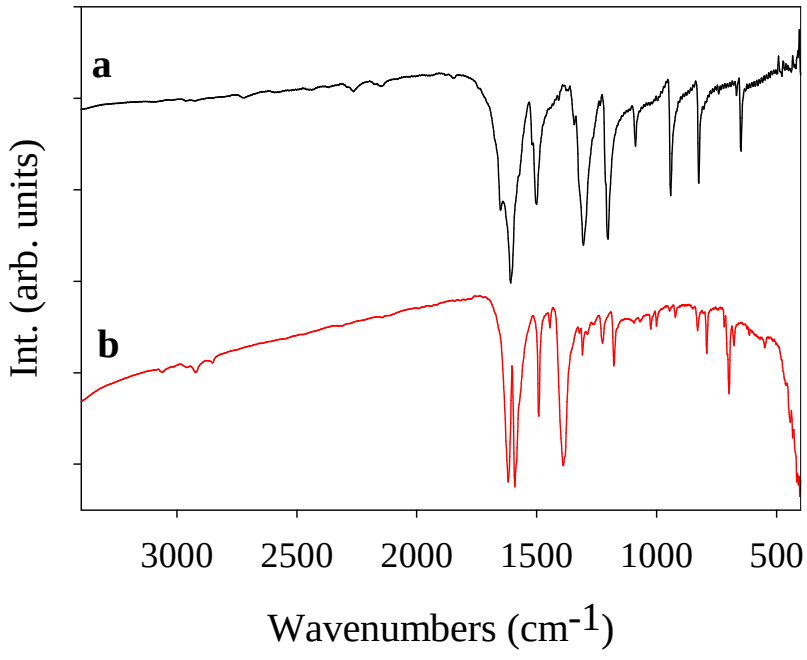

Figure 6.4 - FT-IR spectra of a) TCH and b) TPH.

the meta and para positions of the phenyl ring. Each proton has two vicinal neighbors and will appear as a triplet when the [n+1] rule is applied. When the peaks are integrated, the ratios can be calculated to 15 total protons, as would be expected for TPH. One major impurity peak at 3.33 ppm, this was found to be H_2O present in the DMSO solvent.[185] Analysis of the ^{13}C-NMR spectrum gives shows absorbances: 173.8, 159.2, 134.1, 129.2, and 128.9 ppm. The two most downfield peaks compare very favorably with the heptazine carbons. The peak at 159.2 ppm is very near the reported 158 ppm resonance of the bridgehead carbon. The substituent carbon could be well represented by the 173.8 ppm resonance. The three other peaks are indicative of the protonated carbons of the phenyl rings. No peaks could be found for the quaternary carbon of the phenyl rings. The positions of the phenyl carbons compare very favorably with the shifts of triphenyl-s-triazine.[186] The quaternary carbon of that phenyl could be found at 137 ppm, and this could be expected for TPH as well. It might be questionable then as to the identification of this compound. However, solids probe mass spectrometry was also performed on the recrystallized material. It only showed the parent ion at m/z = 401, along with two isotope peaks. The pattern completely agrees with a compound of the formula $C_{24}H_{15}N_7$. Therefore, the missing quaternary carbon peak is a quandary, but all other evidence points a trisubstituted heptazine ring with three phenyl groups.

Conversion of TCH to 2,5,8-tris(diisopropylamino)-s-heptazine ($C_6N_7(N(C_3H_7)_2)_3$) (TAmH)

The reaction between TCH and diisopropylamine is a straightforward reaction. The TCH undergoes a nucleophilic substitution with the amine and forms the new trisubstituted heptazine and HCl as a byproduct. Since the reaction is occurring neat

diisopropylamine, any forming HCl should react with the base to form the hydrochloride salt as a byproduct. This is washed away in the purification process. The previous report on the diethylamine derivative of heptazine reported[109] performing the reaction in a sealed autoclave, as reported for some amine substituted triazines.[50,187] However, complete substitution was found to occur for TAmH at normal reflux temperatures. Filtering an ethyl acetate solution of the crude product helped to remove the material and incompletely substituted byproducts.

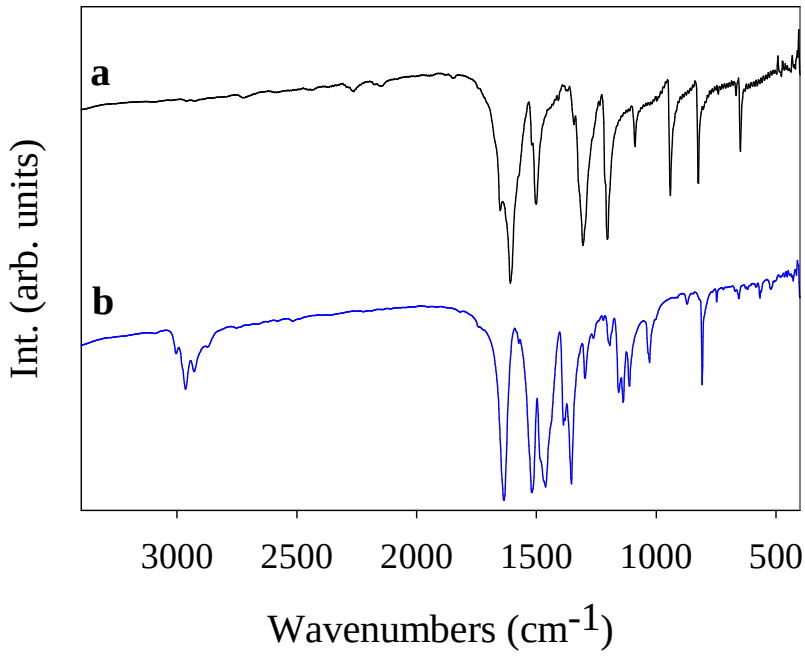

Figure 6.5 - FTIR spectrum of a) TCH and b) TAmH.

FT-IR analysis of the material revealed significant differences in the material when compared to the starting material TCH (Figure 6.5). Namely, that absorbances in the 2900 cm^{-1} region would indicate the presence of alkyl C-H stretches, and the

associated asymmetric C-H stretches occur at 1462 cm^{-1}. The ring vibrations of the heptazine occur at 1646, 1519, 1296, and 808 cm^{-1}. The aromatic C-N stretches of the diisopropyl amine groups occur at in the 1350-1400 cm^{-1} region, while the aliphatic C-N stretches occur in the 1100-1150 cm^{-1} region.

Analysis of TAH by ^{13}C-NMR also confirms the formation of a trisubstituted heptazine with two peaks occurring at 154.2 and 163.0 ppm. This is similar to the previously reported aminoheptazine.[109] The carbons of the isopropyl chains occur at 46.6 and 21.1 ppm, with signal farther downfield representing the carbon bound directly to nitrogen and the upfield signal represent the methyl groups. ^{1}H NMR only showed a multiplet of peaks near 1.2 ppm, which would indicate the presence of alkyl hydrogens. Solids probe mass spectrometry was also used to investigate the molecule as well. The parent peak for $C_{24}H_{42}N_{10}$ occurs at m/z = 470 amu. The major peak occurs at 427 amu and is represented by the ion $[M]^{+}$-C_3H_7. Minor peaks also indicated the successive loss of methyl groups from the parent structure. There are no peaks or isotope patterns to indicate the presence of partially substituted species such as $C_6N_7Cl_2(N(C_3H_7)_2)$.

Conversion of TCH to 2-bis(trimethylsilylamido)-5,8-dichloro-s-heptazine (DCAH)

The reaction between TCH and sodium hexamethyldisilazane (NaHMDS) is a nucleophilic substitution reaction. In a 1:1 ratio, the TCH undergoes attack by the NaHMDS and DCAH is formed along with NaCl as a byproduct. Indeed, powder XRD of the crude material clearly shows the presence of NaCl. Although it was not clearly stated in the reported procedure, toluene was used to wash the crude product. The final

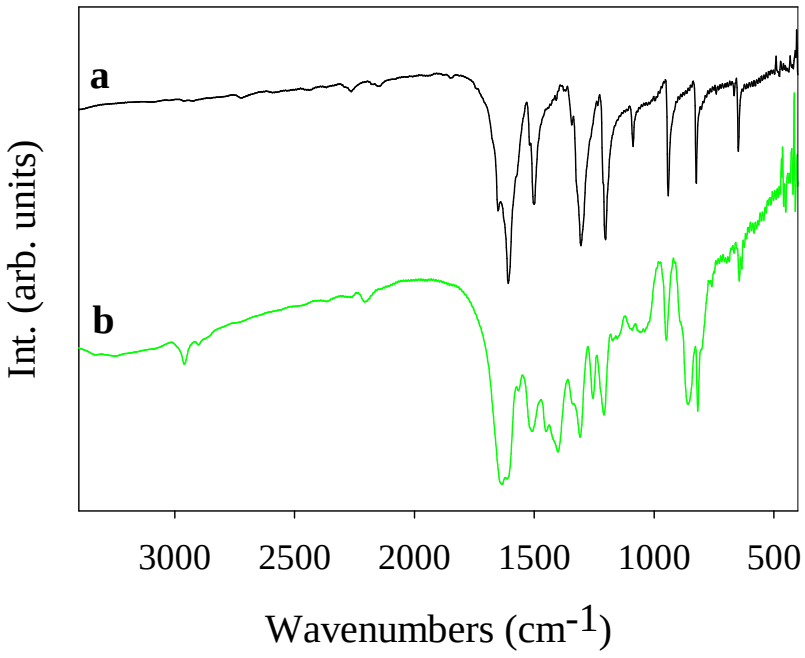

Figure 6.6 - FT-IR spectra of a) TCH and b) DCAH.

product was not soluble in toluene, but any unreacted TCH would be washed away, along with any multiply substituted heptazines. It was rationalized that the addition of lipophilic trimethylsilyl groups should cause the unwanted byproducts to be much more soluble than the desired product.

The FT-IR analysis (see Figure 6.6) of the product reveals the presence of the a heptazine ring with absorbances at 1634, 1508, 1309, and 818 cm^{-1}. The absorbances in the 2900-3000 cm^{-1} represent C-H stretches and the absorbance at 1440 cm^{-1} represent asymmetric C-H stretches. The peaks at 1255, 949 and 859 cm^{-1} are indicative of new Si-C vibrations, while the peaks at 1401 and 1060 cm^{-1} would indicate the presence of C-N and Si-N vibrations, respectively. As noted before, the peak at 645 cm^{-1} indicates the presence of C-Cl stretches. ^{13}C-NMR analysis of the material indicates presence of a

monosubstituted heptazine ring. By only changing one of the substituents of the heptazine, the symmetry is broken and that means there should be four magnetically inequivalent carbons. This was the case, as there were four peaks present in the aromatic region: 174.3, 168.3, 157.5, and 156.1 ppm. There was also one peak present at 1.26 ppm, indicating the presence of trimethylsilyl carbons. These values are in good agreement with the reported values by Horvath-Bordon.[179]

Thermal properties of molecular heptazines

Heptazines are known to be thermally stable materials and the molecular species may have useful applications in high temperature regimes. The thermal stability of the four synthesized species can be found in Figure 6.7. In the case of TAmH and TPH, there was a total mass loss at 300 °C and 450 °C, respectively. There were no endothermic events in the DTA trace to indicate melting, so this suggests the solid proceeds directly to decomposition without going through a phase change. However, another interesting property of these two compounds is that under vacuum pressures of approximately 100 mtorr, TAmH and TPH will sublime near temperatures of 150 °C and 225 °C. So, the complete weight loss of the materials in the TG-DTA may result from a sublimation event, rather than decomposition. The sublimation properties of TAmH and TPH are useful, in that thin films could be made of these types of materials for possible OLED applications.[188,189]

The thermal analysis of TBH indicated three distinct weight loss events. TBH begins to decompose at 350 °C and that a weight loss of approximately 60% occurs by 400 °C. The second event involves an additional weight loss of 20% that occurs near 600 °C and is followed by complete weight loss by 750 °C. The first event corresponds very

well to the loss of three equivalents of Br from the molecular weight. This suggests that the bromine atoms may be initially popping off, leaving behind the C_6N_7 rings, followed by their subsequent decomposition at higher temperatures. The decomposition of DCAH does not show any well defined events. There is a constant, gradual weight loss up to 500 °C, followed by more rapid weight losses up to 700 °C. If the molecule follows the expected decomposition of it triazine analogue,[41] two equivalents of trimethylsilylchloride (TMSCl) should be the expected byproduct, and a weight loss of ~ 47% should occur. The loss of TMSCl was expected to occur up to temperatures of 300 °C followed by fragmentation of heptazine rings by 450 °C.[179] In this case 30% weight loss occurs by 400 °C, indicating that TMSCl is not completely removed from the starting material. Higher temperatures of 550 °C are required to

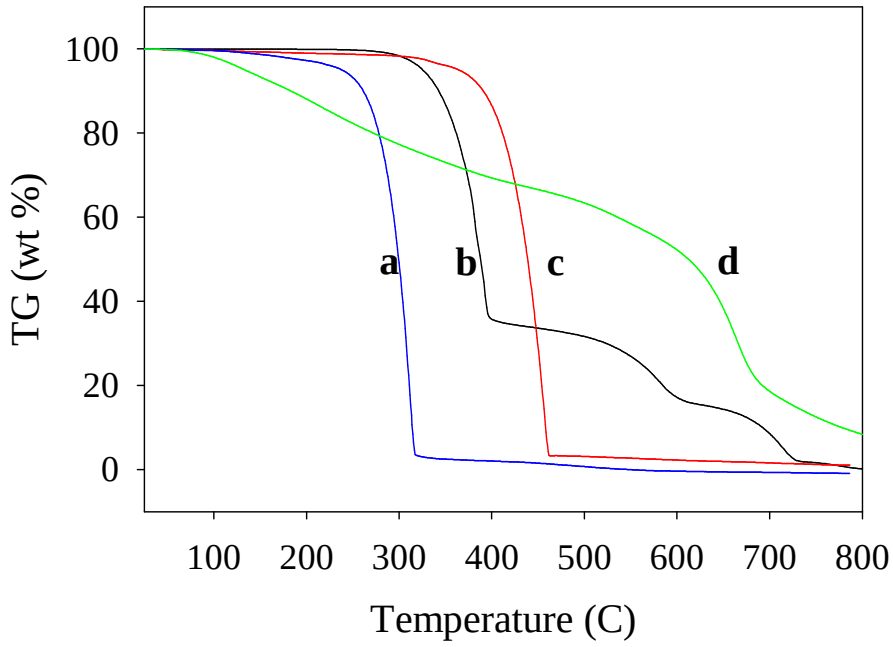

Figure 6.7 - Thermogravimetric analysis of molecular heptazines a) TAmH, b) TBH, c) TPH, and d) DCAH.

induce a near 50 % weight loss, however, this is accompanied by heptazine fragmentation. The decomposition of DCAH will be further explored in Chapter VII.

Optical properties of molecular heptazines

The optical properties of TAmH, TPH, TBH, and DCAH were determined both by UV-Vis and photoluminescence spectroscopy. The solution UV-Vis of the heptazine derivatives are shown in Figure 6.8 for TAmH in ethanol and TPH, TBH, and DCAH in THF. The concentrations were performed in approximate $1x10^{-4}$ M solutions. Given the poor solubility of some of the compounds, the polar THF had to be used since it had the lowest cutoff value (212 nm). The side effect of this is that the finer details are usually lost, and odd interference patterns emerge in the spectra (Figure 6.8b-d). The intense peaks below 300 nm are consistent with n-π* or π-π* electronic transitions. The

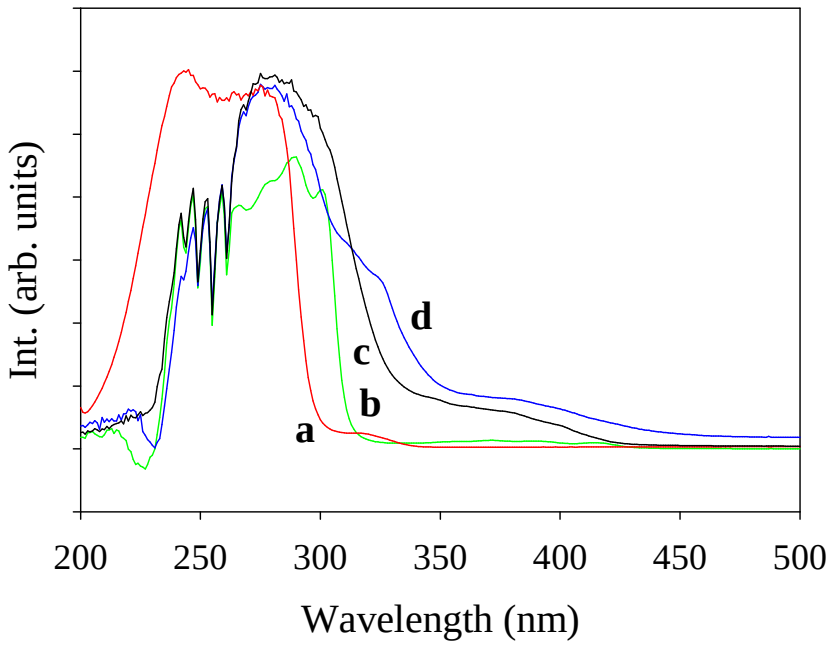

Figure 6.8 - UV-Vis spectra of a) TAmH, b) TBH, c) DCAH, and d) TPH.

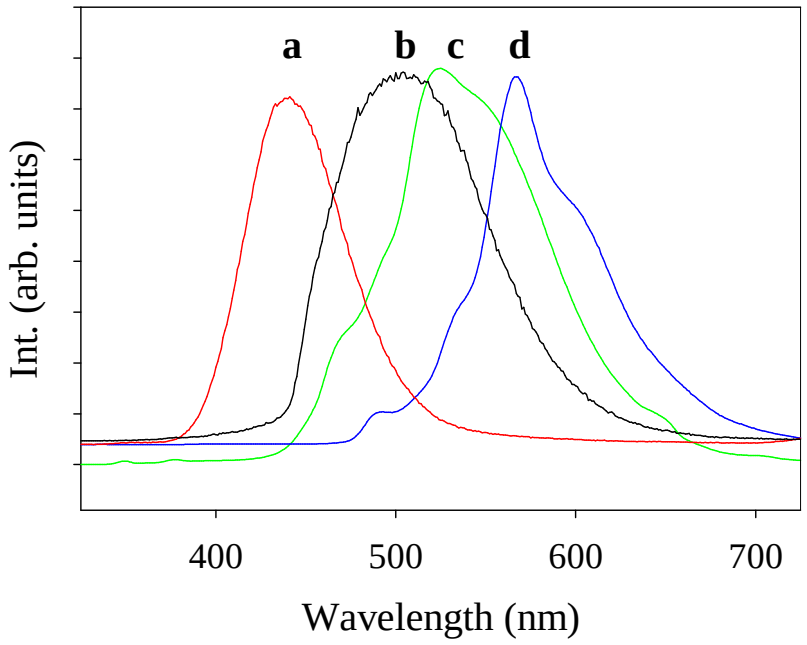

Figure 6.9 - Photoluminescence spectra of: a) TAmH, b) DCAH, c) TBH, and d) TPH.

molecular compounds except TAmH feature tails that extend into the visible region. These tails explain their yellow or orange appearances. TAmH shows no absorbances in the visible region and that would explain its white color. It was also observed that upon illumination with a handheld UV lamp (either 365 or 264 nm light) TAmH, TBH, TPH, and DCAH would show visible luminescence, appearing pale purple, pale green, bright yellow and pale orange.

Photoluminescence spectra for TAmH in ethanol and TBH, TPH, and DCAH in THF are shown in Figure 6.9. TAmH, DCAH, TBH, and TPH show emission at 441, 510, 525, and 566 nm respectively. Theoretical calculations showed TBH to have a HOMO-LUMO gap of 3.98 eV.[190] This energy corresponds to a wavelength of 311 nm, which is in good agreement with the photoluminescence experiments where excitation

wavelengths near 300 nm gave the most intense emission. This was also true of TAmH and DCAH; TPH showed the most intense emission near an excitiation wavelength of 350 nm.

Attempted syntheses of novel molecular heptazines and future experimental work

$\underline{N(C_6N_7Cl_2)_3}$

The goal of this project was to synthesize a model compound featuring three heptazine rings bound to a central nitrogen. Many recent structural models feature this type of bonding in carbon nitride materials, and there has been recent confirmation of this type of bonding arrangement. There have been two reports on the synthesis of the triazine analogue $N(C_3N_3Cl_2)_3$.[191,192] The methods employed solid state reactions of cyanuric chloride ($C_3N_3Cl_3$) with lithium nitride, lithium carbodiimide(Li_2CN_2) or lithium nitridoborate (Li_3BN_2). A molecular product could not be isolated from the series of reactions. Future work on this material may include synthesis of the aminodichloroheptazine ($C_6N_7Cl_2(NH_2)$) via a reported method[193] and subsequent reaction with TCH.

$\underline{C_6N_7(CN)_3}$

The goal of this project was to synthesize the trisubstituted cyanoheptazine compound. Percyano compounds are known to be excellent electron acceptors in charge transfer complexes.[194] A synthesis of tricyanotriazine was reported and the molecule was found to have interesting electrochemical properties.[180] Nitriles are also known to have metal coordination capabilities. Recently, Antonietti, *et al.* discovered a method to

trimerize nitrile compounds into covalent organic frameworks via high temperature reactions in $ZnCl_2$.[195] No cyano stretches were observed in the FTIR of the reaction products and many bands were comparable to starting material. Future work may include using different CN sources such as copper cyanide (CuCN) or tetrabutylammonium cyanide ($(H_9C_4)_4N^+CN^-$).

$\underline{C_6N_7(C{\equiv}CSiMe_3)_3}$

The goal of this project was to rationally synthesize a precursor for the synthesis of acetylene bridged heptazines. The trimethylsilyl groups can be desilylated with KF or KOH in methanol and the subsequent ethynyl compound could be polymerized to form some interesting porous type materials. The reactions attempted did not show any alkyne stretches by FT-IR. Future work would include performing a Negishi coupling that was successful in the triazine case.[196] This would involve a Pd catalyzed reaction of TCH with the reactive $ClZn\text{-}C{\equiv}C\text{-}SiMe_3$ intermediate. Materials of this type will be further explored in Chapter VII.

Conclusions

The synthesis and characterization of 2,5,8-tribromo-s-heptazine (TBH), 2,5,8-triphenyl-s-heptazine (TPH), 2,5,8-tris(diisopropylamino)-s-heptazine (TAmH), 2-bis(trimethylsilyl)amido-5,8-dichloroheptazine (DCAH) was discussed above. Spectroscopic techniques indicated that full substitution occurred in the case of TBH, TPH, and TAmH, while monosubstitution was evident in DCAH. TAmH, DCAH, TBH, and TPH show visible luminescent emission at 441, 510, 525, and 566 nm, respectively. TAmH, TBH, and TPH showed sublimation events in TG-DTA at 300, 350, and 450 °C, respectively. This suggests that these materials may be useful in high temperature OLED

applications. DCAH showed that it may form an extended solid consisting heptazines which will be further discussed in the next chapter. TBH demonstrated slightly better thermal stability and may a better precursor to carbon nitride materials. Its bromine substituents should also be more labile than chlorine, which would also it make it more amenable to substitution than TCH.

CHAPTER VII

SYNTHESIS OF CARBON NITRIDE-BASED EXTENDED MATERIALS FROM HEPTAZINE PRECURSORS

Introduction

It was previously shown in Chapter II that the triazine precursor, TCM, will thermally condense to form a carbon nitride material containing the heptazine species, C_6N_7. Schnick previously confirmed this by showing that melamine ($C_3N_3(NH_2)_3$) and other precursors could be thermally heated to form melem.[4,5,90,99,101] Other reports often include a structural model that features a heptazine nucleus, although they do not fully characterize their materials as containing such.[4,5] There has been very little attention paid towards building carbon nitrides or other materials from heptazine precursors. There is only one report of a heptazine precursor being used in the synthesis of a covalent polymeric material and one report of a heptazine being used in a coordination polymer. Kroke and coworkers reported the synthesis of organic-inorganic hybrid gels with heptazines crosslinked by chlorosilanes.[95] Zhou *et. al.* reported the first metal organic framework featuring a heptazine building block by using the molecular species $C_6N_7(p\text{-}C_6H_4COOH)_3$.[110] These materials represent only a fraction of the avenues that could be applied to polymeric heptazines.

It was the goal of the work reported here to synthesize polymeric materials based on the heptazine nuclei. The two structures that were targeted were: a) a nitrogen-bridged heptazine polymer of the formula C_6N_8; and b) an acetylene-bridged polymer of the formula C_9N_7. The first structure may act as model for structurally ambiguous carbon nitrides that may have been reported as containing heptazine nuclei. The second structure

can act as an open pore framework which could be utilized in gas storage or a catalyst support. The syntheses reported here introduce some attempts at synthesizing heptazine polymers through three different pathways: a high temperature solid-state metathesis route; the thermal decomposition of a single-source precursor, and a low temperature decomposition route in solution.

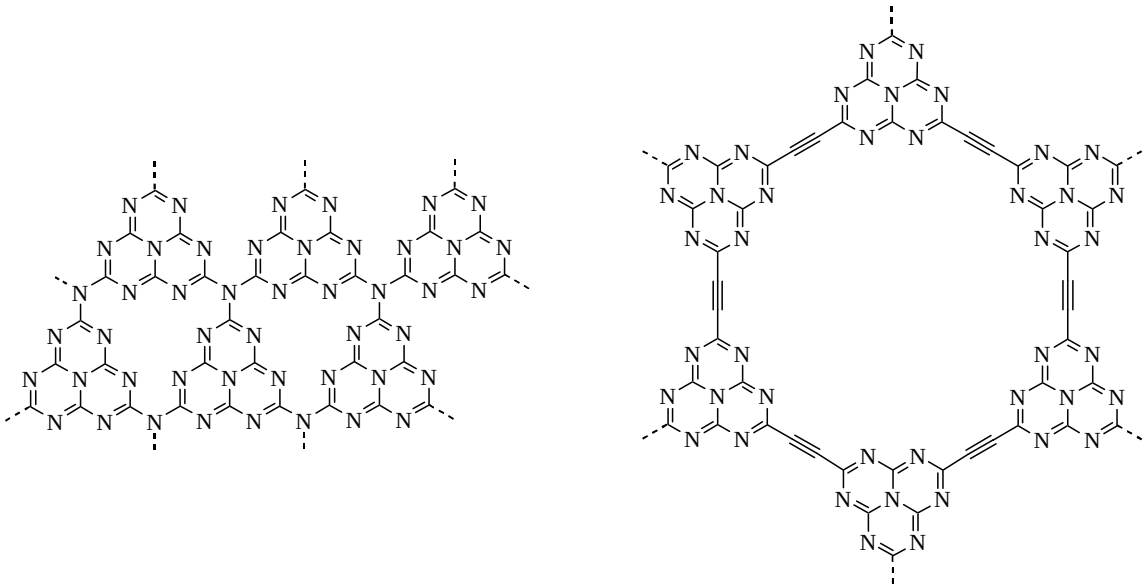

a **b**

Figure 7.1 - Idealized structural models of a) C_6N_8, a nitrogen-bridged heptazine polymer and b) C_9N_7, an acetylene-bridged polymer.

Experimental

Reagents

The following reagents were purchased from Aldrich and used as received: lithium nitride (Li_3N), calcium nitride (Ca_3N_2), calcium carbide (CaC_2), sodium amide

($NaNH_2$), trimethylsilylacetylene ($(H_3C)_3SiC{\equiv}CH$), acetone ($(H_3C)_2CO$). Lithium carbide (Li_2C_2) was purchased from Alfa and methanol (CH_3OH) was purchased from Fisher Scientific. Tetrahydrofuran and toluene were distilled under nitrogen gas over sodium/benzophenone.

Reaction of trichloroheptazine (TCH) with lithium nitride (Li_3N) or calcium nitride (Ca_3N_2)

Trichloroheptazine and lithium nitride

The following manipulations were performed in an argon atmosphere glovebox. To an agate mortar and pestle was added 0.50 g (1.8 mmol) TCH and 0.063 g (1.8 mmol) lithium nitride. The reactants were ground together for three minutes and a tan flour-like powder mixture was obtained. The mixture separated into two batches of 0.28 g and placed into two dried ampules. Using a Cajon valve, the ampules were removed from the glovebox and attached to the Schlenk line. Each ampule was evacuated to 150 mtorr and sealed to a length of 10 cm. The ampules were heated to 300 or 350 °C at a ramp rate of 0.5 °C/min, then held for 72 hours. Once cooled, the ampules were opened, and the crude brown material was washed in methanol, vacuum filtered, then vacuum dried at 150 °C overnight.

Trichloroheptazine and calcium nitride

To an agate mortar and pestle was added 0.50 g (1.8 mmol) TCH and 0.135 g (0.91 mmol) calcium nitride. The reactants were ground together for three minutes and a grayish-brown flour-like powder mixture was obtained. The mixture separated into two batches of 0.31 g and placed into two dried ampules. Using a Cajon valve, the ampules

were removed from the glovebox and attached to the Schlenk line. Each ampule was evacuated to 100 mtorr and sealed to a length of 7 cm. The ampules were heated to 400 or 350 °C at a ramp rate of 2 °C/min, then held for 72 hours. Once cooled, the ampules were opened, and the crude material was washed in methanol, vacuum filtered, then vacuum dried at 150 °C overnight.

Reaction of trichloroheptazine (TCH) with lithium carbide (Li_2C_2) or calcium carbide (CaC_2)

Trichloroheptazine and lithium carbide

To an agate mortar and pestle was added 0.125 g (0.45 mmol) TCH and 0.026 g (0.69 mmol) lithium carbide. The reactants were ground together for three minutes and a pale green flour-like powder mixture was obtained. The mixture was placed in a dried pyrex ampule. A second batch was made by grinding together 0.138 g (0.5 mmol) TCH and 0.028 g (0.74 mmol) lithium carbide for three minutes. Using a Cajon valve, the ampules was removed from the glovebox and attached to the Schlenk line. The first ampule was evacuated to 140 mtorr and the second was evacuated to 150 mtorr and both were sealed to a length of 7 cm. The first ampule were heated to 300 °C at a ramp rate of 1 °C/min and held for 72 hours. The second ampule were heated to 350 °C at a ramp rate of 1 °C/min and held for 60 hours. Once cooled, the ampules were opened, and the crude material was washed in methanol, vacuum filtered, then vacuum dried at 150 °C overnight.

Trichloroheptazine and calcium carbide

To an agate mortar and pestle was added 0.125 g (0.45 mmol) TCH and 0.044 g (0.69 mmol) calcium carbide. The reactants were ground together for three minutes and a pale green flour-like powder mixture was obtained. A second batch was made by grinding together 0.125 g (0.45 mmol) TCH and 0.044 g (0.74 mmol) calcium carbide for three minutes. Both mixtures were placed in separate dried pyrex ampules. Using a Cajon valve, the ampules was removed from the glovebox and attached to the Schlenk line. The first ampule was evacuated to 300 mtorr and second evacuated to 100 mtorr; both were sealed to a length of 7 cm. The first and second ampules were heated to 350 and 400 °C, respectively, at a ramp rate of 1 °C/min, then held for 72 hours. Once cooled, the ampules were opened, and the crude material was washed in methanol, vacuum filtered, then vacuum dried at 150 °C overnight.

Reaction of trichloroheptazine (TCH) with sodium trimethylsilyacetylides (Na-C≡C-Si(CH$_3$)$_3$)

There were two methods employed in the syntheses of an acetylene-bridged heptazine polymer.

Method 1: Ice bath addition of TCH

All manipulations were carried out in an argon atmosphere glovebox or under nitrogen gas via standard Schlenk line techniques. To a 250 mL Schlenk flask was added 0.63 g (16.1 mmol) of ground $NaNH_2$. In a separate 100 mL Schlenk flask was placed 1.11 g (4.0 mmol) TCH. Each flask was removed from the glovebox in which they were charged and attached to the Schlenk line. Under N_2, 75 mL of dry, degassed THF was added to the $NaNH_2$ flask and 25 mL was added to the TCH flask. A reflux condenser is

fitted to the $NaNH_2$ flask under flowing N_2. Using a syringe, 2.25 mL of trimethylsilylacetylene (TMSA) was added dropwise to the $NaNH_2$ suspension. The suspension was then heated at 70 °C for 15 minutes, then further heated to reflux for 2 hours. The milky white suspension of sodium trimethylsilylacetylide was then cooled in an ice bath. Once cooled, the clear TCH solution was added over the course of ten minutes. The milky suspension turned a dark brown/black color within five minutes and was stirred at the ice bath temperature for 20 minutes before being heated to reflux. The black suspension was refluxed for 15 hours then cooled to room temperature. The solvent was removed from the suspension to yield a dark brown solid, which was subsequently washed in toluene, then filtered. Acetone was then added to the solid and briefly stirred then filtered once more. The brown solid was then dried in air overnight to yield 1.96 g of crude material. Approximately 1.46 g of crude material was then washed in methanol to yield a very fine suspension. The suspension was then centrifuged to yield a dark brown solution over a black solid. The supernatant was decanted and the black solid was dried overnight and 0.69 g of black solid was recovered. A Soxhlet extractor charged with methanol was used to further purify 0.6 g of product. Yield: 0.43 g, 90 % (based on formation of material with formula C_9N_7).

Method 2: -84 °C bath addition of TCH

All manipulations were carried out in an argon atmosphere glovebox or under nitrogen gas via standard Schlenk line techniques. To a 250 mL Schlenk flask was added 1.31 g (33.7 mmol) of ground $NaNH_2$. In a separate 100 mL Schlenk flask was placed 2.21 g (8.0 mmol) TCH. Each flask was removed from the glovebox in which they were charged and attached to the Schlenk line. Under N_2, 50 mL of dry, degassed THF was

added to the $NaNH_2$ flask and 50 mL was added to the TCH flask. A reflux condenser is fitted to the $NaNH_2$ flask under flowing N_2. Using a syringe, 4.6 mL of trimethylsilylacetylene (TMSA) was added dropwise to the $NaNH_2$ suspension. The suspension was heated to reflux for 3 hours. The milky white suspension was then cooled in an ethyl acetate/liquid N_2 bath (-84 °C). Once cooled, the clear TCH solution was added over the course of five minutes. The now dark brown/black suspension was warmed to room temperature over the course of 30 minutes before being quickly heated reflux. The black suspension was refluxed for 15 hours then cooled to room temperature. The solvent was removed from the suspension to yield a dark brown solid, which was subsequently washed in chloroform, water, acetone, and methanol. The black solid was then purified with methanol in a Soxhlet extractor for 48 hours. Approximately 16.7 grams of wet solid was recovered. The material was then dried in air, then vacuum dried at 70 °C overnight to yield a black glassy material. Yield: 1.85 g, 112 % (based on formation of material with formula C_9N_7).

Thermal decomposition of 2-bis(trimethylsilylamido)-5,8-dichloro-s-heptazine

Under dynamic vacuum

The precursor 2-bis(trimethylsilylamido)-5,8-dichloro-s-heptazine (DCAH) was synthesized by the procedure mentioned in Chapter VI. A mass of 0.62 g of DCAH was weighed in an argon atmosphere glovebox and placed in a pyrex ampule. The tube was capped with a Cajon valve and removed from the glovebox and immediately attached to a Schlenk line. The tube was evacuated to a pressure of 60 mtorr and heated in a clamshell furnace in 25 °C increments to 300 °C and held for 3 hours. The tube was then heated to

350 °C and held for one additional hour. A mass of 22 mg was recovered. The experiment was repeated with 50 mg of DCAH by heating the precursor to 300 °C at 5 C/min and holding for 10 h. A mass of 28 mg was recovered.

Sealed ampule

A mass of 0.62 g of DCAH was weighed in an argon atmosphere glovebox and placed in a pyrex ampule. The tube was capped with a Cajon valve and removed from the glovebox and immediately attached to a Schlenk line. The tube was evacuated to a pressure of 150 mtorr and sealed to a length of 20 cm. The ampule was placed in a clamshell furnace and heated to a temperature of 300 °C at a rate of 2 °C/min and held for 10 hours. Once cooled, a dark brown solid with a mass of 0.46 g was recovered.

Instrumentation

Thermogravimetric-differential analysis (TG-DTA) was performed on a Seiko ExStar 6300 system under flowing argon. FT-IR absorption spectra were taken with a Nicolet Nexus 670 spectrometer using KBr pellets. Elemental analyses were performed on a Perkin Elmer 2400 CHN/O Analyzer using ultra light weight, ultra clean tin capsules. Powder X-ray diffraction was performed on a Siemens D5000 X-ray diffractometer, using Cu K_{α} radiation on samples mounted on glass slides. Scanning electron microscopy (SEM) was performed on a Hitachi S-4800 SEM with samples mounted on Al stubs and coated with Au-Pd alloy. Energy Dispersive Spectroscopy (EDS) was performed on samples affixed to Al stubs with carbon tape and coated with carbon.

Results and Discussion

Conversion of TCH and alkali or alkaline earth nitrides to C_6N_8 materials

Trichloroheptazine and lithium nitride

This series of experiments were designed to enact a solid state metathesis reaction between trichloroheptazine and lithium nitride (Li_3N) or Ca_3N_2. There are several established reports on the synthesis of carbon nitride materials from solid state reactions between the triazine analog, cyanuric chloride ($C_3N_3Cl_3$), and lithium nitride (Li_3N).[46,115,122,197,198] However, there are no reported syntheses involving the same reaction with trichloroheptazine ($C_6N_7Cl_3$). Therefore, the first steps were to perform the reactions in sealed ampules at high temperatures in order to generate the reaction in Equation 7.1.

$$C_6N_7Cl_3 + Li_3N \rightarrow C_6N_8 + 3LiCl \qquad \text{(Equation 7.1)}$$

From experiments attempting to synthesize $N(C_6N_7Cl_2)_3$ from Chapter VI, it was known that metathesis appeared to occur at temperatures in excess of 300 °C. Therefore, two reactions were performed at 300 and 350 °C. Chocolate brown powders were obtained from the sealed ampules. It was noted that some material had transported down the length of the ampule. It was thought that some of the TCH was subliming during the reaction. From the experiments attempting to synthesize $N(C_6N_7Cl_2)_3$, it was observed that if the end of the ampule was in a cooler zone, the TCH would transport to that cool end during the reaction. Powder X-ray diffraction performed under protective polymers revealed that formation of LiCl, as was expected from Equation 7.1. The reaction

performed at 300 °C also showed peaks that matched crystalline TCH. The data from the powder XRD can be seen in Figure 7.2. After washing, a broad peak near 27° was observed by XRD. It appeared that there were low intensity peaks present within the amorphous pattern, this suggested that there may be a minor amount of crystalline phase present in the sample. A second reaction was performed at a reduced heating rate of 0.1 C/min to 350 °C. After washing, it was revealed that a crystalline phase was present that matched up with the low intensity peaks from the faster heated sample. The results are present in Figure 7.2d. Upon further inspection under an optical microscope, it was found that tiny crystallites were present in the material. This material was compared to the pattern for TDT ($N(C_3N_3Cl_2)_3$) was reported by Yaghi, *et. al.*[17] Assuming that the

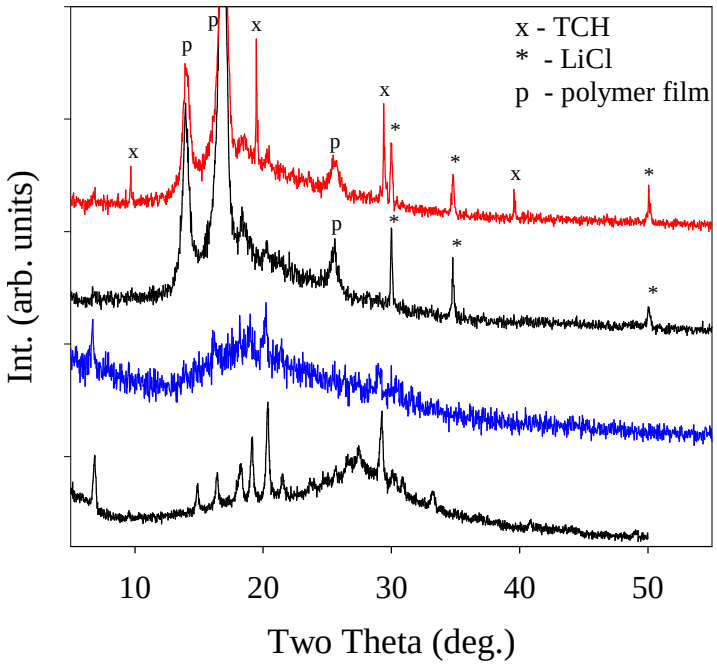

Figure 7.2 - Powder X-ray diffraction patterns for a) crude TCH + Li_3N at 300 °C, b) crude TCH + Li_3N at 350 °C, c) washed TCH + Li_3N at 300 °C, and d) washed TCH + Li_3N at 350 °C (slow heating).

Table 7.1 - Elemental analysis of crude and washed reaction products.

Reaction, Temp	Crude/ Washed	Weight %C	Weight %H	Weight %N	Weight % Diff.	Calc. Formula
TCH + Li_3N, 300	C	22.67	0.42	34.16	42.75	$C_6N_{7.76}H_{1.31}$
TCH + Li_3N, 300	W	17.75	4.59	26.32	51.34	$C_6N_{7.63}H_{18.49}$
TCH + Li_3N, 350	C	22.67	0.38	33.50	43.45	$C_6N_{7.60}H_{1.20}$
TCH + Li_3N, 350	W	20.62	3.79	30.02	45.57	$C_6N_{7.49}H_{13.14}$

first peak is the 110 reflection in a hexagonal crystal system, and the second peak the 20-1 reflection, the unit cell could be indexed to a = 25.876 and c = 6.82, in the same space group as TDT (*R*-3). Unfortunately, Pasteur methods could not be used to separate the crystallites from the bulk amorphous material. Further studies on separation by sublimation will have to be performed.

Elemental analysis was performed on the crude products, in order to establish hydrogen levels prior to washing. The large weight difference is expected due to the presence of lithium chloride salts. The calculated formulas begin to approach that of the expected C_6N_8 stoichiometry, though nitrogen is slightly deficient. As with most reported carbon nitride materials, there is still an inescapable amount of hydrogen present in the sample. This was expected to increase significantly during the washing step. Despite vacuum-drying the materials, it appeared that the brown powders would absorb atmospheric water, as they appeared somewhat wet upon sitting in ambient air. Increased hydrogen content by elemental analysis also would agree with this observation. A large weight difference of non-CHN material is still present. If the residual hydrogen content found in the washed materials is assumed to come from water, then the calculated amount

of oxygen from water was found to be on the order of 30-40 wt%, thus accounting for much of the weight difference. This equates to roughly 3 molecules of water per C_6N_7 unit. Alternately, it is also possible that incomplete combustion of this graphite-like material has occurred or residual lithium has led to Li_2O formation.

The FT-IR spectra of the crude materials were marked by the presence of sharp peaks in the spectra (See Figure 7.3). The spectra reveal multiple, almost identical absorption bands in the region between 1600 and 800 cm^{-1}. Strong, broad absorptions are detected at 1612 and 1332 cm^{-1}; medium to weak, sharp absorptions appear at 2158, 1552, 1514, 1213, 1179, 1093, 943, and 824 cm^{-1}. Figure 7.3a and 7.3b shows a comparison of the IR spectra of crude product with TCH. The differences in the crude

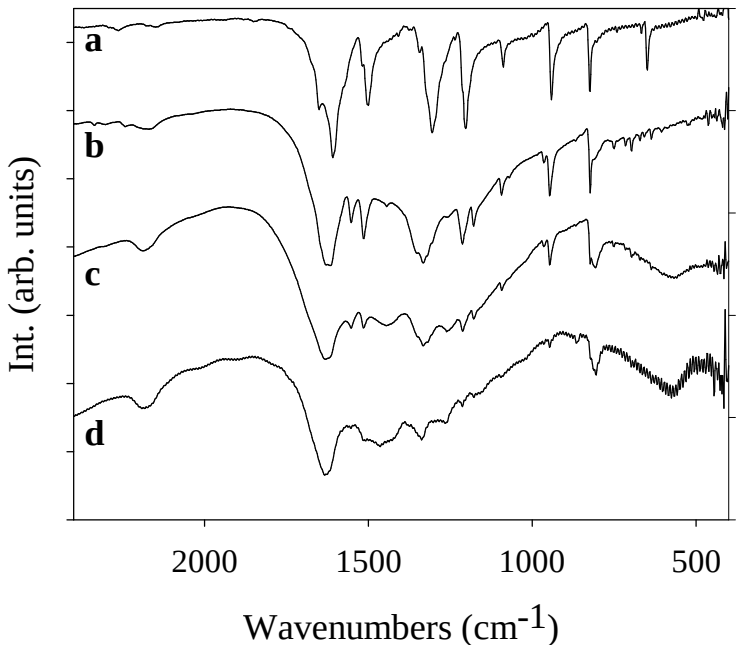

Figure 7.3 - FT-IR spectra of a) TCH b) crude reaction product from reaction with Li_3N at 350 °C, c) washed reaction product from 350 °C, and d) washed reaction product from 300 °C.

product spectrum are new peaks at 2158, 1552, 1179, a shoulder on the 1332 cm^{-1} peak and the decrease in the intensity of the 648 cm^{-1} peak. The peak at 2158 cm^{-1} is indicative of a cyanide C≡N stretch, suggesting that a portion of the material is undergoing ring cleavage. The decrease of the peak at 648 cm^{-1} suggests the loss of C-Cl stretching vibrations, while the shoulder at 1332 cm^{-1} suggests the formation of a C-N stretch from aromatic amines.

Meyer performed a series of reactions between $C_3N_3Cl_3$ and Li_2CN_2, Li_3BN_2, and H_2NCN and every product obtained showed a remarkably similar FTIR spectrum to that of the crude products.[115] His synthesized materials were suggested to come from a $N(C_3N_3Cl_2)_3$ template that was observed to form at temperatures of 200-250 °C. The comparison of spectra between this intermediate and our crude material shows absorptions at 1550, 1515 and 1094 cm^{-1} are found in both spectra at almost the same position and might be assigned to stretching modes of the triazine ring (1550,1515 cm^{-1}) and to a NC_3 stretching mode of tertiary amines (1094 cm^{b}). The sharpness of the peaks suggest that the part of the material causing these vibrations is molecular in nature. Upon washing, the sharp peaks at 1552, 1514, 1213, 1179, 1093, and 943 cm^{-1} are significantly reduced in intensity, suggesting that some material is being washed away (Figure 7.3c,d). The remaining broad peaks are near 1624, 1512, 1429, 1336, 824, and 2180 cm^{-1}. These are peaks that generally have been reported for carbon nitride-type materials. The similarities in IR spectra in this Chapter and Meyer's work suggest that, once again, in his synthesis a triazine precursor is possibly being converted to a heptazine building block during thermal heating (at 500 °C). This was also supported by the work performed in Chapter II.

Trichloroheptazine and calcium nitride

The analogous reaction was performed between TCH and calcium nitride, as demonstrated in Equation 2. Rather than LiCl, the byproduct salt is calcium chloride, $CaCl_2$. An initial reaction at 300 °C showed no change in the tan reactant mixture, so the reaction temperature was increased to 400 °C. The reaction products were recovered as

$$C_6N_7Cl_3 + 0.5Ca_3N_2 \rightarrow C_6N_8 + 1.5CaCl_2 \qquad \text{(Equation 7.2)}$$

brown to dark brown solids. Elemental analysis of the reaction product from 400 °C revealed a composition of 20.34 wt% C, 1.10 wt% H, and 31.51 wt% N, which approaches a chemical formula of $C_6N_{7.97}H_{3.85}$. The powder XRD is shown in Figure 7.4.

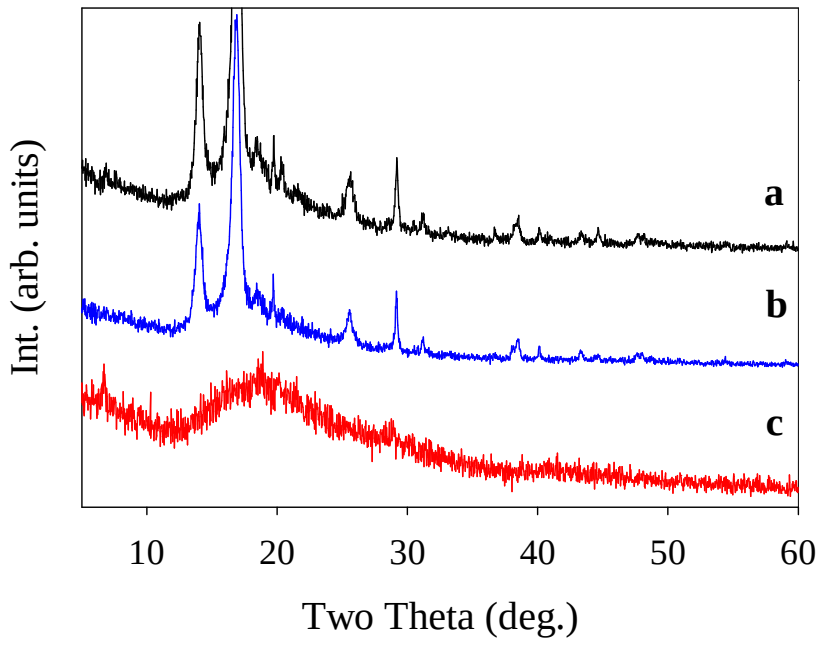

Figure 7.4 - Powder X-ray diffraction patterns of a) crude TCH + 0.5 Ca_3N_2 at 350 °C, b) crude TCH + 0.5 Ca_3N_2 at 400 °C, and c) washed TCH + 0.5Ca_3N_2 at 400 °C.

Powder XRD of the crude products showed that the byproduct $CaCl_2$ was indeed formed (Figure 7.4 a,b). The products were washed in methanol to remove the byproduct salt; amorphous powders were obtained after washing (See Figure 7.4c for example). The washed material had a composition of 23.69 wt% C, 3.19 wt% H, and 34.99 wt% N, corresponding to a chemical formula of $C_6N_{7.60}H_{9.63}$.

FTIR analysis of the crude products showed nearly identical sharp peaks as those obtained from reaction with lithium nitride (Figure 7.5). The only difference is the lack of a peak near 2160 cm^{-1}, suggesting that no cyanide groups are present and perhaps no ring fracture occurred during the reaction. Again, the washing step in methanol leads to a disappearance of the sharp peaks. The remaining peaks correspond with those of the

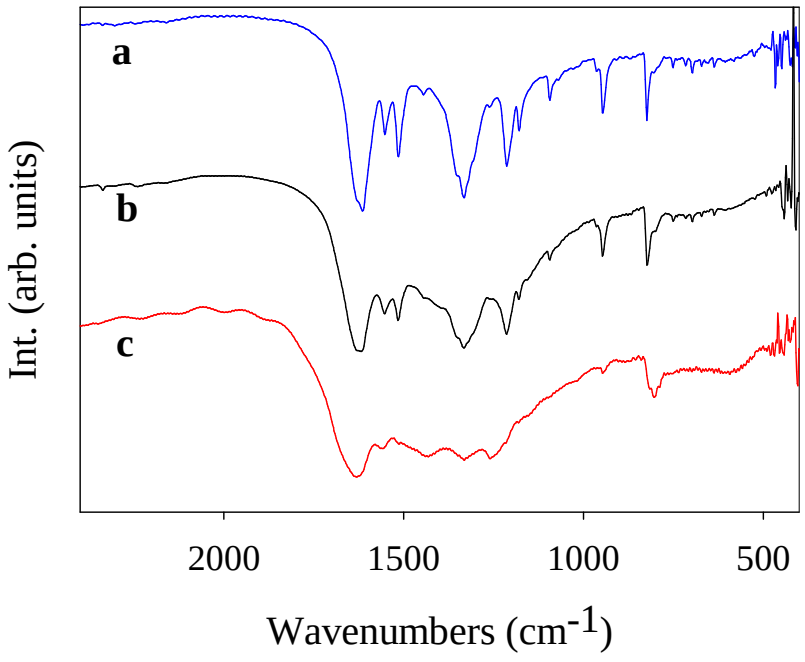

Figure 7.5 - FT-IR spectra of a) crude TCH + 0.5 Ca_3N_2 reacted at 350 °C, b) crude TCH + 0.5 Ca_3N_2 reacted at 400 °C, and c) washed TCH + 0.5 Ca_3N_2 reacted at 400 °C.

products from the lithium nitride reactions: 1624, 1550, 1429, 1336, 1210, 1180, 1094, 943, and 820 cm^{-1}. These results suggest that similar products are being produced by either Li_3N or Ca_3N_2.

Conversion of TCH and metal carbides to C_9N_7 materials

Lithium carbide and calcium carbide are interesting compounds in that they feature the acetylide ($:C\equiv C:^{2-}$) dianion within their crystal structure.[199] They have been used to synthesize graphite and metal carbides in solid state metathesis reactions.[198,200] Therefore, it was proposed that TCH and Li_2C_2 could undergo a similar metathesis reaction as those performed with lithium nitride and calcium nitride to generate carbon-rich carbon nitride materials. The proposed reaction schemes are shown in Equations 7.3 and 7.4. Instead of linking heptazines with a tertiary nitrogen, they could otherwise be bridged by acetylene units.

$C_6N_7Cl_3 + 1.5Li_2C_2 \rightarrow C_6N_7(C\equiv C)_{1.5}$ or "C_9N_7" + 3LiCl (Equation 7.3)

$C_6N_7Cl_3 + 1.5CaC_2 \rightarrow C_6N_7(C\equiv C)_{1.5}$ or "C_9N_7" + $1.5CaCl_2$ (Equation 7.4)

Using the same reaction scheme as that reported for lithium nitride, the reactions were performed at 350 or 400 °C to yield brown or dark brown powders. Again, it was noted that some material had transported down the length of the ampule during the reaction. The crude products were examined using XRD (Figure 7.6). The patterns revealed the formation of LiCl or $CaCl_2$, as was expected from Equation 7.3 or 7.4 (Figure 7.6 a,b). At this time, a control reaction was also performed by heating an ampule of only TCH to 350 °C. The powder pattern of control showed only a broad reflection near 28° (Figure 7.6c).

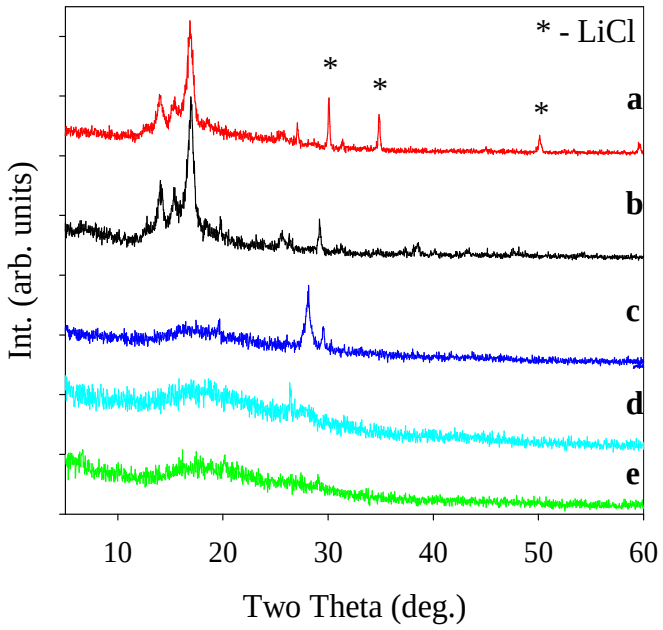

Figure 7.6 - Powder X-ray diffraction patterns of a) crude TCH + 1.5 Li_2C_2 at 350 °C, b) crude TCH + 1.5 CaC_2 at 400 °C, c) TCH at 350, d) TCH+1.5 Li_2C_2 at 300 °C washed, and e) TCH + 1.5 CaC_2, 350 °C washed.

Elemental analysis was performed on some of the crude and washed products. The results can be found in Table 7.2. The calculated formulas approach the predicted stoichiometry of C_9N_7. The washed materials show significant amounts of hydrogen in the formulas. It has been noticed that these materials tend to absorb water from the atmosphere, to the point they were they actually appear clumped and wet. Therefore, this would explain the high values of hydrogen, because they were exposed to ambient air for a significant amount prior to analysis. The calculated formula of the control experiment still shows a stoichiometry consistent with $C_6N_7Cl_3$. The weight percent of chlorine for $C_6N_7Cl_3$ is 38.5%, this is near the weight difference found for the crude material. The

washed materials indicate the presence of the hypothesized C_9N_7 stoichiometry, while also demonstrating high hydrogen content from absorbed water.

Table 7.2 - Elemental analysis of crude and washed products from reactions of TCH with metal carbides.

Reaction, Temp.	Crude/ Washed	Weight %C	Weight %H	Weight %N	Weight % Diff.	Calc. Formula
TCH + 1.5CaC_2, 350 °C	C	25.55	0.88	24.53	49.04	$C_9N_{7.41}H_{3.67}$
TCH + 1.5CaC_2, 350 °C	W	26.37	1.79	21.68	50.16	$C_9N_{6.34}H_{7.28}$
TCH + 1.5Li_2C_2, 350 °C	C	27.67	0.61	24.69	47.03	$C_9N_{6.89}H_{2.36}$
TCH + 1.5Li_2C_2, 350 °C	W	32.80	2.63	29.59	34.98	$C_9N_{6.96}H_{8.60}$
TCH + 1.5CaC_2, 400 °C	C	25.55	1.93	23.58	48.94	$C_9N_{7.12}H_{8.1}$
TCH + 1.5CaC_2, 400 °C	W	32.81	2.53	28.79	35.87	$C_9N_{6.77}H_{8.27}$
TCH, 350 °C	C	27.28	0.06	36.76	35.60	$C_6N_{6.93}H_{0.16}$

Sample FT-IR spectra of selected crude and washed products can be found in the Figure 7.7. All of the crude products revealed the same pattern of absorbances as those found in the crude products from the metal nitride reactions with TCH. One noted absence is a peak in the 2100-2200 cm^{-1} region, which is indicative of alkyne stretches. some of the reactant must be decomposing. The yields for most the washed metathesis products were in the range of 76 - 119% based on either a C_6N_8 or C_9N_7 formula. The only reaction with a low yield was the reaction of Li_2C_2 with TCH at 300 °C, which had a yield of 21%. This was thought to be low because the temperature is too low to drive the reaction to completion and unreacted TCH was washed away in the washing step. The

>100 % yield found to occur in the lithium nitride reactions may due to absorbed water, contributing to increased mass.

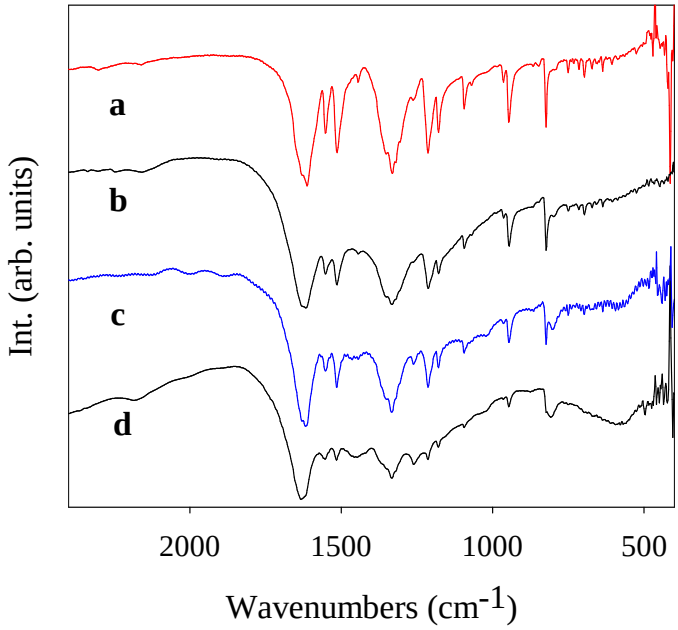

Figure 7.7 - FTIR spectra of a) crude TCH at 350 °C, b) crude TCH+1.5CaC_2 at 400 °C, c) washed TCH+1.5CaC_2 at 400 °C, and d) washed TCH+1.5Li_2C_2 at 350 °C.

Thermal properties of TCH metathesis materials

All thermogravimetric differential thermal analysis (TG-DTA) was performed under argon, and can be found in Figure 7.8. Generally speaking, there were three major events that occurred. The first was the desorption of any unremoved solvent or absorbed water from the atmosphere at temperatures near 100 °C. The C_6N_8 systems (Li_3N, Ca_3N_2) tended to lose more weight (~10-20%) during this step than the C_9N_7 materials (~5-10%). The materials were then subjected to continuous losses from 300-650 °C (30-

35% loss). The third event was a sharp weight loss occurred between 650 and 700 °C. This also happens to be the decomposition temperature of TCM-CN_x. The most thermally stable material was found to be the C_9N_7 product synthesized from CaC_2 at 400 °C. It still had ~40% retention of its original mass at 1000 °C. In fact, all metal carbide reactions all showed carbonaceous residues present after heating to 1000 °C.

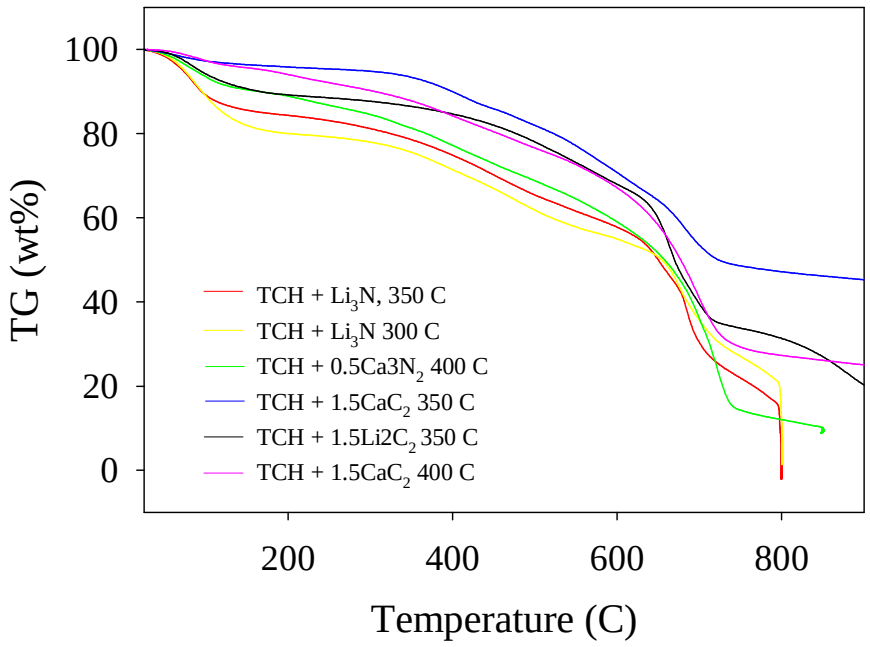

Figure 7.8 - Thermogravimetic analysis of metathesis polymers.

Conversion of TCH and alkali trimethylsilylacetylides to C_9N_7 materials

The idea of this was born out of a similar reaction performed by Kouvetakis *et. al.*[201] A schematic of his reactions are shown in Figure 7.9. While attempting to

synthesize a precursor molecule, 2,4,6-tris(trimethylsilyl)ethynyl-1,3,5-triazine, it was found that a reaction between trichlorotriazine and lithium acetylide would result in a black polymeric material. In order to avoid this, the trifluorotriazine ($C_3N_3F_3$) was used instead to yield the molecular species. Kouvetakis rationalized that reason for the formation of the polymeric material was that the highly exothermic reaction first produced (trimethylsilyl)ethynyl-substituted triazine intermediates which subsequently undergo loss of the protecting trimethylsilyl groups to yield conjugated polymers. The

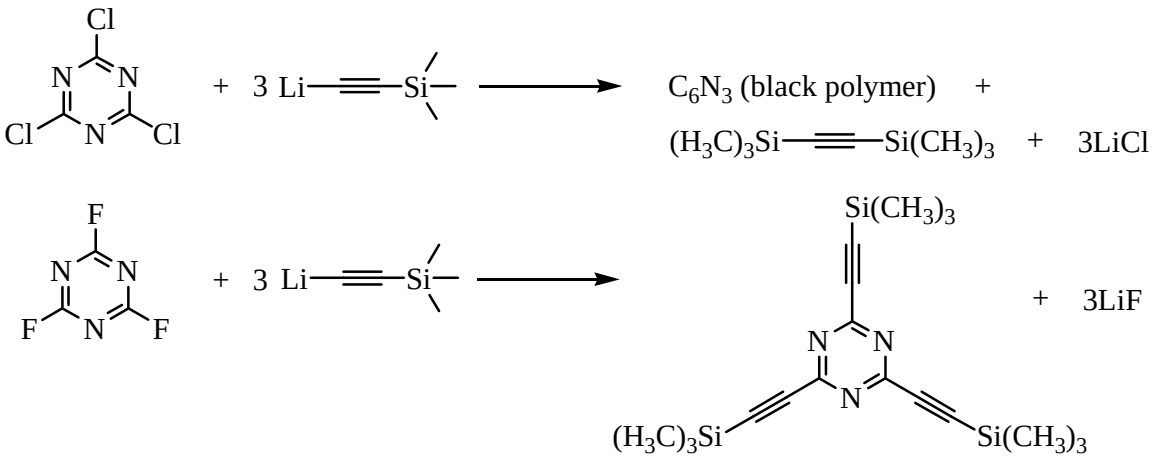

Figure 7.9 - Kouvetakis' reactions of trihalotriazines with lithium trimethylsilylacetylide.[201]

electron-accepting nature of the triazine may have cause destabilization of the Si-C bond, thus allowing the triazine intermediates to react with each other.

Attempts to synthesize the heptazine analogue of the molecular species were briefly summarized in Chapter VI. It was found that reactions between lithium acetylide and TCH analogously resulted in the formation of an dark brown or black material. This

material showed a very strong IR peak at 2170 cm^{-1} and suggested that this material was also polymeric in nature. However attempts to wash this material resulted in fine suspensions in H_2O or methanol and could not be filtered out. It was rationalized that these materials were not sufficiently crosslinked to result in an insoluble polymer.

Therefore two attempts were made to target this black polymeric material. Several factors were considered to be necessary to ensure the formation of a polymeric material: reaction stoichiometry and reaction temperature. It was thought an excess of alkali acetylide would ensure a fully crosslinked material by providing higher probability of that occurring. The reaction temperature was also considered to be important, in that decomposition of any intermediates had to be complete to ensure crosslinking. Therefore, a 1:4 ratio of TCH to alkali acetylide was used and the reaction temperature was probed by initiating the reaction at ice bath temperatures or at cold bath temperatures (-83 °C).

The reaction itself is a metathesis reaction between TCH and the acetylide to form alkali chloride as the byproduct salt. The first step is the formation of alkali acetylide. In this case, trimethylsilylacetylene (TMSA) is reacted with sodium amide ($NaNH_2$) in a THF suspension. The NH_2^- anion is a powerful enough base to deprotonate the slightly acidic alkyne proton of the TMSA and form ammonia gas as the byproduct. Therefore when TMSA is added to a suspension of sodium amide, bubbling is observed which was rationalized as ammonia formation. Refluxing the cloudy suspension resulted in the formation of a milky white suspension as the sodium trimethylsilylacetylide is insoluble in THF. When a solution of TCH in THF was added dropwise to the milky suspension in an ice bath, an immediate darkening is noted. When TCH addition was complete, the

suspension had already turned black. The suspension was quickly heated to reflux temperatures overnight. Once cooled, the solvent was removed under reduced pressure, to yield a large amount dark brown/black solid. Powder X-ray diffraction revealed the presence of crystalline NaCl in the crude material. When the material was washed in methanol, a fine suspension formed which could be separated by centrifugation to yield a black solid and clear dark brown supernatant. ^{1}H-NMR of the supernatant in D_2O showed only residual THF as the only identifiable by product. Since the methanol wash was still dark, it was thought there may still be a considerable amount of soluble byproducts still present. Therefore, the product was washed by Soxhlet extraction of the soluble byproducts in methanol. It was found that a considerable amount of extraction was necessary to remove these byproducts (~ 48 hours). After vacuum-drying the products, they still appeared to absorb H_2O from the atmosphere, but no provisions were made for this.

The two products were characterized by elemental analysis. The ice bath reaction product showed a composition of 35.78 wt% C, 3.52 wt% H, 29.95 wt% N, which corresponds to a empirical formula of $C_9N_{6.46}H_{10.55}$. The cold bath reaction product showed a composition of 43.86 wt% C, 3.41 wt% H, and 28.91 wt% N, which corresponds to an empirical formula of $C_9H_{8.34}N_{5.09}$. If the formulas are compared to the predicted stoichiometry of C_9N_7, it becomes apparent that products approach the appropriate values, but are either deficient in nitrogen, or have an excess of carbon. The excess of carbon seems more likely, given that the non-CHN weight percent is 31 wt% and 23 wt% for the ice bath reaction and cold bath reactions, respectively. This would indicate the presence of remaining trimethylsilyl groups in the final products, or possibly

unreacted chlorides from the TCH. There are also significant amounts of hydrogen in the final product, which could be from the trimethylsilyl groups or absorbed H_2O.

The IR spectra of the reaction products show significant differences from the the starting TCH reactant and can be viewed in Figure 7.10. Each product shows the presence of a peak near 800 cm^{-1}, which indicates the presence of the heptazine ring the final products. What also becomes readily apparent is the presence of a peak near 2150 cm^{-1} in each product. This peak indicates the presence of an alkyne stretch (-C≡C-) in the final products , which follows the suggested structure. In each case, there a very broad absorbances in the 1600-1000 cm^{-1} region; this occurs in the C=N, C=C, C-C, and C-N region. This suggests that heptazine is bonded to the substituent carbon of the alkyne

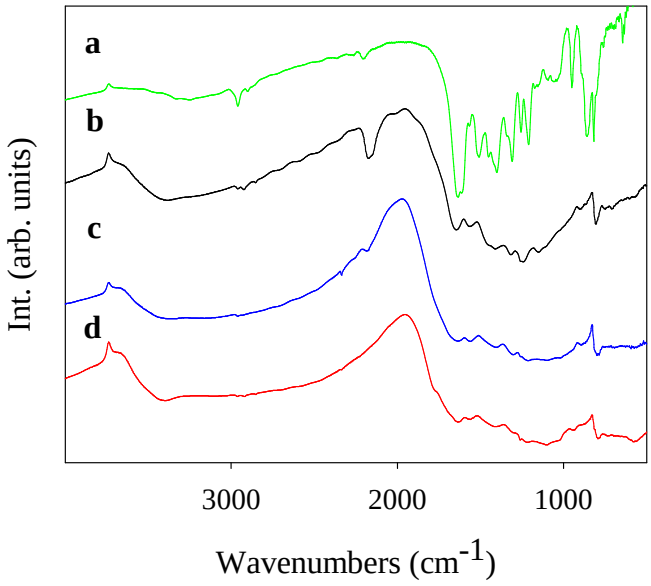

Figure 7.10 - FTIR spectra of TCH + alkali acetylides a) trichloroheptazine (TCH), b) TCH + 4 Na-C≡C-$Si(CH_3)_3$ at 0 °C, and c) TCH + 4 Na-C≡C-$Si(CH_3)_3$ at -83 °C.

group. The cold bath reaction product shows larger absorbances in the 1000-1200 cm^{-1} region. This would be in the C-C region and suggests higher connectivity in the product versus the ice bath reaction. The ice bath reaction product also shows absorbances at 2900 cm^{-1} which would indicate the increased presence of the C-H stretches from remaining trimethylsilyl groups versus the cold bath reaction. Each product spectra has a broad absorbance at 3500 cm^{-1} which follows the previous indication that the products absorbed water from the ambient air.

These products were also characterized by XRD, and it was found that these materials were amorphous and only a broad background peak was observed. All thermogravimetric differential thermal analysis (TG-DTA) was performed under argon. The thermal analysis of the products showed similar responses upon heating to 1000 °C. Each product showed losses near 100 °C, which suggests desorption of residual solvent and absorbed H_2O. The products lost ~10-15 wt% up to 400 °C, at which point, a considerable step loss of 15-20 wt% was observed. The materials then showed gradual losses up to 1000 °C. The cold bath product appeared to be more thermally stable as approximately 40 wt% of material remained in comparison to 25 wt% for the ice bath product.

Decomposition of DCAH to C_6N_8 materials

The synthesis of the precursor molecule 2,5-dichloro-8-bis(trimethylsilyl)amidoheptazine (DCAH) was performed as described by Horvath-Bordon.[179] The synthesis was based on previous reports for the triazine analogue.[35,41,202,203] The idea was that DCAH would decompose following the pathway as was proposed by Kouvetakis, *et. al.* and portrayed in Figure 7.11.[41] The single source

precursor would thermally decompose to form a polymeric material and generate chlorotrimethylsilane, $(H_3C)_3SiCl$, as a byproduct, as described in Figure 7.11. Very little characterization was given to the thermal decomposition of the precursor except for mentioning that the product recovered from a TGDTA measurement by heating DCAH to 350 °C contained an empirical formula of $C_{6.9}N_{6.8}Si_{0.18}$. This decomposition was studied in further detail to elucidate the formation of the material.

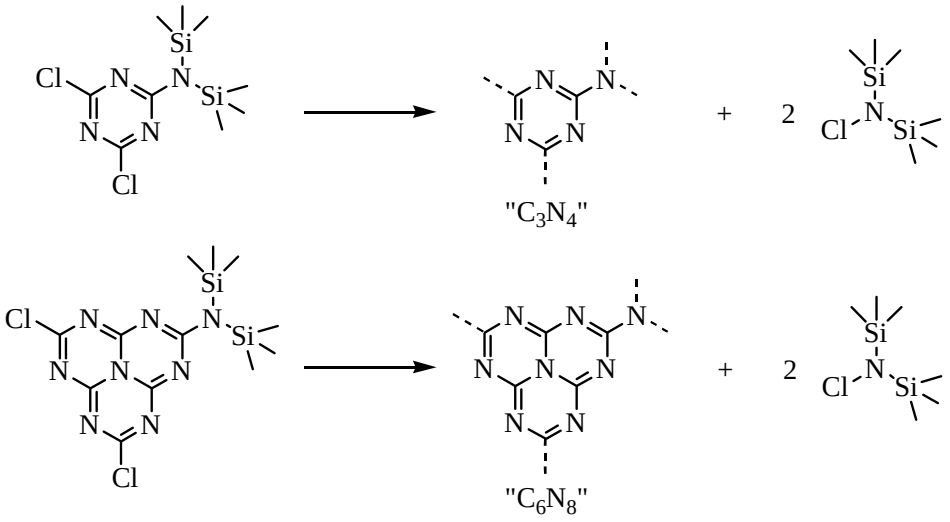

Figure 7.11 - Decomposition pathway of $C_3N_3Cl_2[Si(CH_3)_3]$ and $C_6N_7Cl_2[Si(CH_3)_3]$ (DCAH) to yield carbon nitride materials and generate chlorotrimethylsilane as a byproduct.

Two methods were used to explore this decomposition reaction: heating DCAH under dynamic vacuum at 300 and 350 °C or heating DCAH in a sealed ampule at 300 °C. In both cases, a dark brown glassy material was formed. Elemental analysis of the material heated to 350 °C under vacuum had a composition of 26.89 wt% C, 2.62 wt% H, and 38.60 wt% N, which corresponds to a calculated formula of $C_6N_{7.39}H_{6.97}$. The

ampule product had a composition of 30.58 wt% C, 3.26 wt% H, and 39.31 wt% N, which corresponds to a formula of $C_6N_{6.61}H_{7.62}$. These materials have higher carbon content than the proposed C_6N_8 stoichiometry considers. This would suggest that materials are incompletely decomposed and have residual trimethylsilyl groups remaining in the material. There was also a non-CHN component of uncombusted

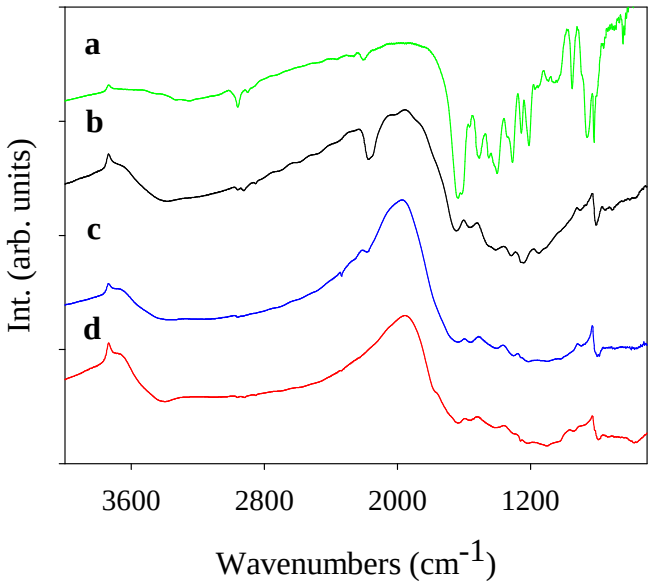

Figure 7.12 - FTIR spectra of DCAH decomposition products a) DCAH, b) DCAH decomposed under dynamic vacuum at 350 °C, c) DCAH decomposed under dynamic vacuum at 300 °C, and d) DCAH decomposed sealed ampule at 300 °C.

materials in the decomposition products. This may be due to absorbed H_2O, residual NaCl from the synthesis of DCAH, or residual silicon that oxidizes to form SiO_2. In the case of the ampule decomposition product, a liquid byproduct had formed in the cool end of the ampule. ^{1}H-NMR of this material showed a singlet at 0.45 ppm, which

corresponds well with the methyl hydrogens of trimethylsiylchloride ($(H_3C)_3SiCl$). This suggests that within this temperature regime, the proposed decomposition pathway is valid.

The FTIR spectra of the DCAH decomposition products can be found in Figure 7.12. The products show significant differences from the starting DCAH material. The products show a disappearance of the peak at 850 cm^{-1} and the peak at 640 cm^{-1}. As previously mentioned in Chapter VI, these peaks represent the Si-N and C-Cl stretches, respectively. Each product shows a peak at 800 cm^{-1}, indicating that the heptazine ring is still present in the product. The products showed broad absorbances in the 1000-1200 cm-1 region. This is in the C-N stretching region and would suggest that the rings are being linked to nitrogen during DCAH decomposition. Each product shows broad absorbances in the 1600-1300 cm^{-1} region, which indicates the continued presence of C=N-type frequencies, as had been observed in the TCM-CN_x products of Chapter II. The products also show broad absorbances in the 3500 cm^{-1} regions, which suggests some H_2O absorption in the final products. One difference of note was the peak at 2200 cm-1 for the product decomposed at 350 °C. This suggested that the heptazine rings may have decomposed, so it was thought that heating above 300 °C was excessive.

Further structural analysis was carried out by XRD (Figure 7.13). The product heated under vacuum at 350 °C, showed peaks corresponding to residual NaCl from the synthesis of DCAH. Otherwise, the material was amorphous. For the the products heated to 300 °C, the material heated under dynamic vacuum showed a broad shoulder on the background peak near 27°. The ampule product also showed a broad peak at 27°. This suggests that these materials are forming a graphite-like ordering in the final

products, which is typical of layered material. These materials also were examined by TGDTA. The products showed decomposition temperatures near 660 °C which is very similar to the TCM-CN_x products from Chapter II. This suggests that the material still retains its heptazine character.

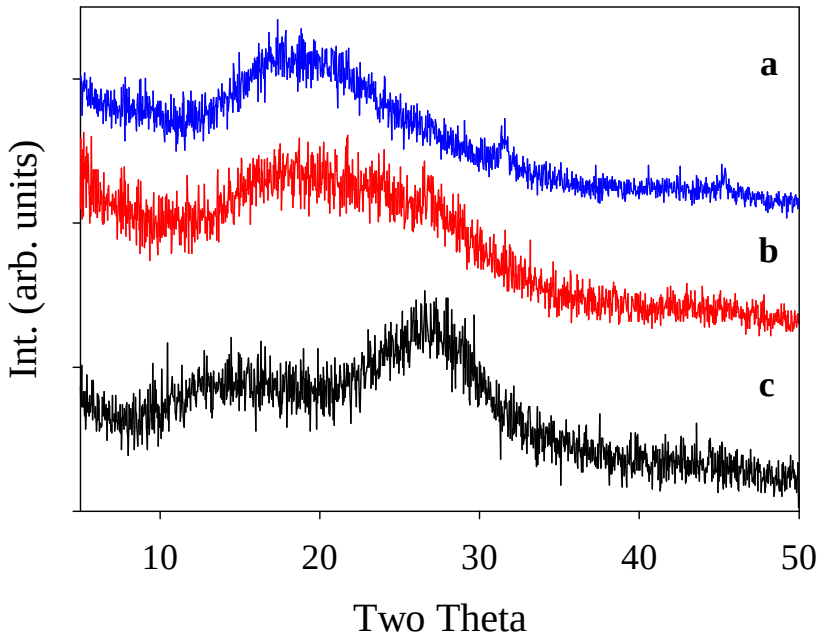

Figure 7.13 - Powder X-ray diffraction patterns of a) DCAH, b) DCAH decomposed under dynamic vacuum at 350 °C, c) DCAH decomposed under dynamic vacuum at 300 °C, and d) DCAH decomposed in a sealed ampule at 300 °C.

Conclusions

Several attempts were made to synthesize polymeric heptazine materials using heptazine precursors. Some extended solids with the C_6N_8 and C_9N_7 stoichiometry were made through the solid state metathesis reaction between trichloroheptazine and either

lithium nitride or lithium carbide. Powder X-ray diffraction indicated that salt formation was occurred during these reactions and products had roughly the desired C-N stoichiometry. A polymeric heptazine material, linked by acetylene units was also synthesized from a low temperature reaction of TCH with alkali acetylides. FT-IR analysis revealed that products contained the appropriate heptazine and acetylene-based absorbances. These materials proved to be quite thermally stable materials, though the materials did not appear to be completely polymerized. A polymeric heptazine material was produced from the thermal decomposition of 2,5-dichloro-8-(bistrimethylsilylamido)heptazine (DCAH). Analysis of the byproducts showed that trimethylsilylchloride is eliminated from this molecular precursor. The products also did not appear to be completely polymerized by IR and elemental analysis.

CHAPTER VIII

OTHER MODIFICATIONS OF TRICHLOROMELAMINE DECOMPOSITION FOR METAL CATALYST AND CONDUCTING CN_X APPLICATIONS; FINAL THOUGHTS AND FUTURE OUTLOOK

Introduction

Previous work by Dale Miller made attempts to synthesize metallated carbon nitride materials with the incorporation of copper and platinum salts into TCM-CN_x/carbon black blends for the use as catalyst supporting materials in fuel cells.[151] It was found that some his materials showed performance as good, if not better than a commercial material of Pt on carbon black. Currently, there are many variations of fuel cells, but one of them is the proton exchange membrane fuel cell (PEMFC). The PEMFCs are highly desirable, in that they have low operating temperatures and only produce energy and water as products. One of the limiting factors has been the O_2 reduction reaction (ORR) that occurs at the cathode of the cell (Equation 8.1).[204]

$$O_2 + 4H^+ + 4e^- \rightarrow 2H_2O \qquad \text{(Equation 8.1)}$$

The cathode catalyst of choice is currently Pt distributed on carbon; however, the reaction is still sluggish despite high catalyst loading. Pt is a very expensive and economically unfeasible, so other less expensive electrocatalysts are desired in order to make the PEMFC viable. In the 1970's it was found that heat-treating cobalt phthalocyanines resulted in good candidates for ORR catalysis.[205] Recently, Birss *et. al.* reported sol-gel preparations of heat-treated Co-N-C catalysts that showed ORR activity.[206,207] It was therefore proposed that two different pathways could lead to

materials that would be ultimately applicable to catalyst supports for ORR activity. The incorporation of a metal phthalocyanine into TCM decomposition may provide a new pathway toward metal incorporation into the TCM-CN_x product. The employment of lithium carbide (Li_2C_2) or anthracene in the TCM reaction may provide a carbon source that helps to improve conductivity of the TCM-CN_x support.

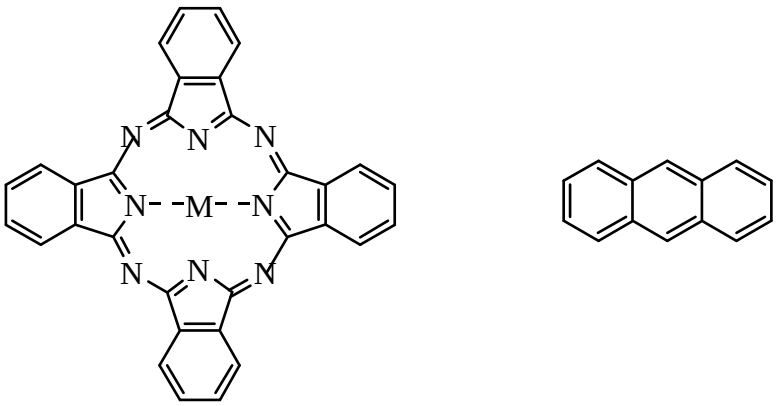

a) b)

Figure 8.1 - Structures of organic carbon sources a) metal phthalocyanine (MPc, $MC_{32}H_{16}N_8$) and b) anthracene ($C_{14}H_{10}$).

Experimental

Reagents

Methanol was purchased from Fisher Scientific. Trichloromelamine (TCM, $C_3N_3(NHCl)_3$, 98%) and lithium nitride (Li_3N) were purchased from Aldrich. Lithium carbide (Li_2C_2) was purchased from Alfa; anthracene ($C_{14}H_{10}$) was purchased from

Scintillation Chemical, and copper phthalocyanine (CuPc, $CuC_{32}H_{16}N_8$, technical grade) was purchased from Matheson Coleman & Bell.

Solid state incorporation of copper phthalocyanine or anthracene into trichloromelamine decomposition

In argon atmosphere glovebox, 1g TCM (4.4 mmol) was mixed with 0.33 g copper phthalocyanine (0.57 mmol) in a ceramic mortar and pestle for 15 minutes. The mixture was transferred to a Parr reactor. The reactor was removed from the glovebox and assembled under flowing N_2 gas. Using a custom mantle, the reactor was heated to an internal temperature of 205 °C, then slowly cooled to room temperature. Upon opening the reactor, there was a fluffy brown material present on the walls of the reactor accompanied by a mass of blue gray material with a mass of 0.71 g. The material was washed in methanol for 1h, then vacuum filtered. The collected solid was then subjected to vacuum drying at 75 °C overnight. A mass of 0.66 g of product was recovered.

In argon atmosphere glovebox, 1g TCM (4.4 mmol) was mixed with 0.33 g anthracene (2.2 mmol) in an agate mortar and pestle for 5 minutes. 1.25 g of the mixture was transferred to a Parr reactor. The reactor was removed from the glovebox and assembled under flowing N_2 gas. Using a custom mantle, the reactor was heated to an internal temperature of 205 °C, then slowly cooled to room temperature. Upon opening the reactor, there was a fluffy brown material present on the walls of the reactor accompanied by a mass of dark gray material with a mass of 0.71 g. 0.39 g of material was washed in methanol for 1h, then vacuum filtered. The collected solid was then subjected to vacuum drying at 75 °C overnight. A mass of 0.25 g of product was recovered.

Solid state Li_2C_2 incorporation into trichloromelamine decomposition

Three different ratios of Li_2C_2 were employed in the reaction and can be found in Table 8.1. A typical synthesis is as follows. In argon atmosphere glovebox, 3.0 g (13.1 mmol) TCM was mixed with 0.74 g (19.7 mmol) Li_2C_2 in an agate mortar and pestle for 5 minutes. 3.45 g of the mixture was transferred to a filament reactor (See Chapter III for details). The reactor was removed from the glovebox and attached to a Variac. Using a setting of 10%, the reaction was initiated, a large amount of vapor escaped from the reactor. Upon cooling and opening the reactor, a mass of black material was present. The material was washed in methanol, then vacuum filtered. The collected solid was then subjected to vacuum drying at 75 °C overnight. A mass of 0.23 g of product was recovered.

Table 8.1 - Summary of lithium compounds incorporated into TCM decomposition.

Reactants	**Mass TCM (g)**	**TCM:Li_2C_2 molar ratio**	**Heating Method**	**Appearance**	**Recovered Mass (g)**
Li_2C_2	3.0	1:1.5	Filament	black	0.23
Li_2C_2	3.0	1:0.75	Filament	black	0.21
Li_2C_2	3.0	1:0.375	Filament	brown	0.80

Instrumentation

Thermogravimetric-differential analysis (TG-DTA) was performed on a Seiko ExStar 6300 system under flowing argon. FT-IR absorption spectra were taken with a

Nicolet Nexus 670 spectrometer using KBr pellets. Elemental analyses were performed on a Perkin Elmer 2400 CHN/O Analyzer using ultra light weight, ultra clean tin capsules. Powder X-ray diffraction was performed on a Siemens D5000 X-ray diffractometer, using Cu K_α radiation on samples mounted on glass slides. Scanning electron microscopy (SEM) was performed on a Hitachi S-4800 SEM with samples mounted on Al stubs and coated with Au-Pd alloy.

Results and Discussion

Solid state incorporation of CuPc and Anthracene in TCM Decomposition

The reactions between TCM and CuPc or anthracene were originally formulated to reflect a final product mixture of 1:1 TCM-CNx/CuPc(or anthracene) by mass. This translates to molar mixtures of 7.72:1 TCM/CuPc and 2:1 TCM/anthracene. On a 1 g scale, a TCM decomposition reaction will yield approximately 0.33 g of TCM-CN_x. The CN_x/CuPc product mass was 197 % larger than expected when compared to the same scale decomposition of TCM alone. The CN_x/anthracene product was approximately 76% of the expected TCM-CN_x product mass. This suggests that the CuPc may not be thermally decomposing during reaction, while the anthracene is partially decomposing during reaction. The first obvious evidence of something other than a normal TCM-CN_x product and these mixtures is the color of the products. The CN_x/CuPc product is a bluish gray color and the CN_x/anthracene product is black, while TCM-CN_x is an orange tan color. No elemental analysis was collected on these products, but a higher C wt% and H wt% would be expected. More work would be necessary to reveal the effect of different molar mixtures.

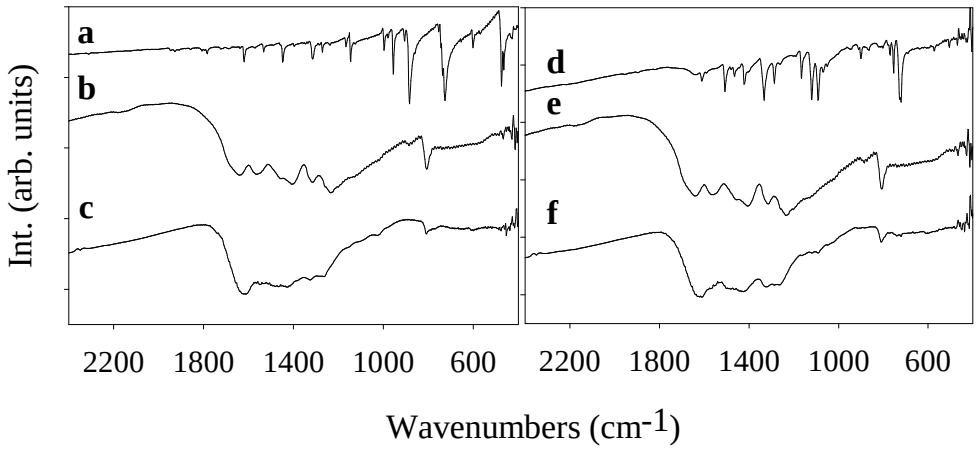

Figure 8.2 - FT-IR spectra of a) anthracene, b) TCM-CN_x, c) CNx/Anthracene, d) CuPc, e) TCM-CN_x, and f) CN_x/CuPc. The range of analysis is 2400-400 cm^{-1}.

A comparison of the IR between the two reactants and the final product reveals that in both the cases of CN_x/CuPc and CN_x/anthracene, the product is not a heterogeneous mixture of TCM-CN_x and CuPc or anthracene. The IR product spectra reveals broad absorbances occurring in the region of 1650-1100 cm^{-1}, which is consistent with extended carbon nitride solids, as well as the peak near 800 cm^{-1} indicating the presence of, what is assumed to be heptazine rings. Although it is not shown, there were vibrations near 2900 cm^{-1} in the washed products indicating the presence of a C-H stretch, most likely from the CuPc and anthracene components. There is also an increased intensity in the 1600-1500 cm^{-1} region; this could mean the presence of more C=N type bonding within the structure.

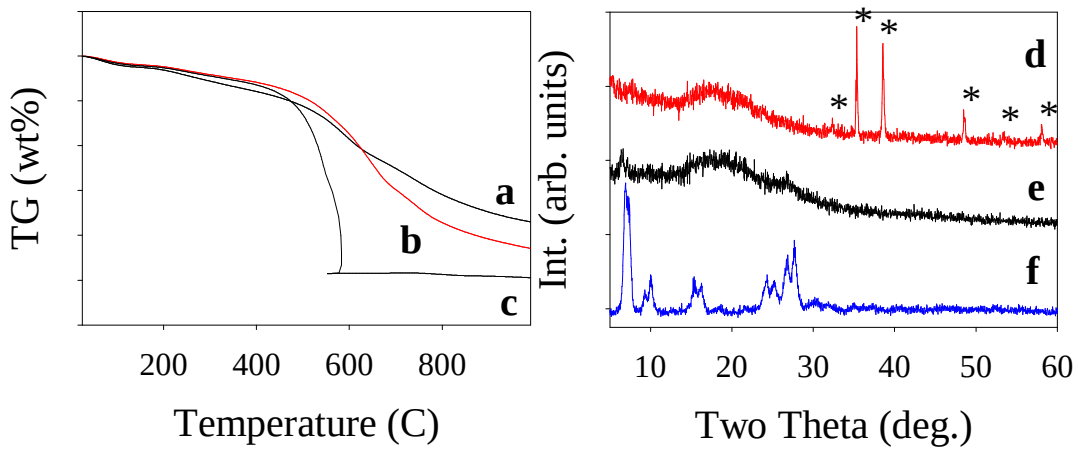

Figure 8.3 - Thermogravimetric analysis of a) CN_x/Anthracene, b) CN_x/CuPc under Ar gas, and c) TG-DTA of CN_x/CuPc under O_2 gas. Powder X-ray diffraction patterns of d) CN_x/CuPc heated to 1000 °C under oxygen (* denotes CuO), e) CN_x/CuPc product, and f) CuPc.

The thermal stability of the materials are roughly the same and are shown in Figure 8.3a-c. Low temperature weight loss (<100 °C) occur, presumably to absorbed methanol from the washing process. Under inert conditions, gradual weight losses of 15-20% occurred for CN_x/CuPc until approximately 600 °C, where a further 76% weight loss up to 1000 °C. The CN_x/anthracene product showed a more gradual weight loss over the same temperature range. When the CN_x/CuPc material was heated in oxygen to 1000 °C, the material was stable to ~550 °C, then reacted exothermically. Powder XRD analysis revealed the presence of CuO in the oxidized product (Figure 8.3d).

Powder XRD of the CN_x/CuPc material revealed a broad peak near 27° 2θ, which is a common feature for graphitic carbon nitrides (Figure 8.3e). The product also features a small peak near 7° 2θ, which corresponds with the largest peak of CuPc (Figure 8.3f). This suggests that the structures may involve a graphite-like carbon nitride material

embedded with regions of poorly crystalline CuPc. Although not shown, there was a similar peak near 27° 2θ for the CN_x/anthracene product, indicating similar graphitic structures. Further structural observations were made with scanning electron microscopy (SEM). A smooth glassy type of morphology was observed for both products, which is similar to that of TCM-CN_x (See Chapter II).

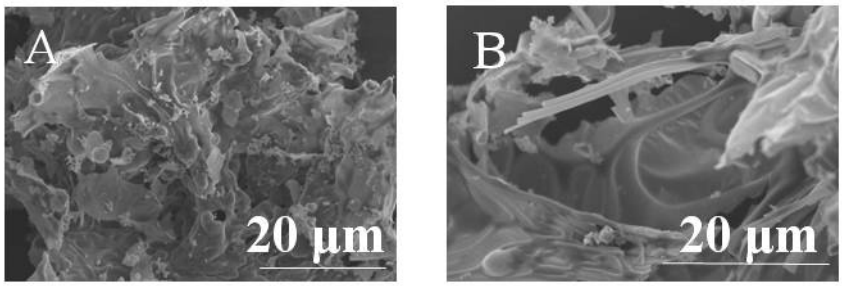

Figure 8.4 - Scanning electron micrographs of A) CN_x/CuPc and B) CN_x/anthracene.

Solid state Li_2C_2 incorporation into trichloromelamine decomposition

The reaction was considered to proceed in a manner analogous to the BCN reactions described in Chapter IV and form a carbon-rich carbon nitride (CCN) type of material, gaseous byproducts, and lithium chloride. In order to easily designate these materials, the products will be named CCN-*n*, where *n* indicates the molar equivalent of Li_2C_2 added to TCM , Black or dark brown products were initially obtained directly from the filament reactor. The material would immediately appear deliquescent after the reactions. It was thought that any LiCl that had formed would hydrolyze in air following

the reaction, so the materials were immediately washed in methanol to remove the solid byproducts. Therefore, no LiCl could be resolved by powder XRD. Except for CCN-0.375, the products had significantly lower yields than a similar scale TCM decomposition. CCN-0.375 had approximately 80% yield (assuming that 3 g of TCM yields 1g of TCM-CN_x), while CCN-1.5 and CCN-0.75 had yields of 23 and 21% respectively. A larger yield was expected for CCN-0.75, but it was difficult to collect all of the wet solids from the reactor.

Elemental analysis revealed that these materials were indeed carbon rich materials, when compared to TCM-CN_x. CCN-1.5 was found to contain 62.99 C wt%, 0.99 H wt% and 12.01 N wt%, while CCN-0.75 was found to contain 49.86 C wt%, 1.67 H wt% and 23.35 N wt%, and CCN-0.375 contained 26.93 C wt%, 4.54 H wt% and

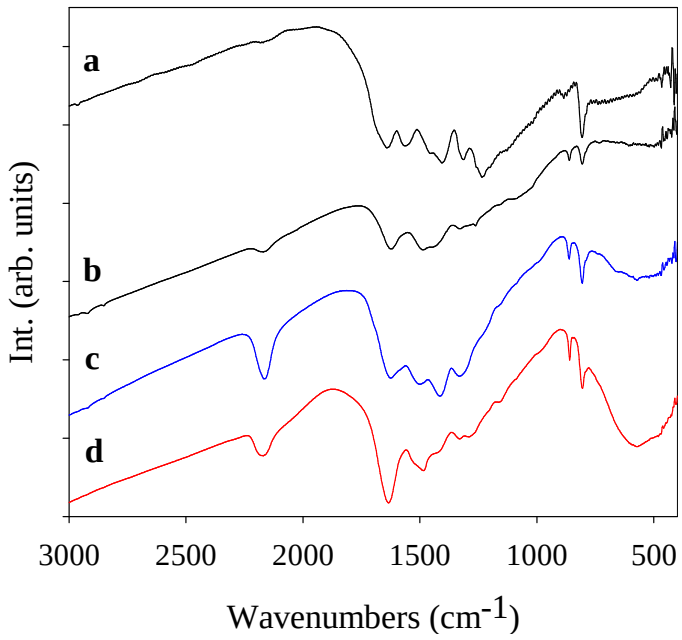

Figure 8.5 - FT-IR comparison of CCN materials a) TCM-CN_x, b) CCN-1.5 c) CCN-0.75 d) CCN-0.375.

36.58 N wt%. Therefore the formulas were calculated for each CCN: CCN-1.5 = $CN_{0.16}H_{0.19}$; CCN-0.75 = $CN_{0.40}H_{0.40}$ and CCN-0.375 = $CN_{1.16}H_{2.01}$. Further analysis of these materials by XPS may help to elucidate their local bonding structures.

FT-IR spectroscopy revealed a broad group of absorbances indicating C-N, C=N, and N-H stretching in the 1650-1100 cm^{-1} region (Figure 8.5). There were also large peaks at 3400 and 1650 cm^{-1} that are consistent with O-H vibrational modes of water. Each CCN material featured the absorbance near 800 cm^{-1} indicative of heptazine or triazine rings. There are no C-H stretches, but these may be covered up by water. There is also a peak near 2170 cm^{-1}, which is indicative of either an alkyne or nitrile stretch. There is a notable amount of broadening of the peaks, and this indicates the formation of an extended-type of material.

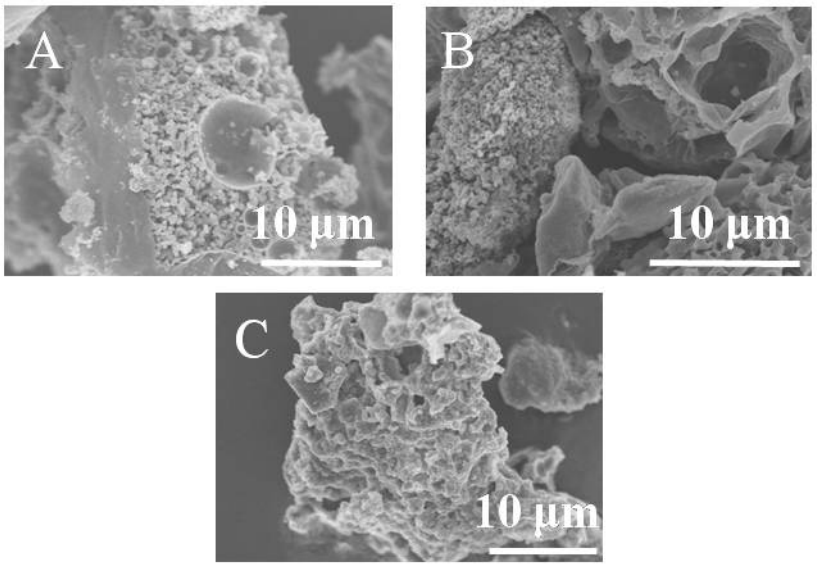

Figure 8.6 - Scanning electron micrographs of A) CCN-1.5, B) CCN-0.75, and C) CCN-0.375.

The thermal stability of the CCN products under argon flow were measured by TG-DTA. CCN-1.5 showed 35% weight loss up to 1000 °C, CCN-0.75 showed 74% weight loss, and CCN-0.375 showed 89% weight loss. The losses for CCN-1.5 were gradual throughout heating, while CCN-0.75 and CCN-0.375 showed considerable weight losses near 650 °C. This suggests that these two compounds may possess a considerable amount of carbon nitride character, while CCN-1.5 may consist of a larger amount of thermally stable amorphous carbon regions.

SEM revealed smooth glassy surfaces for the CCN materials. This suggests that a molten state may be formed during the reaction, which ultimately cools to room temperature. Li_2C_2 has been used to synthesize carbon nanotubes by solid state metathesis using reactions with C_2Cl_6.[200] Temperatures were calculated to be near 2030 °C during that reaction. Our solid state metathesis type of reaction may also be getting hot enough to melt the materials involved.

Final Thoughts

It is hoped that by now the reader will realize that heptazine-based carbon nitride materials are an interesting class of compounds and deserve further exploration into their practical utility. The research presented here represents only a fraction of the applicability of the heptazine ring structure to molecular and extended structures. It was demonstrated here that a rapid exothermic decomposition of the triazine precursor trichloromelamine generates a structure containing linked heptazines, TCM-CN_x. The fact that the true identity of this material initially eluded detection is a testament to the difficulty of disordered materials characterization.

Trichloromelamine continues to show great promise as a precursor to many types of materials. It was found that the morphology could be altered to obtain carbon nitride type materials with open pore structures. These open frameworks may be amenable to metal support materials in the areas of catalysis. It was also found that incorporation of boron leads to a novel thermally robust BCN material, through a facile route that is significantly faster than other reported pathways. This could result in hard, thermally-stable lightweight ceramics.

The potassium cyamelurate ($K_3C_6N_7O_3$) that is generated from the hydrolysis of TCM-CN_x has many chemical applications. It was found that the potassium can be exchanged with a series of transition metals to form novel metal cyamelurates. These materials proved to be formidable opponents in the areas of recrystallization and structure elucidation. Potassium cyamelurate is also the precursor to a series of heptazine derivatives: trichloroheptazine ($C_6N_7Cl_3$), tribromoheptazine ($C_6N_7Br_3$), triphenylheptazine ($C_6N_7(C_6H_5)_3$), and 2-bis(trimethyl)silylamido-5,8-dichloroheptazine ($C_6N_7Cl_2(N(SiMe_3)_2)$). All these exhibit photoluminescence and may have interesting applications in organic light-emitting diodes (OLEDs). Finally, molecular heptazines were used in the synthesis of new heptazine-based polymers.

Future Outlook

The future of the work described herein could follow any of these paths.

Physically Modified Carbon Nitride Materials

The morphology of carbon nitride materials could be altered through the use of different gas-forming additives as well as some simple inorganic templates. Thus, in order to optimize these materials, it would be prudent to quantify the changes to the

surface area of the CN_x products through further BET measurements. Once a suitable candidate is found, then perhaps metal catalyst loading could be used to explore improvements in catalytic activity. It may also be useful to explore the possibility of these materials as organocatalysts. It also may help to exploit the Lewis basicity of the nitrogens in CN_x, by exploring BH_3 bonding in possible hydrogen storage applications.

Boron Carbon Nitride Materials

The BCN types of materials synthesized from TCM and $NaBH_4$ showed excellent thermal stability and the structures of the high boron content materials were explored through the use of XPS. It may be useful to explore the structure of the materials with lower boron content to come to a better understanding of the bonding arrangements found in the materials.

Metal Cyamelurates

The metal cyamelurates proved to be problematic to recrystallize. Further explorations of new solvent systems may be required in order to form crystalline materials. An alternative synthesis might be to perform the reaction in superheated H_2O in an autoclave. Some initial attempts to solve the structure of copper cyamelurate from powder data were made. An unambiguous method for refining the structure will have to be explored.

Molecular Heptazines

The triphenylheptazine and triaminoheptazine derivatives were found to be sublimable. It may be possible to form thin films of these materials for the application of electroluminescent devices. The possibilities for novel molecular heptazines are far from

limited, but there may be different avenues to the as yet unsynthesized materials. For example, it may be useful to explore the synthesis of trifluoroheptazine through a reaction of TCH with KF in DMF. The trifluoro derivative may be more amenable to a reaction with lithium acetylides; this is analogous to the case for triazine. Otherwise, tribromoheptazine may be a better starting material in the palladium-catalyzed Sonogashira reactions. As for palladium catalysts, it has been reported that they can be used to promote synthesis of aryl cyanides, which may be useful in the synthesis of tricyanoheptazine. Another route to $N(C_6N_7Cl_2)_3$ may be to use partial substitution of TCH at two chlorine sites in order to effectively bind three heptazines to a central nitrogen.

Polymeric Heptazines

The solid state reactions involving TCH and Li_3N and Li_2C_2 may be more effective with the more thermally stable tribromoheptazine. It also may be useful to perform the reaction in a molten salt flux. Further studies on the decomposition of DCAH may have to be carried out in order to determine effects on structure. As with all polymeric heptazine structures, solid state NMR would be useful in order to further characterize the material. The acetylene bridged heptazine polymer appears to undergo significant shrinkage on drying; it may be interesting to try lyophilizing or supercritical drying in order to obtain an aerogel-type porous CN_x material.

REFERENCES

(1) Goettmann, F.; Thomas, A.; Antonietti, M. *Angewandte Chemie-International Edition* **2007**, *46*, 2717-2720.

(2) Thomas, A.; Fischer, A.; Goettmann, F.; Antonietti, M.; Muller, J. O.; Schlogl, R.; Carlsson, J. M. *Journal of Materials Chemistry* **2008**, *18*, 4893-4908.

(3) Goettmann, F.; Fischer, A.; Antonietti, M.; Thomas, A. *Chemical Communications* **2006**, 4530-4532.

(4) Goettmann, F.; Fischer, A.; Antonietti, M.; Thomas, A. *Angewandte Chemie-International Edition* **2006**, *45*, 4467-4471.

(5) Groenewolt, M.; Antonietti, M. *Advanced Materials* **2005**, *17*, 1789-+.

(6) Kim, M.; Hwang, S.; Yu, J. S. *Journal of Materials Chemistry* **2007**, *17*, 1656-1659.

(7) Mutsukura, N. *Diamond and Related Materials* **2001**, *10*, 1152-1155.

(8) Zhong, D. Y.; Zhang, G. Y.; Liu, S.; Wang, E. G.; Wang, Q.; Li, H.; Huang, X. J. *Applied Physics Letters* **2001**, *79*, 3500-3502.

(9) Bai, X. D.; Zhong, D. Y.; Zhang, G. Y.; Ma, X. C.; Liu, S.; Wang, E. G.; Chen, Y.; Shaw, D. T. *Applied Physics Letters* **2001**, *79*, 1552-1554.

(10) Abedinov, N.; Popov, C.; Yordanov, Z.; Rangelow, I. W.; Kulisch, W. *Applied Physics a-Materials Science & Processing* **2004**, *79*, 531-536.

(11) Cohen, M. L. *Physical Review B* **1985**, *32*, 7988-7991.

(12) Sung, C.-M. *unpublished patent* **1984**.

(13) Liu, A. Y.; Cohen, M. L. *Physical Review B* **1990**, *41*, 10727-10734.

(14) Liu, A. Y.; Cohen, M. L. *Science* **1989**, *245*, 841-842.

(15) Teter, D. M.; Hemley, R. J. *Science* **1996**, *271*, 53-55.

(16) Teter, D. M. *MRS Bulletin* **1998**, *23*, 22-27.

(17) Vodak, D. T.; Kim, K.; Iordanidis, L.; Rasmussen, P. G.; Matzger, A. J.; Yaghi, O. M. *Chemistry--A European Journal* **2003**, *9*, 4197-4201.

(18) Liu, A. Y.; Wentzcovitch, R. M. *Physical Review B* **1994**, *50*, 10362-10365.

(19) Ortega, J.; Sankey, O. F. *Physical Review B* **1995**, *51*, 2624-2627.

(20) Kroll, P.; Hoffmann, R. *Journal of the American Chemical Society* **1999**, *121*, 4696-4703.

(21) Kroke, E.; Schwarz, M. *Coordination Chemistry Reviews* **2004**, *248*, 493-532.

(22) Goglio, G.; Foy, D.; Demazeau, G. *Materials Science & Engineering R-Reports* **2008**, *58*, 195-227.

(23) Matsumoto, S.; Xie, E. Q.; Izumi, F. *Diamond and Related Materials* **1999**, *8*, 1175-1182.

(24) Muhl, S.; Mendez, J. M. *Diamond and Related Materials* **1999**, *8*, 1809-1830.

(25) Hellgren, N.; Guo, J. H.; Luo, Y.; Sathe, C.; Agui, A.; Kashtanov, S.; Nordgren, J.; Agren, H.; Sundgren, J. E. *Thin Solid Films* **2005**, *471*, 19-34.

(26) Rodil, S. E. *Diamond and Related Materials* 2005, p 1262-1269.

(27) Ferrari, A. C.; Rodil, S. E.; Robertson, J. *Physical Review B* **2003**, *67*.

(28) Ronning, C.; Feldermann, H.; Merk, R.; Hofsass, H.; Reinke, P.; Thiele, J. U. *Physical Review B* **1998**, *58*, 2207-2215.

(29) Escobar-Alarcon, L.; Villarreal-Barajas, J. E.; Camps, E.; Muhl, S.; Haro-Poniatowski, E.; Romero, S.; Salinas, B. *Materials Science and Engineering B-Solid State Materials for Advanced Technology* **2002**, *90*, 79-83.

(30) Escobar-Alarcon, L.; Camps, E.; Romero, S.; Olea-Mejia, O.; Muhl, S.; Arrieta, A.; Haro-Poniatowski, E. *Applied Physics a-Materials Science & Processing* **2004**, *79*, 1133-1135.

(31) Zhou, Z. B.; Cui, R. Q.; Pang, Q. J.; Hadi, G. M.; Ding, Z. M.; Li, W. Y. *Solar Energy Materials and Solar Cells* **2002**, *70*, 487-493.

(32) Kulisch, W.; Popov, C.; Zambov, L. *New Diamond and Frontier Carbon Technology* **2001**, *11*, 53-76.

(33) Iwasaki, T.; Aono, M.; Nitta, S.; Habuchi, H.; Itoh, T.; Nonomura, S. *Diamond and Related Materials*, **1999**, *8*, 440-445.

(34) Aono, M.; Nitta, S.; Katsuno, T.; Itoh, T.; Nonomura, S. *Applied Surface Science*, **2000**, *159*, 341-344.

(35) Ivanov, B. L.; Zambov, L. M.; Georgiev, G. T.; Popov, C.; Plass, M. F.; Kulisch, W. *Chemical Vapor Deposition* **1999**, *5*, 265-273.

(36) Xu, S.; Kumar, S.; Li, Y. A.; Jiang, N.; Lee, S. *Journal of Physics-Condensed Matter* **2000**, *12*, L121-L126.

(37) Zhang, Z. H.; Guo, H. X.; Xu, Y.; Zhang, W.; Fan, X. J. *Journal of Materials Science Letters* **1999**, *18*, 685-687.

(38) Wei, J.; Hing, P.; Mo, Z. Q. *Wear*, **1999**, *225*, 1141-1147.

(39) Gu, Y. S.; Zhang, Y. P.; Chang, X. R.; Tian, Z. Z.; Chen, N. X.; Shi, D. X.; Zhang, X. F.; Yuan, L. *Science in China Series a-Mathematics* **2000**, *43*, 185-198.

(40) MartinGil, J.; MartinGil, F. J.; Sarikaya, M.; Qian, M. X.; JoseYacaman, M.; Rubio, A. *Journal of Applied Physics* **1997**, *81*, 2555-2559.

(41) Kouvetakis, J.; Todd, M.; Wilkens, B.; Bandari, A.; Cave, N. *Chemistry of Materials* **1994**, *6*, 811-14.

(42) Montigaud, H.; Tanguy, B.; Demazeau, G.; Courjault, S.; Birot, M.; Dunogues, J. *Comptes Rendus de l'Academie des Sciences* **1997**, *325 series II b*, 229.

(43) Fu, Q.; Cao, C. B.; Zhu, H. S. *Chemical Physics Letters* **1999**, *314*, 223-226.

(44) Montigaud, H.; Tanguy, B.; Demazeau, G.; Alves, I.; Courjault, S. *Journal of Materials Science* **2000**, *35*, 2547-2552.

(45) Oku, T.; Kawaguchi, M. *Diamond and Related Materials* **2000**, *9*, 906-910.

(46) Khabashesku, V. N.; Zimmerman, J. L.; Margrave, J. L. *Chemistry of Materials* **2000**, *12*, 3264-3270.

(47) Huynh, M.-H. V.; Hiskey, M. A.; Hartline, E. L.; Montoya, D. P.; Gilardi, R. *Angewandte Chemie, International Edition* **2004**, *43*, 4924-4928.

(48) Guo, Q.; Xie, Y.; Wang, X.; Zhang, S.; Hou, T.; Lu, S. *Chemical Communications* **2004**, 26-27.

(49) Guo, Q. X.; Yang, Q.; Zhu, L.; Yi, C. Q.; Zhang, S.; Xie, Y. *Solid State Communications* **2004**, *132*, 369-374.

(50) Katritzky, A. R.; Oniciu, D. C.; Ghiviriga, I.; Barcock, R. A. *Journal of the Chemical Society, Perkin Transactions 2: Physical Organic Chemistry* **1995**, 785-792.

(51) Quirke, J. M. E. In *Comprehensive Heterocyclic Chemistry*; Boulton, A. J., McKillop, A., Eds.; Pergamon: Elmsford, NY, 1984; Vol. 3, Part 2B, p 457-530.

(52) Zhang, W.; Simanek, E. E. *Organic Letters* **2000**, *2*, 843-845.

(53) Le Fur, E.; Demers, E.; Maris, T.; Wuest, J. D. *Chemical Communications* **2003**, 2966-2967.

(54) Katritzky, A. R.; Rogovoy, B. V.; Vvedensky, V. Y.; Hebert, N.; Forood, B. *Journal of Organic Chemistry* **2001**, *66*, 6797-6799.

(55) Miller, D. R.; Wang, J.; Gillan, E. G. *Journal of Materials Chemistry* **2002**, *12*, 2463-2469.

(56) Gillan, E. G. *Chemistry of Materials* **2000**, *12*, 3906-3912.

(57) Wang, J.; Gillan, E. G. *Thin Solid Films* **2002**, *422*, 62-68.

(58) Wang, J.; Miller, D. R.; Gillan, E. G. *Chemical Communications* **2002**, 2258-2259.

(59) Wang, J.; Miller, D. R.; Gillan, E. G. *Carbon* **2003**, *41*, 2031-2037.

(60) Miller, D. R.; Swenson, D. C.; Gillan, E. G. *Journal of the American Chemical Society* **2004**, *126*, 5372-5373.

(61) Miller, D. R.; Holst, J. R.; Gillan, E. G. *Inorganic chemistry* **2007**, *46*, 2767-2774.

(62) Gmelin, L. *Handbook of Chemistry* **1855**, *9*, 378-394.

(63) Liebig, J. v. *Annalen der Pharmacie* **1834**, *10*, 1-48.

(64) Liebig, J. *Annalen der Chemie und Pharmacie* **1844**, *50*, 337.

(65) Liebig, J. *Annalen der Chemie und Pharmacie* **1845**, *53*, 330.

(66) Liebig, J. *Annalen der Chemie und Pharmacie* **1855**, *95*, 257.

(67) Voelckel *Poggendorff Annalen* **1843**, *58*, 151.

(68) Gmelin, L. *Annalen der Pharmacie* **1835**, *15*, 252.

(69) Franklin, E. C. *Journal of the American Chemical Society* **1922**, *44*, 486-509.

(70) Pauling, L.; Sturdivant, J. H. *Proceedings of the National Academy of Sciences of the United States of America* **1937**, *23*, 615-620.

(71) Redemann, C. E.; Lucas, H. J. *Journal of the American Chemical Society* **1939**, *61*, 3420-3424.

(72) Redemann, C. E.; Lucas, H. J. *Journal of the American Chemical Society* **1940**, *62*, 842-846.

(73) Boitsov, E. N.; Finkel'shtein, A. I. *Zhurnal Obshchei Khimii* **1962**, *32*, 321-2.

(74) Finkel'shtein, A. I. *Optika i Spektroskopiya* **1962**, *12*, 204-7.

(75) Finkel'shtein, A. I.; Spiridonova, N. V. *Uspekhi Khimii* **1964**, *33*, 900-11.

(76) Finkel'shtein, A. I.; Spiridonova, N. V. *Zhurnal Organicheskoi Khimii* **1965**, *1*, 606-9.

(77) Finkel'shtein, A. I. Application: SU, 1966.

(78) Spiridonova, N. V.; Finkel'shtein, A. I. *Trudy po Khimii i Khimicheskoi Tekhnologii* **1967**, 38-40.

(79) Spiridonova, N. V.; Finkel'shtein, A. I.; Buchnev, I. F.; Zagranichnyi, V. I.; Molev, I. I.; (Dzerzhinsk Branch of the State-Scientific Research and Design Institute of the Nitrogen Industry and of Products of Organic Synthesis). Application: SU, 1967.

(80) Simkina, L. A.; Finkel'shtein, A. I.; Gal'perin, V. A. *Zavodskaya Laboratoriya* **1973**, *39*, 287.

(81) Karlik, V. M.; Gal'perin, V. A.; Zagranichnyi, V. I.; Finkel'shtein, A. I. Application: SU, 1974.

(82) Zhagrova, N. I.; Spiridonova, N. V.; Finkel'shtein, A. I. *Zhurnal Prikladnoi Khimii (Sankt-Peterburg, Russian Federation)* **1975**, *48*, 452-3.

(83) Spasskaya, R. I.; Finkel'shtein, A. I.; Zil'berman, E. N.; Gal'perin, V. A. *Plast. Massy* **1977**, 10-11.

(84) Karlik, V. M.; Rozhnova, M. V.; Finkel'shtein, A. I.; Zagranichnyi, V. I.; Al'tshuler, L. N.; (USSR). Application: SU.

(85) Finkel'shtein, A. I.; Karlik, V. M.; Al'tshuler, L. N.; Rozhnova, M. V.; Zagranichnyi, V. I.; (USSR). Application: SU

(86) Schroeder, H.; Kober, E. *Journal of Organic Chemistry* **1962**, *27*, 4262-&.

(87) Hosmane, R. S.; Rossman, M. A.; Leonard, N. J. *Journal of the American Chemical Society* **1982**, *104*, 5497-5499.

(88) Kroke, E.; Schwarz, M.; Horath-Bordon, E.; Kroll, P.; Noll, B.; Norman, A. D. *New Journal of Chemistry* **2002**, *26*, 508-512.

(89) Horvath-Bordon, E.; Kroke, E.; Svoboda, I.; Fuess, H.; Riedel, R. *New Journal of Chemistry* **2005**, *29*, 693-699.

(90) Jurgens, B.; Irran, E.; Senker, J.; Kroll, P.; Muller, H.; Schnick, W. *Journal of the American Chemical Society* **2003**, *125*, 10288-10300.

(91) Komatsu, T.; Nakamura, T. *Journal of Materials Chemistry* **2001**, *11*, 474-478.

(92) Komatsu, T. *Macromolecular Chemistry and Physics* **2001**, *202*, 19-25.

(93) Komatsu, T. *Journal of Materials Chemistry* **2001**, *11*, 799-801.

(94) Komatsu, T. *Journal of Materials Chemistry* **2001**, *11*, 802-805.

(95) El-Gamel, N. E. A.; Schwarz, M.; Brendler, E.; Kroke, E. *Chemical Communications* **2006**, 4741-4743.

(96) Riedel, R.; Horvath-Bordon, E.; Nahar-Borchert, S.; Kroke, E.; Suzuki, H. K. K. S. M., Ed. *Key Engineering Materials*, **2003**, *247*, 121-128.

(97) Jurgens, B.; Irran, E.; Schneider, J.; Schnick, W. *Inorganic chemistry* **2000**, *39*, 665-670.

(98) Lotsch, B. V.; Schnick, W. *Chemistry of Materials* **2005**, *17*, 3976-3982.

(99) Lotsch, B. V.; Schnick, W. *Chemistry of Materials* **2006**, *18*, 1891-1900.

(100) Sattler, A.; Schnick, W. *Zeitschrift Fur Anorganische Und Allgemeine Chemie* **2006**, *632*, 238-242.

(101) Lotsch, B. V.; Schnick, W. *Chemistry-a European Journal* **2007**, *13*, 4956-4968.

(102) Lotsch, B. V.; Doblinger, M.; Sehnert, J.; Seyfarth, L.; Senker, J.; Oeckler, O.; Schnick, W. *Chemistry-a European Journal* **2007**, *13*, 4969-4980.

(103) Sehnert, J.; Baerwinkel, K.; Senker, J. *Journal of Physical Chemistry B* **2007**, *111*, 10671-10680.

(104) Redemann, C. E.; Lucas, H. J. *Journal of the American Chemical Society* **1940**, *62*, 842-6.

(105) Shahbaz, M.; Urano, S.; Lebreton, P. R.; Rossman, M. A.; Hosmane, R. S.; Leonard, N. J. *Journal of the American Chemical Society* **1984**, *106*, 2805-2811.

(106) Halpern, A. M.; Rossman, M. A.; Hosmane, R. S.; Leonard, N. J. *Journal of Physical Chemistry* **1984**, *88*, 4324-4326.

(107) Schwarz, M. R.; Ehrenberg, H.; Kloc, M. A.; Kroke, E. *Heterocycles* **2006**, *68*, 2499-2507.

(108) Tragl, S.; Meyer, H. J. *Zeitschrift Fur Anorganische Und Allgemeine Chemie* **2005**, *631*, 2300-2302.

(109) Traber, B.; Oeser, T.; Gleiter, R.; Goebel, M.; Wortmann, R. *European Journal of Organic Chemistry* **2004**, 4387-4390.

(110) Ke, Y. X.; Collins, D. J.; Sun, D. F.; Zhou, H. C. *Inorganic chemistry* **2006**, *45*, 1897-1899.

(111) Horvath-Bordon, E.; Kroke, E.; Svoboda, I.; Fuess, H.; Riedel, R.; Neeraj, S.; Cheetham, A. K. *Dalton Transactions* **2004**, 3900-3908.

(112) El-Gamel, N. E. A.; Seyfarth, L.; Wagler, J.; Ehrenberg, H.; Schwarz, M.; Senker, J.; Kroke, E. *Chemistry-a European Journal* **2007**, *13*, 1158-1173.

(113) Komatsu, T. *Physical Chemistry Chemical Physics* **2004**, *6*, 878-880.

(114) Riedel, R.; Horvath-Bordon, E.; Nahar-Borchert, S.; Kroke, E. *Key Engineering Materials* **2003**, *247*, 121-128.

(115) Tragl, S.; Gibson, K.; Glaser, J.; Duppel, V.; Simon, A.; Meyer, H. J. *Solid State Communications* **2007**, *141*, 529-534.

(116) Zheng, W. X.; Wong, N. B.; Wang, W. Z.; Zhou, G.; Tian, A. M. *Journal of Physical Chemistry A* **2004**, *108*, 97-106.

(117) Guo, Q. X.; Yang, Q.; Yi, C. Q.; Zhu, L.; Xie, Y. *Carbon* **2005**, *43*, 1386-1391.

(118) Holst, J. R.; Gillan, E. G. *Journal of the American Chemical Society* **2008**, *130*, 7373-7379.

(119) Aoki, S.; Shiro, M.; Koike, T.; Kimura, E. *Journal of the American Chemical Society* **2000**, *122*, 576-584.

(120) Seifer, G. B. *Russian Journal of Coordination Chemistry* **2002**, *28*, 301-324.

(121) Zhang, Z.; Leinenweber, K.; Bauer, M.; Garvie, L. A. J.; McMillan, P. F.; Wolf, G. H. *Journal of the American Chemical Society* **2001**, *123*, 7788-7796.

(122) Zimmerman, J. L.; Williams, R.; Khabashesku, V. N.; Margrave, J. L. *Nano Letters* **2001**, *1*, 731-734.

(123) Derbyshire, F.; Jagtoyen, M.; Thwaites, M. *Porosity in Carbons*; Edward Arnold: London, 1995.

(124) *Handbook of Porous Solids*; Wiley-VCH: Weinheim, 2002; Vol. 1.

(125) Thomas, A.; Goettmann, F.; Antonietti, M. *Chemistry of Materials* **2008**, *20*, 738-755.

(126) Cooper, A. I.; JIang, J.-X.; Trewin, A.; Su, F.; Tan, B.; Stockel, E.; Niu, H.; Campbell, N. L.; Ganin, A.; Rosseinsky, M. J.; Khimyak, Y. Z. *PMSE Preprints* **2007**, *97*, 116.

(127) Thomas, A.; Pierre-Kuhn, P.; Weber, J.; Titrici, M.-M.; Antonietti, M. *Macromol. Rapid Commun.* **2009**, *30*, 221-236.

(128) Stober, W.; Fink, A.; Bohn, E. *Journal of Colloid and Interface Science* **1968**, *26*, 62-&.

(129) Johnson, S. A.; Ollivier, P. J.; Mallouk, T. E. *Science* **1999**, *283*, 963-965.

(130) Xia, Y. N.; Gates, B.; Yin, Y. D.; Lu, Y. *Advanced Materials* **2000**, *12*, 693-713.

(131) Xia, Y. N.; Gates, B.; Li, Z. Y. *Advanced Materials* **2001**, *13*, 409-413.

(132) Edrington, A. C.; Urbas, A. M.; DeRege, P.; Chen, C. X.; Swager, T. M.; Hadjichristidis, N.; Xenidou, M.; Fetters, L. J.; Joannopoulos, J. D.; Fink, Y.; Thomas, E. L. *Advanced Materials* **2001**, *13*, 421-425.

(133) Stein, A. *Microporous and Mesoporous Materials* **2001**, *44*, 227-239.

(134) Goettmann, F.; Fischer, A.; Antonietti, M.; Thomas, A. *New Journal of Chemistry* **2007**, *31*, 1455-1460.

(135) Hwang, S.; Lee, S.; Yu, J. S. *Applied Surface Science* **2007**, *253*, 5656-5659.

(136) Perera, S.; Zelenski, N.; Gillan, E. G. *Chemistry of Materials* **2006**, *18*, 2381-2388.

(137) Paine, R. T.; Narula, C. K. *Chemical Reviews* **1990**, *90*, 73-91.

(138) Wentorf, R. H. *Journal of Chemical Physics* **1957**, *26*, 956-956.

(139) Chopra, N. G.; Luyken, R. J.; Cherrey, K.; Crespi, V. H.; Cohen, M. L.; Louie, S. G.; Zettl, A. *Science* **1995**, *269*, 966-967.

(140) Kaner, R. B.; Kouvetakis, J.; Warble, C. E.; Sattler, M. L.; Bartlett, N. *Materials Research Bulletin* **1987**, *22*, 399-404.

(141) Kawaguchi, M. *Advanced Materials* **1997**, *9*, 615-625.

(142) Kawaguchi, M.; Bartlett, N. *Chemistry, Physics and Applications of Fluorine-Carbon and Fluoride-Carbon Compounds*; Marcel Dekker: New York, 1995.

(143) Morita, M.; Hanada, T.; Tsutsumi, H.; Matsuda, Y.; Kawaguchi, M. *Journal of the Electrochemical Society* **1992**, *139*, 1227-1230.

(144) Kosolapova, T.; Makarenko, G.; Serebryakova, T.; Prilutskii, E.; Khorpyakov, O.; Chernysheva, O. *Poroshkovaya Metallurgiya* **1971**, *1*.

(145) Badzian, A.; Niemyski, T.; Appenheimer, S.; Olkusnik, E. In *Proceedings of the 3rd International Conference on Chemical Vapor Deposition* Pennington, NJ, 1972, p 747.

(146) Badzian, A.; Niemyski, T.; Appenheimer, S.; Olkusnik, E. *Khimiya Svyaz Poluprodnikov Polumet* **1972**, 362.

(147) Sasaki, T.; Bartlett, N. In *Proceedings of the 197th ACS National Meeting*; ACS: Dallas, TX, 1989, p 46.

(148) Kouvetakis, J.; Kaner, R. B.; Sattler, M. L.; Bartlett, N. *Journal of the Chemical Society-Chemical Communications* **1986**, 1758-1759.

(149) Kouvetakis, J.; Sasaki, T.; Shen, C.; Hagiwara, R.; Lerner, M.; Krishnan, K. M.; Bartlett, N. 1990, p 1-7.

(150) Kawaguchi, M.; Kawashima, T. *Journal of the Chemical Society-Chemical Communications* **1993**, 1133-1134.

(151) Miller, D. R. **2004**, Ph.D. Dissertation, University of Iowa, pp220.

(152) Komatsu, T.; Goto, A. *Journal of Materials Chemistry* **2002**, *12*, 1288-1293.

(153) Stephan, O.; Ajayan, P. M.; Colliex, C.; Redlich, P.; Lambert, J. M.; Bernier, P.; Lefin, P. *Science* **1994**, *266*, 1683-1685.

(154) Bai, S. Z.; Yao, B.; Xing, G. Z.; Zhang, K.; Su, W. H. *Physica B-Condensed Matter* **2007**, *396*, 214-219.

(155) Komatsu, T. *Journal of Materials Chemistry* **2004**, *14*, 221-227.

(156) Volger, K. W.; Kroke, E.; Gervais, C.; Saito, T.; Babonneau, F.; Riedel, R.; Iwamoto, Y.; Hirayama, T. *Chemistry of Materials* **2003**, *15*, 755-764.

(157) Darmstadt, H.; Roy, C.; Kaliaguine, S.; Xu, G. Y.; Auger, M.; Tuel, A.; Ramaswamy, V. *Carbon* **2000**, *38*, 1279-1287.

(158) Goze-Bac, C.; Latil, S.; Lauginie, P.; Jourdain, V.; Conard, J.; Duclaux, L.; Rubio, A.; Bernier, P. *Carbon* **2002**, *40*, 1825-1842.

(159) Gervais, C.; Babonneau, F. *Journal of Organometallic Chemistry*, **2002**, *657*, 75-82.

(160) Marchetti, P. S.; Kwon, D. K.; Schmidt, W. R.; Interrante, L. V.; Maciel, G. E. *Chemistry of Materials* **1991**, *3*, 482-486.

(161) Lee, Y.; Han, D. Y.; Lee, D.; Woo, A. J.; Lee, S. H.; Kim, Y. K. *Carbon* **2002**, *40*, 403-408.

(162) Shchukarev, A.; Boily, J. F.; Felmy, A. R. *Journal of Physical Chemistry C* **2007**, *111*, 18307-18316.

(163) Wagner, C.; Naumkin, A.; Kraut-Vass, A.; Allison, J.; Powell, C.; Rumble, J. In *NIST X-ray Photoelectron Spectroscopy Database* 2003.

(164) Komatsu, T.; Goto, A. *Journal of Materials Chemistry* **2002**, *12*, 1288-1293.

(165) Pels, J. R.; Kapteijn, F.; Moulijn, J. A.; Zhu, Q.; Thomas, K. M. *Carbon* **1995**, *33*, 1641-1653.

(166) Wojtowicz, M. A.; Pels, J. R.; Moulijn, J. A. *Fuel* **1995**, *74*, 507-516.

(167) Sattler, A.; Schnick, W. *Zeitschrift Fur Anorganische Und Allgemeine Chemie* **2006**, *632*, 531-533.

(168) Cheary, R. W.; Coelho, A. A. In *XFIT* 1996.

(169) Shirley, R. In *The CRYSFIRE System for Automatic Powder Indexing*.

(170) Favre-Nicolin, V.; Cerny, R. *Journal of Applied Crystallography* **2002**, *35*, 734-743.

(171) Kirk-Othmer *Encyclopedia of Chemical Technology*; Fourth ed.; John Wiley & Sons, Inc.: New York, 1997; Vol. 23.

(172) Rathke *Berichte der Deutschen Chemischen Gesellshaft* **1879**, *12*, 778.

(173) Rathke *Berichte der Deutschen Chemischen Gesellshaft* **1890**, *23*, 1675.

(174) Cotton, F. A.; Wilkinson, G. *Advanced Inorganic Chemistry, 5th Edition* **1988**, 702.

(175) Nakamoto, K. *Infrared and Raman Spectra of Inorganic and Coordination Compounds, 4th Ed.* **1986**.

(176) Sattler, A.; Schnick, W. *Zeitschrift Fur Anorganische Und Allgemeine Chemie* **2008**, *634*, 457-460.

(177) Sattler, A.; Seyfarth, L.; Senker, J.; Schnick, W. *Zeitschrift Fur Anorganische Und Allgemeine Chemie* **2005**, *631*, 2545-2554.

(178) Sattler, A.; Schnick, W. *Zeitschrift Fur Anorganische Und Allgemeine Chemie* **2008**, *634*, 1063-1066.

(179) Horvath-Bordon, E., Ph.D. Dissertation, Darmstadt, 2004.

(180) Del Sesto, R. E.; Arif, A. M.; Novoa, J. J.; Anusiewicz, I.; Skurski, P.; Simons, J.; Dunn, B. C.; Eyring, E. M.; Miller, J. S. *Journal of Organic Chemistry* **2003**, *68*, 3367-3379.

(181) Friedrich, K.; Steiert, P. *Journal Fur Praktische Chemie-Chemiker-Zeitung* **1995**, *337*, 313-314.

(182) Chinchilla, R.; Najera, C. *Chemical Reviews* **2007**, *107*, 874-922.

(183) Harris, G. S.; Payne, D. S. *Journal of the Chemical Society* **1958**, 3732-3733.

(184) Dudchik, G. P.; Polyachenok, O. G. *Zh. Neorg. Khim.* **1980**, *25*, 2599-2602.

(185) Gottlieb, H. E.; Kotlyar, V.; Nudelman, A. *Journal of Organic Chemistry* **1997**, *62*, 7512-7515.

(186) Cui, D.; Nishiura, M.; Hou, Z. *Angewandte Chemie-International Edition* **2005**, *44*, 959-962.

(187) Katritzky, A. R.; Ghiviriga, I.; Steel, P. J.; Oniciu, D. C. *Journal of the Chemical Society, Perkin Transactions 2: Physical Organic Chemistry* **1996**, 443-7.

(188) Inomata, H.; Goushi, K.; Masuko, T.; Konno, T.; Imai, T.; Sasabe, H.; Brown, J. J.; Adachi, C. *Chemistry of Materials* **2004**, *16*, 1285-1291.

(189) Pang, J.; Tao, Y.; Freiberg, S.; Yang, X. P.; D'Iorio, M.; Wang, S. N. *Journal of Materials Chemistry* **2002**, *12*, 206-212.

(190) Zheng, W. X.; Wong, N. B.; Zhou, G.; Liang, X. Q.; Li, J. S.; Tian, A. M. *New Journal of Chemistry* **2004**, *28*, 275-283.

(191) Vodak, D. T.; Kim, K.; Iordanidis, L.; Rasmussen, P. G.; Matzger, A. J.; Yaghi, O. M. *Chemistry-a European Journal* **2003**, *9*, 4197-4201.

(192) Tragl, S.; Gibson, K.; Meyer, H. J. *Zeitschrift Fur Anorganische Und Allgemeine Chemie* **2004**, *630*, 2373-2376.

(193) Gibson, K.; Glaser, J.; Milke, E.; Marzini, M.; Tragl, S.; Binnewies, M.; Mayer, H. A.; Meyer, H. J. *Materials Chemistry and Physics* **2008**, *112*, 52-56.

(194) Zhang, X. H.; Li, Q. S.; Ingels, J. B.; Simmonett, A. C.; Wheeler, S. E.; Xie, Y. M.; King, R. B.; Schaefer, H. F.; Cotton, F. A. *Chemical Communications* **2006**, 758-760.

(195) Kuhn, P.; Antonietti, M.; Thomas, A. *Angewandte Chemie-International Edition* **2008**, *47*, 3450-3453.

(196) Sonoda, M.; Inaba, A.; Itahashi, K.; Tobe, Y. *Organic Letters* **2001**, *3*, 2419-2421.

(197) Kawaguchi, M.; Tokimatsu, Y.; Nozaki, K.; Kaburagi, Y.; Hishiyama, Y. *Chemistry Letters* **1997**, 1003-1004.

(198) Gibson, K.; Strobele, M.; Blaschkowski, B.; Glaser, J.; Weisser, M.; Srinivasan, R.; Kolb, H. J.; Meyer, H. J. *Zeitschrift Fur Anorganische Und Allgemeine Chemie* **2003**, *629*, 1863-1870.

(199) Juza, R.; Wehle, V.; Schuster, H. U. *Zeitschrift Fur Anorganische Und Allgemeine Chemie* **1967**, *352*, 252-&.

(200) Mack, J. J.; Tari, S.; Kaner, R. B. *Inorganic chemistry* **2006**, *45*, 4243-4246.

(201) Kouvetakis, J.; Grotjahn, D.; Becker, P.; Moore, S.; Dupon, R. *Chemistry of Materials* **1994**, *6*, 636-639.

(202) Kouvetakis, J.; Todd, M. In *U.S.*; (Arizona Board of Regents, USA). Us, 1997, p 9 pp.

(203) Solozhenko, V. L.; Solozhenko, E. G.; Late, K. *Sverkhtverdye Materialy* **2002**, 95-96.

(204) Chang, C. K.; Liu, H. Y.; Abdalmuhdi, I. *Journal of the American Chemical Society* **1984**, *106*, 2725-2726.

(205) Jahnke, H.; Schonborn, M.; Zimmerman, G. *Topics in Current Chemistry* **1976**, *61*, 133.

(206) Sirk, A. H. C.; Campbell, S. A.; Birss, V. I. *Electrochemical and Solid State Letters* **2005**, *8*, A104-A107.

(207) Sirk, A. H. C.; Campbell, S. A.; Birss, V. I. *Journal of the Electrochemical Society* **2008**, *155*, B592-B601.